Activity of Py-Im polyamides in anti-androgen resistant prostate cancer models

Thesis by

Alexis Anna Kurmis

In Partial Fulfillment of the Requirements for

the degree of

Doctor of Philosophy

CALIFORNIA INSTITUTE OF TECHNOLOGY

Pasadena, California

2019

(Defended February 25, 2019)

Alexis Anna Kurmis
ORCID: 0000-0002-8427-2198

ACKNOWLEDGEMENTS

First, I would like to thank Professor Peter Dervan for the opportunity to join his lab, and for the chances he has given me to explore new fields throughout my time here. Not everything has worked out, but I did get the valuable opportunity to learn skills from basic cell culture to xenograft work to electron microscopy to sequencing data analysis.

I would also like to thank the other members of the Dervan lab for all their help over the last few years. Alissa, JJ, Tim, Thomas, and Jerzy, thank you for your support and answering all my questions as I adjusted to working on more biological experiments. Amanda, Tiezheng, Paul, and Alice were all also a pleasure to work with. I would also like to thank Nick for helpful suggestions and critical review of the work presented here, and Vicky for always being a source of great conversation (and not minding giving me the same grant number many many times!)

None of the work presented here would have been possible without the many wonderful Caltech employees who are always willing to help. I would particularly like to thank the animal care staff, including Dr. Karen Lencioni for her help with protocols, and Gwen Williams and Gloria Martinez for taking excellent care of my little guys. Vijaya Kumar and Igor Antoshechkin in the sequencing facility were also tremendously helpful.

Finally, I would like to thank my family and friends. Alice Chang was an excellent roommate for our first two years here, and definitely helped make the adjustment to life at Caltech easier. Sophie Zhang-Bullock is an excellent camping companion (but terrible hike planner), who has given me leads on many exciting jobs such as puppy petter and chocolate

ambassador. My mom, dad, and sisters Kari, Taylor, and Hannah have also all been there to remind me that they believe in me even when things are difficult (and to provide cat and baby pictures to cheer me up). Last, the past five years would not have been nearly as fun without my wonderful husband Fei, who has taken me on adventures all over southern California, Utah, and Arizona. I look forward to many more in the future!

ABSTRACT

The antiproliferative effects of Py-Im polyamides have been evaluated in several cancer models. The work presented here focuses on prostate cancer and the application of Py-Im polyamides targeted to the sequence 5'-WGWWCW-3', which is found in a subset of androgen response elements. We begin by exploring the effect of a Py-Im polyamide in the VCaP model, which overexpresses wildtype AR and is genomically unstable due to ERG overexpression caused by the *TMPRSS2-ERG* translocation. In this model, Py-Im polyamide treatment reduces ERG protein level and DNA fragmentation, and reduces VCaP xenograft growth. Transcriptomic analysis of Py-Im polyamide treated VCaP cells provides a novel potential mechanism of blockage of topoisomerase I and II activity by polyamides. We next evaluate the activity of a second generation Py-Im polyamide in two models of anti-androgen resistant prostate cancers, and demonstrate growth inhibition in both cell culture and tumor models. Transcriptomic analysis of the model cell lines revealed suppression of androgen receptor signaling. Further, expression profiles are consistent with transcription inhibition in both cell samples and tumor samples. Finally, we examine the effect of a Py-Im polyamide on the AR cistrome in prostate cancer cells. We find through ChIP-Seq analysis that loci differentially affected by Py-Im polyamide treatment are enriched for potential ARE half-sites consistent with the polyamide target site. In summary, we find that Py-Im polyamides interfere with several DNA dependent processes, similar to other DNA minor groove binders, and we show through AR cistromic analysis that Py-Im polyamides reduce AR occupancy in a pattern that is predicted by Py-Im polyamide pairing rules.

PUBLISHED CONTENT AND CONTRIBUTIONS

Chapter 2:

Hargrove AE, Martinez TF, Hare AA, Kurmis AA, Phillips JW, Sud S, Pienta KJ, and Dervan PB. (2015) Tumor Repression of VCaP Xenografts by a Pyrrole-Imidazole Polyamide. PLoS ONE 10(11):e0143161. Doi:10.1371/journal.pone.0143161

AAK performed RNA-seq experiments, analyzed data, and participated in the writing of the manuscript.

Chapter 3:

Kurmis AA, Yang F, Welch TR, Nickols NG, and Dervan PB. (2017) A Pyrrole-Imidazole Polyamide is Active against Enzalutamide-Resistant Prostate Cancer. *Cancer Res.* 77:2207-2212. Doi: 10.1158/0008-5472.CAN-16-2503

AAK participated in the design and conception of experiments (with FY, NGN, and PBD), performed RNA-seq and xenograft experiments, analyzed data, and participated in the writing of the manuscript.

Chapter 4:

Kurmis AA and Dervan PB. (2019) Sequence specific suppression of androgen receptor-DNA binding in vivo by a Py-Im polyamide. *Nucleic Acids Research.* Doi: 10.1093/nar/gkz153

AAK participated in the design and execution of all experiments, analyzed data, and participated in the writing of the manuscript.

THESIS OUTLINE

LIST OF FIGURES

Chapter 1

Introduction

1.1 Background and significance

Advancements in medical research have significantly changed health care needs in the last century. In 1900, the top three causes of death in the United States were 1) pneumonia and influenza, 2) tuberculosis, and 3) diarrhea, enteritis, and ulceration of the intestines. (1) Improved living standards, along with medical advances, have greatly reduced the prevalence of these communicable diseases and increased global life expectancy. This, in turn, has led to an increase in diseases that typically affect elderly patients. As of 2016, heart disease and cancer were the leading causes of death by a significant margin in both the 50-70+ year old population and overall (Fig 1.1 A). For comparison, the leading causes of death in the 5-14 year old population are malaria and road accidents. (2)

As a result of this change in health care needs, significant efforts and resources have been invested into the study of the underlying causes of heart disease and cancer. Cancer in particular has been found to have a myriad of molecular mechanisms contributing to its development, which can vary based on the tissue of origin. Among these, cancers of the breast, colon, and prostate are the most commonly diagnosed world-wide (Fig 1.1 B). (3) For many cancers, the standard of care involves the use of chemotherapeutic toxins, which are effective largely because highly proliferative cancer cells are more sensitive than healthy cells. The side effects of these treatments, however, do not spare normal cells, and

extensive DNA damage increases the risk of secondary cancer, particularly in pediatric cancers. (4, 5)

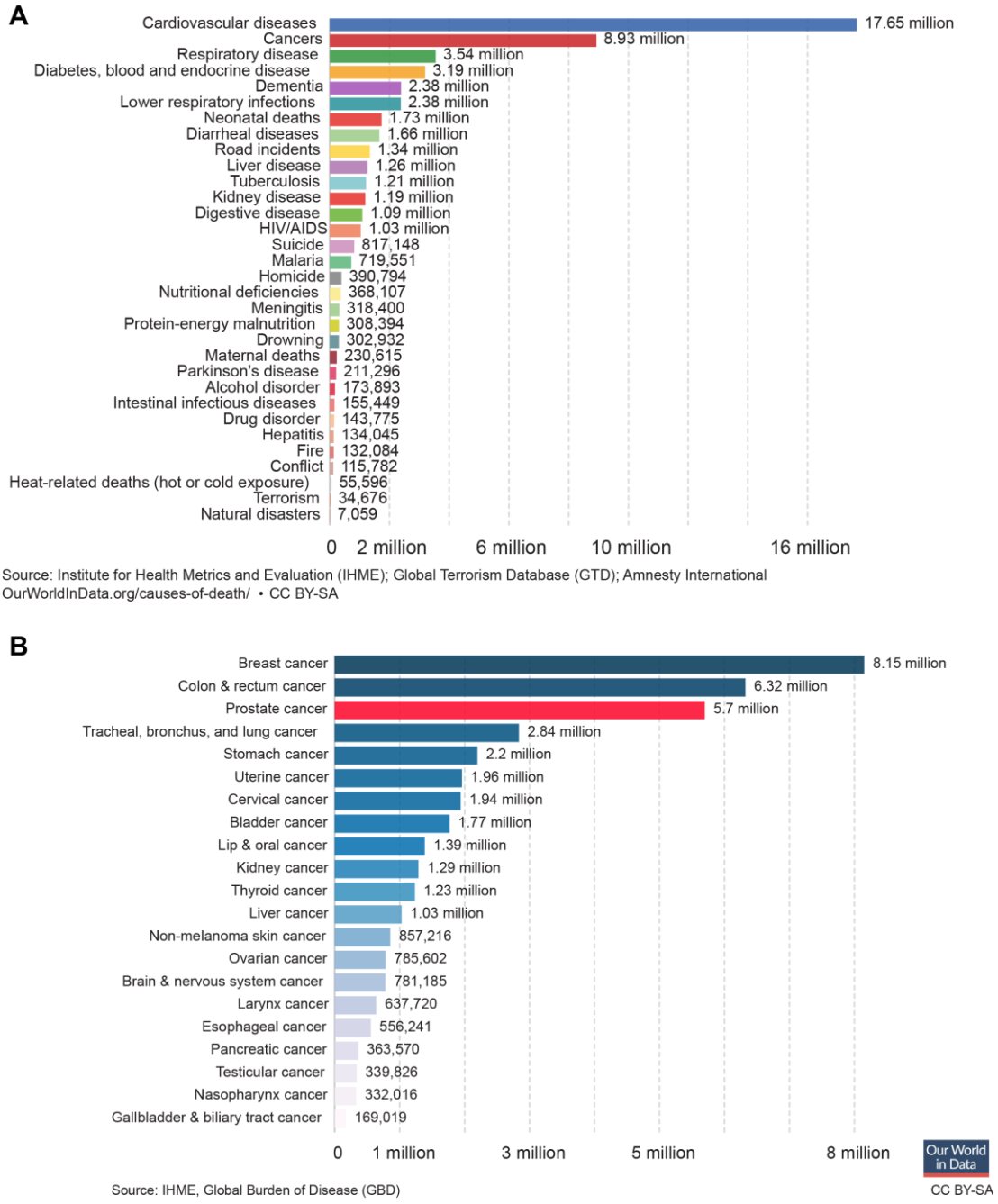

Figure 1.1 A) Top causes of death in the world, by number of cases in 2016. **B)** Number of people in the world with cancer, by type, in 2016.

The most common histologies of breast and prostate cancer represent a type of disease where a single dysfunctioning protein drives progression. The estrogen receptor (ER) is a well-established marker for breast cancer; the first experiments connecting ER status to treatment response were conducted in the 1970s. (6) Today, ERα status is an important predictor of survival and it is known that ERα positive tumors are more likely to respond to anti-estrogen therapy. (7) Similarly, it has been known since the early 1940s that the progression of prostate cancer can be slowed by androgen deprivation. (8) Therefore, inhibition of the estrogen receptor in breast cancer and the androgen receptor in prostate cancer have been mainstays in the treatment of these diseases.

1.2 Prostate cancer biology and treatment

Prostate cancer is the one of the most commonly diagnosed cancers, and the second leading cause of cancer death in men, with an estimated 161,360 new cases and 26,730 deaths in the United States in 2017. (9) Early diagnosis and treatment is often curative with a five year survival of 98.2%. (10) After peaking in 1993, the mortality rate of prostate cancer steadily declined through 2015, due to more widespread screening and advances in diagnostics and treatment options. (11) However, prostate cancer with distal metastasis, which accounts for 5% of all prostate cancer cases, only has a five year survival rate of 29%. (9) This precipitous drop in treatment outcome is largely due to the development of heterogeneous disease. (10)

The androgen receptor is a nuclear hormone receptor that is important in the development of sex characteristics and muscle development. (12, 13) AR is normally sequestered in the cytosol by heat shock proteins and is activated when dihydrotestosterone (DHT) binding to the AR ligand binding domain induces structural changes to the receptor. (Fig 1.2 A, adapted from (14–16). Upon release, AR homodimerizes and translocates to the nucleus, where it binds to specific sequences on the DNA known as androgen response elements (ARE) (Fig 1.2 B+C). Subsequent recruitment of transcriptional machinery results in the activation of gene expression programs collectively referred to as AR signaling.

Androgen receptor activity is key to the survival of approximately 80-90% of prostate cancers at diagnosis, and often persists through multiple rounds of treatment. (17–20) If the disease is caught at an early stage, surgery and localized radiation is often sufficient for treatment, however, distal metastatic disease requires systemic treatment. The current treatment strategy for metastatic prostate cancer utilizes a combination of drugs that antagonizes the activity of the androgen receptor, collectively called androgen deprivation therapy (ADT).

As implied by the name, ADT functions by blocking AR signaling through the interference of DHT-AR interactions or by depleting physiological levels of DHT or its precursor testosterone. The classical ADT drugs leuprolide and bicalutamide function by shutting down approximately 90-95% of testosterone production in the pituitary gland and blocking

DHT-AR interactions, respectively. (21) Abiraterone, enzalutamide, and apalutamide have also been approved recently, and have the same goal of reducing AR signaling. (22–24)

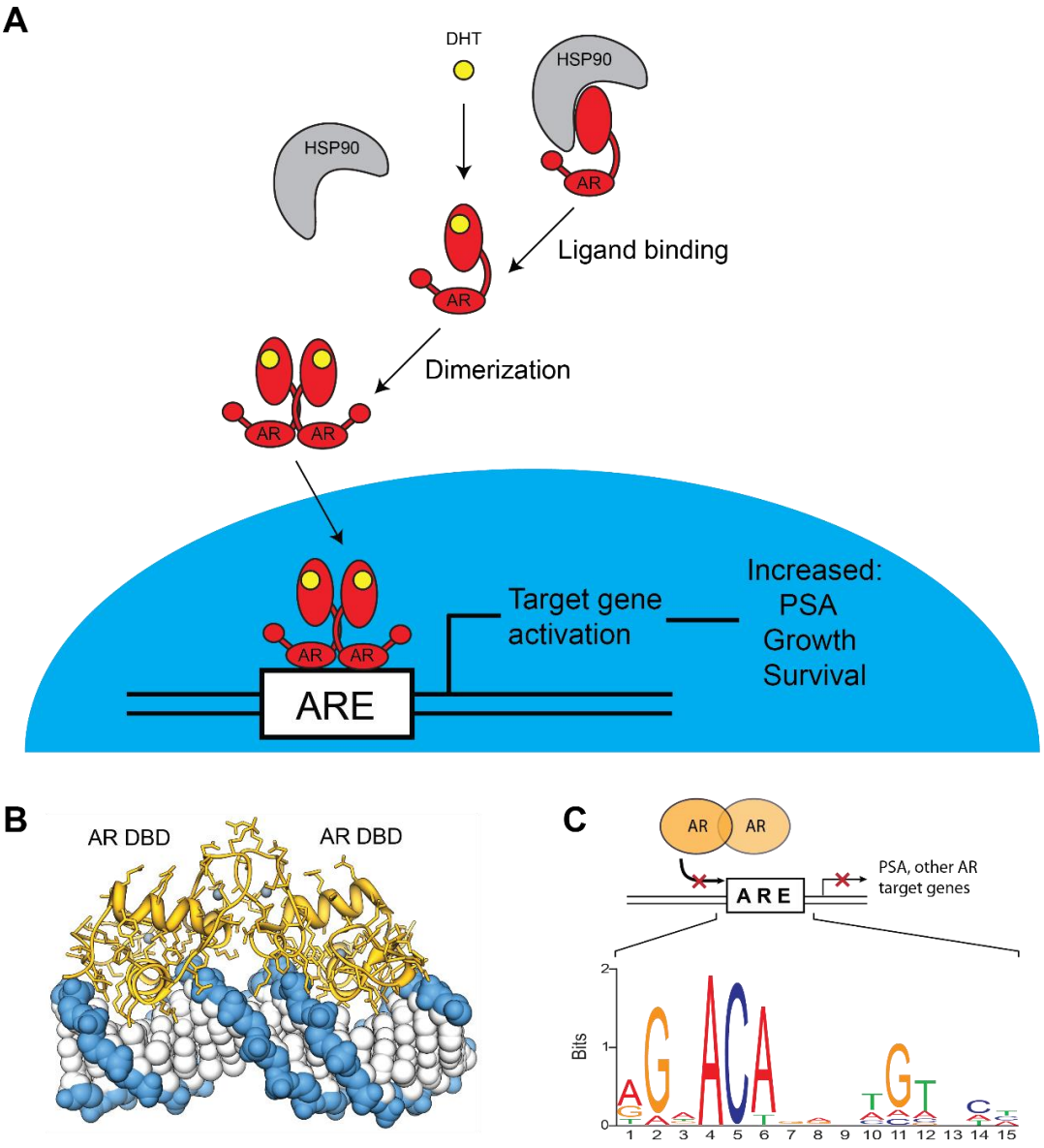

Figure 1.2 A) The androgen receptor is a nuclear hormone receptor that is sequestered in the cytosol until activation. Upon DHT binding, it translocates into the nucleus as a homodimer, binds to androgen response elements (AREs) and activates gene expression. **B)** X-ray crystal structure of the AR DNA binding domain (DBD) docked to the major groove. **C)** Consensus sequence of the ARE.

1.3 Limitations of current treatments

While initially effective, relapse is often the inevitable outcome of ADT due to genomic variability, preexisting or acquired, and presence of compensatory pathways as shown in figure 2. (16, 25, 26) One example of circumvention of ADT is the bypass of testosterone depletion by leuprolide. Leuprolide is a peptide GnRH analog that over activates the GnRH receptors in the pituitary gland and abolishes the pulsatile stimulations required for normal sex hormone production. (27) To overcome the depletion of ligand, cancer cells can develop endogenous production of DHT through the utilization of the CYP17A1 enzyme. Inhibitors of this enzyme such as abiraterone have been developed to inhibit this enzyme and can be used collectively with classical ADT to deplete DHT levels. (28)

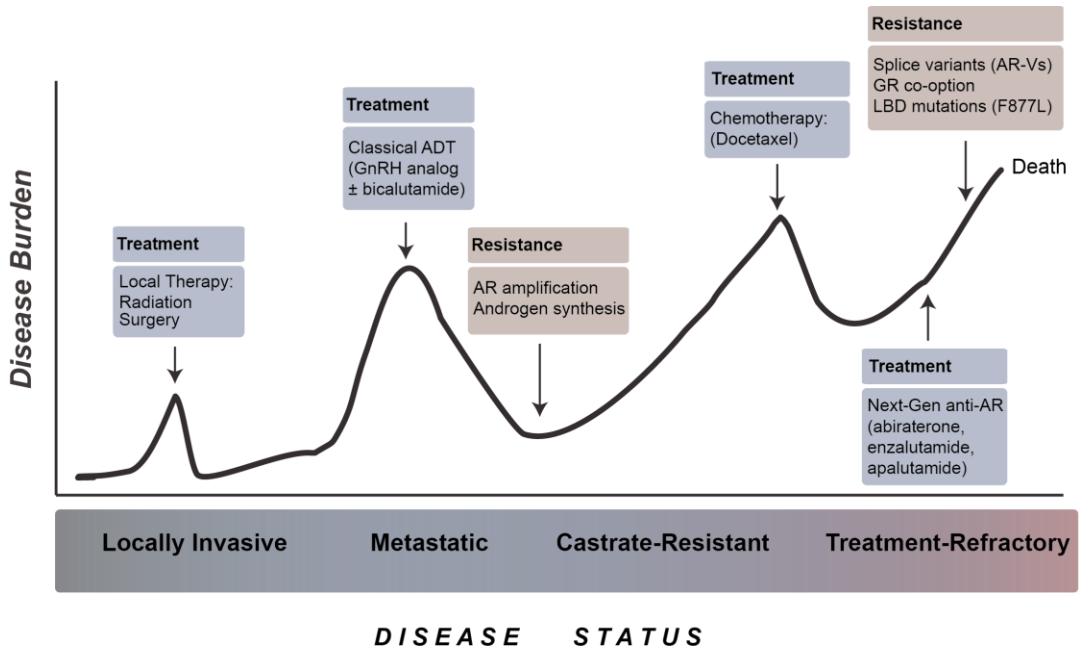

Figure 1.3 Progression of prostate cancer and treatment options at each stage. Local disease is typically curable, but metastatic disease gives rise to genetic heterogeneity and increases the likelihood of treatment evasion in later stages of cancer. Treatment-refractory disease is non-curable and treatment only serves to extend survival.

Modifications to or amplification of AR can overcome the absence of ligand. (25, 26, 29–31) Classic anti-AR drugs, including bicalutamide, enzalutamide, and apalutamide, target the ligand binding domain of AR and prevent AR-DHT interaction. However, in certain conditions bicalutamide is a weak agonist of AR, and cancer cells can often compensate by overexpressing AR and regain sufficient signaling to continue survival. (32) Enzalutamide, a second generation anti-AR drug approved in 2012, was developed to supplement lost bicalutamide activity, but recent studies indicate that the clinically relevant F877L/T878A mutations to the ligand binding domain can also result in receptor agonism. (25) Apalutamide, approved in early 2018, is an enzalutamide analog with superior pharmacokinetics; however, the same mutations confers resistance to both drugs. (24, 33, 34) Furthermore, expression of splice variants of AR lacking the ligand binding domain altogether renders most anti-AR treatment completely ineffective. (26) Interestingly, many patients have been found to possess AR splice variants prior to enzalutamide or abiraterone treatment. (35)

In addition to changes to the AR axis that renders ADT in effective, compensatory signaling mechanisms can also maintain disease viability in the absence of AR signaling. Recently, the glucocorticoid receptor, another nuclear hormone receptor with a nearly identical DNA response element was found to replace a subset of AR driven transcription in xenografts and patients treated with enzalutamide. (16) Collectively, these and other mechanism that confers resistance to treatment makes metastatic prostate cancer an incurable disease.

Due to the necessity for DNA binding for the activation of AR signaling, one potential way to attenuate transcription programs that drive disease progression is to target the DNA and block protein-DNA interactions of nuclear hormone receptors and their respective response elements through the use of pyrrole-imidazole (Py-Im) polyamides.

1.4 Py-Im polyamides as anticancer agents

Py-Im polyamides are minor groove binding molecules with modular sequence specificity and binding to targeted DNA sites with affinities comparable to DNA binding proteins. (36, 37) Upon binding to the minor groove, Py-Im polyamides cause a distortion to the local helix that is characterized by an expansion of the minor groove and a corresponding compression in the opposing major groove. (38, 39) These molecules have been shown to affect gene expression in inducible transcription systems, including those induced by AR and GR. (40, 41) Additionally, polyamides are able interfere with DNA dependent processes like RNA polymerase II elongation, DNA polymerase replication, and topoisomerase activity. (38, 42) They have also been shown to activate p53 and induce apoptosis without genotoxicity, and to have demonstrated antitumor activity in prostate cancer cell lines and xenograft models with little toxicity to the host mice. (42, 43)

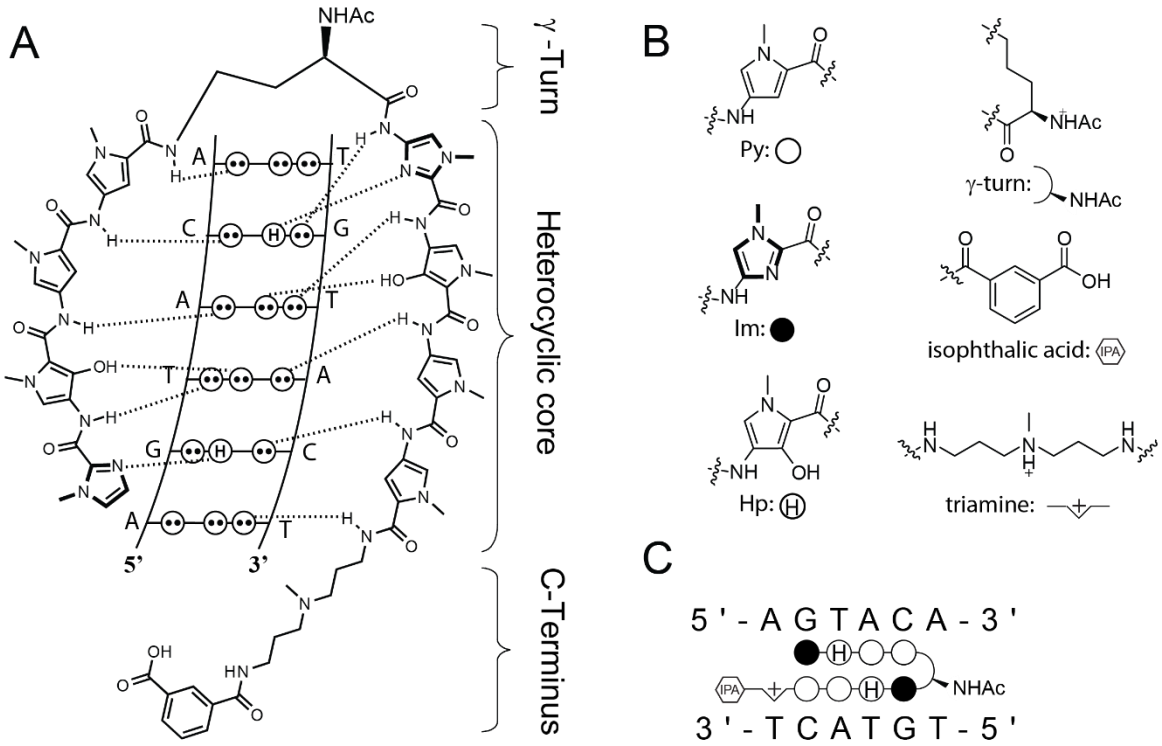

Figure 1.4 DNA recognition by hairpin Py-Im polyamides. **A)** Sequence specificity is determined by the antiparallel pairing of aromatic heterocycles in the minor groove. Py/Im pairing recognizes C/G base pairing, Im/Py pairing recognizes G/C pairing, Hp/Py pairing recognizes T/A pairing, and Py/Py pairing is degenerate for T/A or A/T. The γ-turn and the c-terminal tail are degenerate for T/A or A/T. **B)** Ball and stick representation of individual monomers. **C)** A ball and stick representation of a Py-Im polyamide bound to a target sequence.

Minor groove sequence recognition is determined by the side by side pairing of N-methylimidazole (Im) and N-methylpyrrole (Py) in the minor groove of DNA, which allows specific hydrogen bonding to DNA base pairs (Fig 1.4 A). (44–46) The sequence recognized is dependent on the arrangement of the Im and Py monomers in the hairpin structure: an Im/Py pair will recognize a G•C pair in the DNA, Py/Im will recognize C•G, and Py/Py will bind to either A•T or T•A as shown in Figure 4. (38, 44, 47) The polyamides used in this thesis target the sequence 5'-WGWWCW-3', which is found in a subset of response elements common to AR and GR.

1.5 Scope of this work

The work presented here focuses on the use of Py-Im polyamides in treatment resistant prostate cancer models. Chapter 2 describes the application of a Py-Im polyamide targeted to the 5'-WGWWCW-3' sequence found in the androgen response element to a model expressing both GR and AR splice variants in addition to high levels of AR. Chapter 3 details the characterization of a next generation, less toxic hairpin polyamide targeted to the same sequence in the enzalutamide resistant prostate cancer models VCaP and LREX`. In Chapter 4, we further evaluate the *in vivo* targeting of androgen receptor binding in an additional treatment resistant prostate cancer model. Appendix A describes structural modifications made to hairpin polyamides to increase their solubility, and Appendix B details the testing of a single hairpin in many formulations.

References

1. CDC on Infectious Diseases in the United States: 1900-99 (1999) *Popul. Dev. Rev.*, **25**, 635–640.
2. Roser M and Ritchie H (2019) Causes of Death. *Published online at OurWorldInData.org*. Retrieved from: 'https://ourworldindata.org/causes-of-death' [Online Resource]
3. Roser M and Ritchie H (2019) Cancer. *Published online at OurWorldInData.org*. Retrieved from: 'https://ourworldindata.org/cancer' [Online Resource]
4. Travis LB, Curtis RE, Fraumeni JF, Boice JD, Storm H, Andersson M, Hall P, Bergfeldt K, Holowaty E, Clarke EA, *et al.* (1997) Risk of Second Malignant Neoplasms Among Long-term Survivors of Testicular Cancer. *JNCI J. Natl. Cancer Inst.*, **89**, 1429–1439.
5. Felix CA (2001) Leukemias related to treatment with DNA topoisomerase II inhibitors. *Med. Pediatr. Oncol.*, **36**, 525–535.
6. Jensen EV, Block GE, Smith S. Kyser K and DeSombre ER (1971) Estrogen receptors and breast cancer response to adrenalectomy. *Natl. Cancer Inst. Monogr. 34 55-70 1971*.
7. Burns KA and Korach KS (2012) Estrogen receptors and human disease: an update. *Arch. Toxicol.*, **86**, 1491–1504.
8. Huggins C and Hodges CV (1941) Studies on Prostatic Cancer. I. The Effect of Castration, of Estrogen and of Androgen Injection on Serum Phosphatases in Metastatic Carcinoma of the Prostate. *Cancer Res.*, **1**, 293.
9. Siegel RL, Miller KD and Jemal A (2017) Cancer statistics, 2017. *CA. Cancer J. Clin.*, **67**, 7–30.
10. Noone A, Howlader N, Krapcho M, Miller D, Brest A, Yu M, Ruhl J, Tatalovich Z, Mariotto A, Lewis D, *et al.* eds. (2018) SEER Cancer Statistics Review, 1975-2015.
11. Negoita S, Feuer EJ, Mariotto A, Cronin KA, Petkov VI, Hussey SK, Benard V, Henley SJ, Anderson RN, Fedewa S, *et al.* (2018) Annual Report to the Nation on the Status of Cancer, part II: Recent changes in prostate cancer trends and disease characteristics: Recent Changes in Prostate Cancer Trends. *Cancer*, **124**, 2801–2814.
12. Vlahopoulos S, Zimmer WE, Jenster G, Belaguli NS, Balk SP, Brinkmann AO, Lanz RB, Zoumpourlis VC and Schwartz RJ (2005) Recruitment of the androgen receptor via serum response factor facilitates expression of a myogenic gene. *J. Biol. Chem.*, **280**, 7786–7792.
13. Sinisi AA, Pasquali D, Notaro A and Bellastella A (2003) Sexual differentiation. *J. Endocrinol. Invest.,* **26**, 23–28.
14. Feldman BJ and Feldman D (2001) The development of androgen-independent prostate cancer. *Nat. Rev. Cancer*, **1**, 34–45.
15. Shaffer PL, Jivan A, Dollins DE, Claessens F and Gewirth DT (2004) Structural basis of androgen receptor binding to selective androgen response elements. *Proc. Natl. Acad. Sci. U. S. A.,* **101**, 4758–4763.

16. Arora VK, Schenkein E, Murali R, Subudhi SK, Wongvipat J, Balbas MD, Shah N, Cai L, Efstathiou E, Logothetis C, *et al.* (2013) Glucocorticoid receptor confers resistance to antiandrogens by bypassing androgen receptor blockade. *Cell*, **155**, 1309–1322.
17. Heinlein CA and Chang C (2004) Androgen Receptor in Prostate Cancer. *Endocr. Rev.,* **25**, 276–308.
18. van der Kwast TH, Schalken J, Ruizeveld de Winter JA, van Vroonhoven CC, Mulder E, Boersma W and Trapman J (1991) Androgen receptors in endocrine-therapy-resistant human prostate cancer. *Int. J. Cancer*, **48**, 189–193.
19. Sadi MV, Walsh PC and Barrack ER (1991) Immunohistochemical study of androgen receptors in metastatic prostate cancer. Comparison of receptor content and response to hormonal therapy. *Cancer*, **67**, 3057–3064.
20. Chodak GW, Kranc DM, Puy LA, Takeda H, Johnson K and Chang C (1992) Nuclear localization of androgen receptor in heterogeneous samples of normal, hyperplastic and neoplastic human prostate. *J. Urol.,* **147**, 798–803.
21. Rove KO and Crawford ED (2013) Androgen annihilation as a new therapeutic paradigm in advanced prostate cancer: *Curr. Opin. Urol.*, **23**, 208–213.
22. Tran C, Ouk S, Clegg NJ, Chen Y, Watson PA, Arora V, Wongvipat J, Smith-Jones PM, Yoo D, Kwon A, *et al.* (2009) Development of a Second-Generation Antiandrogen for Treatment of Advanced Prostate Cancer. *Science*, **324**, 787–790.
23. Attard G, Reid AHM, A'Hern R, Parker C, Oommen NB, Folkerd E, Messiou C, Molife LR, Maier G, Thompson E, *et al.* (2009) Selective Inhibition of CYP17 With Abiraterone Acetate Is Highly Active in the Treatment of Castration-Resistant Prostate Cancer. *J. Clin. Oncol.*, **27**, 3742–3748.
24. Clegg NJ, Wongvipat J, Joseph JD, Tran C, Ouk S, Dilhas A, Chen Y, Grillot K, Bischoff ED, Cai L, *et al.* (2012) ARN-509: A Novel Antiandrogen for Prostate Cancer Treatment. *Cancer Res.*, **72**, 1494–1503.
25. Korpal M, Korn JM, Gao X, Rakiec DP, Ruddy DA, Doshi S, Yuan J, Kovats SG, Kim S, Cooke VG, *et al.* (2013) An F876L mutation in androgen receptor confers genetic and phenotypic resistance to MDV3100 (enzalutamide). *Cancer Discov.*, **3**, 1030–1043.
26. Li Y, Chan SC, Brand LJ, Hwang TH, Silverstein KAT and Dehm SM (2013) Androgen receptor splice variants mediate enzalutamide resistance in castration-resistant prostate cancer cell lines. *Cancer Res.,* **73**, 483–489.
27. Crawford ED, Eisenberger MA, McLeod DG, Spaulding JT, Benson R, Dorr FA, Blumenstein BA, Davis MA and Goodman PJ (1989) A controlled trial of leuprolide with and without flutamide in prostatic carcinoma. *N. Engl. J. Med.*, **321**, 419–424.
28. de Bono JS, Logothetis CJ, Molina A, Fizazi K, North S, Chu L, Chi KN, Jones RJ, Goodman OB, Saad F, *et al.* (2011) Abiraterone and increased survival in metastatic prostate cancer. *N. Engl. J. Med.*, **364**, 1995–2005.
29. Dehm SM. and Tindall DJ (2011) Alternatively spliced androgen receptor variants. *Endocr. Relat. Cancer*, **18**, R183-196.

30. Koivisto P, Kononen J, Palmberg C, Tammela T, Hyytinen E, Isola J, Trapman J, Cleutjens K, Noordzij A, Visakorpi T, *et al.* (1997) Androgen receptor gene amplification: a possible molecular mechanism for androgen deprivation therapy failure in prostate cancer. *Cancer Res.*, **57**, 314–319.
31. Li Y, Alsagabi M, Fan D, Bova GS, Tewfik AH and Dehm SM (2011) Intragenic rearrangement and altered RNA splicing of the androgen receptor in a cell-based model of prostate cancer progression. *Cancer Res.,* **71**, 2108–2117.
32. Chen CD, Welsbie DS, Tran C, Baek SH, Chen R, Vessella R, Rosenfeld MG and Sawyers CL (2004) Molecular determinants of resistance to antiandrogen therapy. *Nat. Med.*, **10**, 33–39.
33. Joseph JD, Lu N, Qian J, Sensintaffar J, Shao G, Brigham D, Moon M, Maneval EC, Chen I, Darimont B, *et al.* (2013) A Clinically Relevant Androgen Receptor Mutation Confers Resistance to Second-Generation Antiandrogens Enzalutamide and ARN-509. *Cancer Discov.*, **3**, 1020–1029.
34. Nelson WG and Yegnasubramanian S (2013) Resistance Emerges to Second-Generation Antiandrogens in Prostate Cancer. *Cancer Discov.*, **3**, 971–974.
35. Antonarakis ES, Lu C, Wang H, Luber B, Nakazawa M, Roeser JC, Chen Y, Mohammad TA, Chen Y, Fedor HL, *et al.* (2014) AR-V7 and Resistance to Enzalutamide and Abiraterone in Prostate Cancer. *N. Engl. J. Med.*, **371**, 1028–1038.
36. Hsu CF, Phillips JW, Trauger JW, Farkas ME, Belitsky JM, Heckel A, Olenyuk BZ, Puckett JW, Wang CCC and Dervan PB (2007) Completion of a Programmable DNA-Binding Small Molecule Library. *Tetrahedron*, **63**, 6146–6151.
37. Trauger JW, Baird EE and Dervan PB (1996) Recognition of DNA by designed ligands at subnanomolar concentrations. *Nature*, **382**, 559–561.
38. Chenoweth DM and Dervan PB (2010) Structural Basis for Cyclic Py-Im Polyamide Allosteric Inhibition of Nuclear Receptor Binding. *J. Am. Chem. Soc.*, **132**, 14521–14529.
39. Chenoweth DM and Dervan PB (2009) Allosteric modulation of DNA by small molecules. *Proc. Natl. Acad. Sci.*, **106**, 13175–13179.
40. Muzikar KA, Nickols NG and Dervan PB (2009) Repression of DNA-binding dependent glucocorticoid receptor-mediated gene expression. *Proc. Natl. Acad. Sci. U. S. A.*, **106**, 16598–16603.
41. Nickols NG and Dervan PB (2007) Suppression of androgen receptor-mediated gene expression by a sequence-specific DNA-binding polyamide. *Proc. Natl. Acad. Sci.*, **104**, 10418–10423.
42. Yang F, Nickols NG, Li BC, Marinov GK, Said JW and Dervan PB (2013) Antitumor activity of a pyrrole-imidazole polyamide. *Proc. Natl. Acad. Sci.*, **110**, 1863–1868.
43. Yang F, Nickols NG, Li BC, Szablowski JO, Hamilton SR, Meier JL, Wang C-M and Dervan PB (2013) Animal Toxicity of Hairpin Pyrrole-Imidazole Polyamides Varies with the Turn Unit. *J. Med. Chem.*, **56**, 7449–7457.

44. Kielkopf CL, White S, Szewczyk JW, Turner JM, Baird EE, Dervan PB and Rees DC (1998) A structural basis for recognition of A.T and T.A base pairs in the minor groove of B-DNA. *Science*, **282**, 111–115.
45. Foister S, Marques MA, Doss RM and Dervan PB (2003) Shape selective recognition of T.A base pairs by hairpin polyamides containing N-terminal 3-methoxy (and 3-chloro) thiophene residues. *Bioorg. Med. Chem.*, **11**, 4333–4340.
46. White S, Baird EE and Dervan PB (1997) On the pairing rules for recognition in the minor groove of DNA by pyrrole-imidazole polyamides. *Chem. Biol.*, **4**, 569–578.
47. Kielkopf CL, Baird EE, Dervan PB and Rees DC (1998) Structural basis for G.C recognition in the DNA minor groove. *Nat. Struct. Biol.*, **5**, 104–109.

Chapter 2

Tumor Repression of VCaP Xenografts by a Pyrrole-Imidazole Polyamide

The text of this chapter is taken from a manuscript coauthored with Amanda E. Hargrove[1], Thomas F. Martinez[1], Alissa A. Hare[1], John W. Phillips[1], Sudha Sud[2], Kenneth J. Pienta[2], and Peter B. Dervan[1].

1 Division of Chemistry and Chemical Engineering,
California Institute of Technology, Pasadena, CA

2 Department of Urology,
University of Michigan Medical School, Ann Arbor, MI

Hargrove AE, Martinez TF, Hare AA, Kurmis AA, Phillips JW, Sud S, Pienta KJ and Dervan PB. (2015) Tumor Repression of VCaP Xenografts by a Pyrrole-Imidazole Polyamide. PLoS ONE 10(11):e0143161. Doi:10.1371/journal.pone.0143161

Abstract

Pyrrole-imidazole (Py-Im) polyamides are high affinity DNA-binding small molecules that can inhibit protein-DNA interactions. In VCaP cells, a human prostate cancer cell line overexpressing both AR and the *TMPRSS2-ERG* gene fusion, an androgen response element (ARE)-targeted Py-Im polyamide significantly downregulates AR driven gene expression. Polyamide exposure to VCaP cells reduced proliferation without causing DNA damage. Py-Im polyamide treatment also reduced tumor growth in a VCaP mouse xenograft model. In addition to the effects on AR regulated transcription, RNA-seq analysis revealed inhibition of topoisomerase-DNA binding as a potential mechanism that contributes to the antitumor effects of polyamides in cell culture and in xenografts. These studies support the therapeutic potential of Py-Im polyamides to target multiple aspects of transcriptional regulation in prostate cancers without genotoxic stress.

2.1 Introduction

Pyrrole imidazole (Py-Im) polyamides are non-covalent, sequence specific DNA binders that can alter DNA architecture. (1, 2) Upon high affinity binding to the DNA minor groove, the molecules cause a 4 angstrom widening of the minor groove walls and a corresponding compression of the opposing major groove. (3, 4) Despite the relatively large molecular weight of Py-Im polyamides, these molecules are cell permeable and localize to the cell nucleus to affect endogenous gene expression.(5–10) Due to their modular sequence specificity, Py-Im polyamides can be synthesized to target DNA sequences of similar size to a protein-DNA interaction site and therefore used to antagonize gene expression driven by specific transcription factors. (7, 9–13) One such transcription factor that has been studied previously is the androgen receptor (AR). (9)

The AR is a dihydrotestosterone (DHT) inducible nuclear hormone receptor whose transcriptional program has been implicated in the progression of prostate cancer. (14–16) Upon ligand induction, AR will homodimerize, translocate to the nucleus and bind to conserved sequences known as the androgen response element (ARE) to regulate transcription. (17) Each monomeric unit binds to a half site of the sequence 5’-TGTTCT-3’. (18) Polyamide 1 (Fig 2.1) was designed to target the sequence 5’-WGWWCW-3’ (W = A/T), found in a subset of ARE half-sites, and has been shown to prevent AR binding at select AREs and attenuate AR signaling. (9)

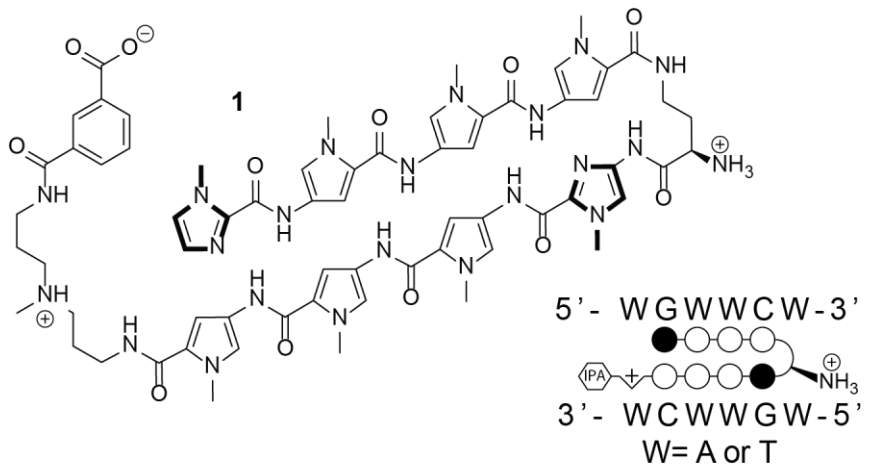

Figure 2.1 Chemical structure of a Py-Im polyamide (**1**) designed to target the DNA sequence 5'-WGWWCW-3'. A ball and stick notation used to represent binding to the target DNA sequence. Pairing of an imidazole heterocycle (black circle) with a pyrrole heterocycle (white circle) allows G▪C recognition, and the pairing of two pyrrole heterocycles recognizes A▪T or T▪A base pairs.

In addition to antagonizing AR signaling, polyamide **1** is also cytotoxic towards prostate cancer cells. (19) Experiments in mice have shown that polyamide **1** is bioavailable via several routes of administration, with a serum half-life of 5.2 hours. (20, 21) In xenograft experiments, polyamide **1** has been shown to be active towards LNCaP xenografts at doses of 1 mg/kg. (19) LNCaP, however, expresses a mutated androgen receptor, and as a result, may not be representative of the majority of human disease. (22) It would therefore be useful to evaluate the efficacy of **1** against other forms of prostate cancer.

The VCaP human prostate cancer cell line expresses wild type AR and contains the *TMPRSS2-ERG* fusion. (23) Gene fusions between the *TMPRSS2* 5'-untranslated region and the *ERG* oncogene are found in approximately half of prostate cancer cases. (24) The fusion allows the AR regulated *TMPRSS2* promoter to drive the expression of *ERG*, and

overexpression of *ERG* in patients has been linked with higher incidences of metastasis and poor disease prognosis. (25) In cell culture, *ERG* overexpression in immortalized prostate RPWE epithelial cells and in primary prostate epithelial cells (PrEC) has been shown to increase cellular invasiveness. (26) Due to these characteristics, the VCaP cell line presents an ideal model for the study of Py-Im polyamide activity towards this common subtype of prostate cancer. In this study, we evaluated the activity of the ARE targeted polyamide **1** in VCaP cells.

2.2 Materials and Methods

Synthesis and quantitation of Py-Im polyamide 1

Chemicals were obtained from Sigma Aldrich or Fisher Scientific unless otherwise noted. Synthesis was performed using previously reported procedures as indicated. (7, 27) Briefly, polyamides were synthesized by microwave-assisted solid phase synthesis on Kaiser oxime resin (Nova Biochem) (27) and then cleaved from the resin with neat 3,3'-diamino-N-methyldipropylamine. The triamine-conjugated polyamides were purified by reverse phase HPLC and subsequently modified at the C-terminus with isophthalic acid (IPA) or fluorescein-5-isothiocyanate (FITC isomer I, Invitrogen). (7) The amine substituents of the γ-aminobutyric acid (GABA) turn units of the polyamides were deprotected using neat trifluoroacetic acid. (28, 29) The final polyamide was purified by reverse phase HPLC, lyophilized to dryness, and stored at -20°C. The identity and purity of the final compounds were confirmed by matrix-assisted laser desorption/ionization time-of-flight (MALDI-TOF)

spectrometry and analytical HPLC. Chemical structures are represented in Fig 2.1 and Fig S2.1 Mass spectrometry characterization data are represented in Fig S2.2.

Py-Im polyamides were dissolved in sterile dimethylsulfoxide (DMSO, ATCC) and quantitated by UV spectroscopy in either 4:1 0.1% TFA (aqueous):acetonitrile (ε(310nm) = 69,500 M-1cm-1) or 9:1 water:DMSO (ε(310nm) = 107,100 M-1cm-1) as dictated by solubility. Polyamides were added to cell culture solutions at 1000x concentration to give 0.1% DMSO solutions.

Cell culture

The VCaP cell line was obtained from the laboratories of Dr. Kenneth J. Pienta and Dr. Arul M. Chinnaiyan at the University of Michigan Department of Pathology, where the cell line was derived. (30) VCaP cells were received at passage 19 and cultured in Dulbecco's modified eagle medium (DMEM, Gibco 10313–039) with 4 mM glutamine (Invitrogen) and fetal bovine serum (FBS, Omega Scientific) on Corning CellBind flasks. All experiments were performed below passage 30.

Cellular uptake studies

For visualization of uptake using FITC-analog polyamides, VCaP cells were plated in 35-mm optical dishes (MatTek) at 7.5×10^4 cells per dish and allowed to adhere for 48 h. Media was then changed and cells were treated with 0.1% DMSO with polyamide for 24 or 48 h. Cells were imaged at the Caltech Beckman Imaging Center using a Zeiss LSM 5 Exciter inverted

laser scanning microscope equipped with a 63x oil immersion lens as previously described. (5)

WST-1 proliferation assay

VCaP cells were plated at $2x10^4$ per well in 96-well plates coated with poly-L-lysine (BD BioCoat). After 24 h, an additional volume of medium containing vehicle or polyamide was added to each well. All medium was removed following polyamide incubation at the indicated time points and replaced with one volume of WST-1 reagent (Roche) in medium according to manufacturer protocol. After 4 h of incubation at 37°C, the absorbance was measured on a FlexStation3 plate reader (Molecule Devices). The value of A(450 nm)-A(630 nm) of treated cells was referenced to vehicle treated cells. Non-linear regression analysis (Prism software, Graphpad) was performed to determine IC_{50} values.

Gene expression analysis by quantitative RT-PCR (qPCR)

For DHT induction experiments, VCaP cells were plated in 6-well plates coated with poly-L-lysine (BD BioCoat) in charcoal-treated FBS containing media at a density of $31k/cm^2$ ($3x10^5$ cells per well). The cells were allowed to adhere for 24 h and then dosed with 0.1% DMSO with or without polyamide 1 for 72 h followed by the addition of 0.01% ethanol in PBS with or without DHT (1 nM final concentration). Cells were harvested after additional 24 h incubation. Cells treated with etoposide and camptothecin (Sigma) were co-treated with DHT (1 nM) and harvested after a 16 h incubation. For native expression experiments, VCaP cells were plated as above but using standard FBS media and harvested after 72 h of

treatment. For all experiments, the mRNA was extracted using the QIAGEN RNeasy mini kit following the standard purification protocol. Samples were submitted to DNAse treatment using the TURBO DNA-*free* Kit (Ambion), and the mRNA was reverse-transcribed by using the Transcriptor First Strand cDNA Synthesis Kit (Roche). Quantitative PCR was performed by using the FastStart Universal SYBR Green Master (Rox) (Roche) on an ABI 7300 Real Time PCR System. Gene expression was normalized against *GUSB*. Primers used are referenced in Fig S2.3.

Immunoblot of ERG protein levels

For assessment of ERG and beta-actin protein levels, $3x10^6$ VCaP cells were plated in 10 cm diameter dishes with charcoal-treated FBS containing media for 24 h before treatment with 0.1% DMSO vehicle with or without polyamide 1 for an additional 72 h. Ethanol (0.01%) in PBS with or without DHT (1 nM final concentration) was then added. After 24 h incubation, cells were lysed in TBS-Tx buffer (50 mM Tris-HCl pH 7.4, 150 mM NaCl, 1 mM EDTA, 1% Triton X100) containing fresh 1 mM phenylmethanesulfonylfluoride (PMSF) and protease inhibitors (Roche). The samples were quantified by Bradford assay, denatured by boiling in Laemmli buffer, and total protein was separated by SDS-PAGE. After transfer to the polyvinyl difluoride (PVDF) membrane (Bio-Rad) and blocking with Odyssey Blocking Buffer (LI-COR), primary antibodies were incubated overnight at 4°C. Rabbit monoclonal anti-ERG antibody (Epitomics 2805–1) and rabbit polyclonal anti-actin antibody (Sigma A2066) were used. Goat anti-rabbit near-IR conjugated secondary antibody (LI-COR) was added and the

bands were visualized on an Odyssey infrared imager (LI-COR). The experiment was conducted in duplicate and the data are representative of both trials.

Single cell electrophoresis (COMET) assay

VCaP cells ($3x10^6$ cells) were plated in 10 cm cell culture dishes and allowed to adhere for 24 h before addition of DMSO vehicle or polyamide stock in DMSO. After 72 h incubation, cells were washed with warm PBS (37°C), gently scraped, and counted. Samples were centrifuged, resuspended at $1x10^5$ cells/mL, and treated according to manufacturer protocol (Trevigen) for neutral electrophoresis. Slides were stained with SybrGreen (Trevigen) and imaged at the Caltech Beckman Imaging Center using a Zeiss LSM 5 Pascal inverted laser scanning microscope equipped with a 5x air objective lens. Overlayed fluorescence and bright field images were obtained using standard filter sets for fluorescein. Images were analyzed using Comet IV software (Perceptive Instruments Ltd) with 200–600 comets measured per sample. A random sampling of 200 comets per condition was used for two-way analysis of variance (ANOVA) analysis (Prism software, GraphPad) of three biological replicates.

Xenograft assays

Male severe combined immunodeficiency (SCID) mice (4–6 weeks old) were obtained from a breeding colony maintained by the University of Michigan. Tumors were induced by subcutaneous injection of $1x10^6$ VCaP cells (10 mice per dose group) in 200 µL of Matrigel (BD Biosciences, Inc., San Jose, CA) above the right flank. Tumor growth was monitored by

caliper measurement until the tumor size reached 100 mm^3 using the formula 0.56 x L x W^2. Groups were randomized and all mice were treated subcutaneously with control (DMSO) or with polyamide **1** as reported (3 times per week, 10 total injections). Tumor growth was followed weekly by caliper measurements. Animal husbandry and daily care and medical supervision was provided by the staff of the Unit for Laboratory Animal Medicine (ULAM) under the guidance of supervisors who are certified as Animal Technologists by the American Association for Laboratory Animal Science (AALAS) at the University of Michigan. Animals were monitored twice daily by both the research team and the veterinary staff. Health was monitored by weight (twice weekly), food and water intake, and general assessment of animal activity, panting, and fur condition. The experiments were performed in accordance with the guidelines on the care and use of animals set by the University Committee for the Use and Care of Animals (UCUCA) of the University of Michigan, and all procedures in this study were specifically approved by the UCUCA (Protocol Number 3848). In all cases, appropriate measures were taken to minimize discomfort to animals. All injections or surgical procedures were performed using sterile technique with efforts made to minimize trauma to the animals. When necessary, animals were anesthetized with a mixture of 1.75% isofluorane/air. Following injections animals were closely monitored and any that appeared moribund were immediately euthanized by administration of anesthesia, followed by inhalation of carbon dioxide until breathing ceased. Death was then ensured through cervical dislocation.

RNA-seq analysis

VCaP cells ($1x10^6$ cells) were plated in 20 cm cell culture dishes and allowed to adhere for 72 h in DMEM containing 10% FBS and 4 mM glutamine. Polyamide **1** or 0.1% DMSO vehicle were then added in fresh media and allowed to incubate for 96 h. Total RNA was collected by trizol extraction. Library building and sequencing were performed at the Caltech Millard and Muriel Jacobs Genetics and Genomics Laboratory. Sequenced reads were mapped against the human genome (hg19) with Tophat2 using Ensembl GRCh37 gene annotations. (31) Exon alignment was performed with htseq-count and differential expression was determined with DESeq2. (32, 33) Genes with padj < 0.05 and |log2(fold change)| ≥ 1 were submitted for connectivity map analysis online at http://lincscloud.org.

Topoisomerase inhibition assay

Topoisomerase inhibition kits were purchased from Topogen (Port Orange, FL). For Top2 relaxation assays, 540 ng Top2α-p170 fragment (16 units) was added to 250 ng supercoiled pHOT1 DNA in assay buffer (0.05 M Tris-HCl (pH 8), 0.15 M NaCl, 10 mM MgCl2, 0.5 mM dithiothreitol) plus 2 mM ATP with or without test compounds in a total volume of 20 µL. The DMSO concentration was standardized to 1% for all samples except the no-DMSO solvent controls. Reactions were incubated at 37°C for 30 min and then quenched with 2 µL 10% sodium dodecyl sulfate solution. Samples were then extracted with chloroform: isoamyl alcohol 24:1, mixed with 2 µL 10x glycerol loading buffer and loaded onto 1%

agarose gels in tris-acetic acid-EDTA (TAE) buffer with or without 0.5 μg/mL ethidium bromide (EtBr). Gels run without EtBr were post-stained with SYBR-Gold (Invitrogen).

For Top1 assays, 0.5 μL Top1 (5 units) was added to 250 ng supercoiled pHOT1 DNA in assay buffer (10 mM Tris-HCl (pH 7.5), 1 mM EDTA) plus 2 μL reaction buffer (10 mM Tris-HCl (pH 7.9), 1 mM EDTA, 0.15 M NaCl, 0.1% BSA, 0.1 mM spermidine, 5% glycerol) with or without test compounds in a total volume of 20 μL. The DMSO concentration was again standardized to 1% for all samples except the no-DMSO solvent controls. Reactions were incubated at 37°C for 30 min and then quenched with 4 μL stop buffer (0.125% bromphenol blue, 25% glycerol, 5% Sarkosyl). Samples were then loaded onto 1% agarose gels in tris-acetic acid-EDTA (TAE) buffer with or without 0.5 μg/mL ethidium bromide (EtBr). Gels run without EtBr were post-stained with SYBR-Gold.

2.3 Results

Nuclear uptake and cytotoxicity of Py-Im polyamide

To test the nuclear uptake potential of polyamide **1**, a FITC-labeled derivative was prepared (**1-FITC**) and incubated with VCaP cells prior to imaging by confocal microscopy (Fig S2.1). Polyamide **1-FITC** signal was observed in the nucleus and also showed significant membrane binding. The overall level of uptake in VCaP cells was found to be qualitatively less than that in LNCaP cells. (21) Next, polyamide **1** was evaluated for antiproliferation effects in VCaP cells using the WST-1 assay under conditions similar to the gene expression experiment. After a 96 h incubation with polyamide, an IC_{50} value of 6.5 ± 0.3 μM was

determined for polyamide **1** (Fig 2.2A). At 72 h, the IC_{50} value for polyamide **1** in VCaP cells was found to be over 30 μM (data not shown). For comparison, polyamide **1** has been found to have an IC_{50} of 7 ± 3 μM after 72 h incubation in LNCaP cells. (19)

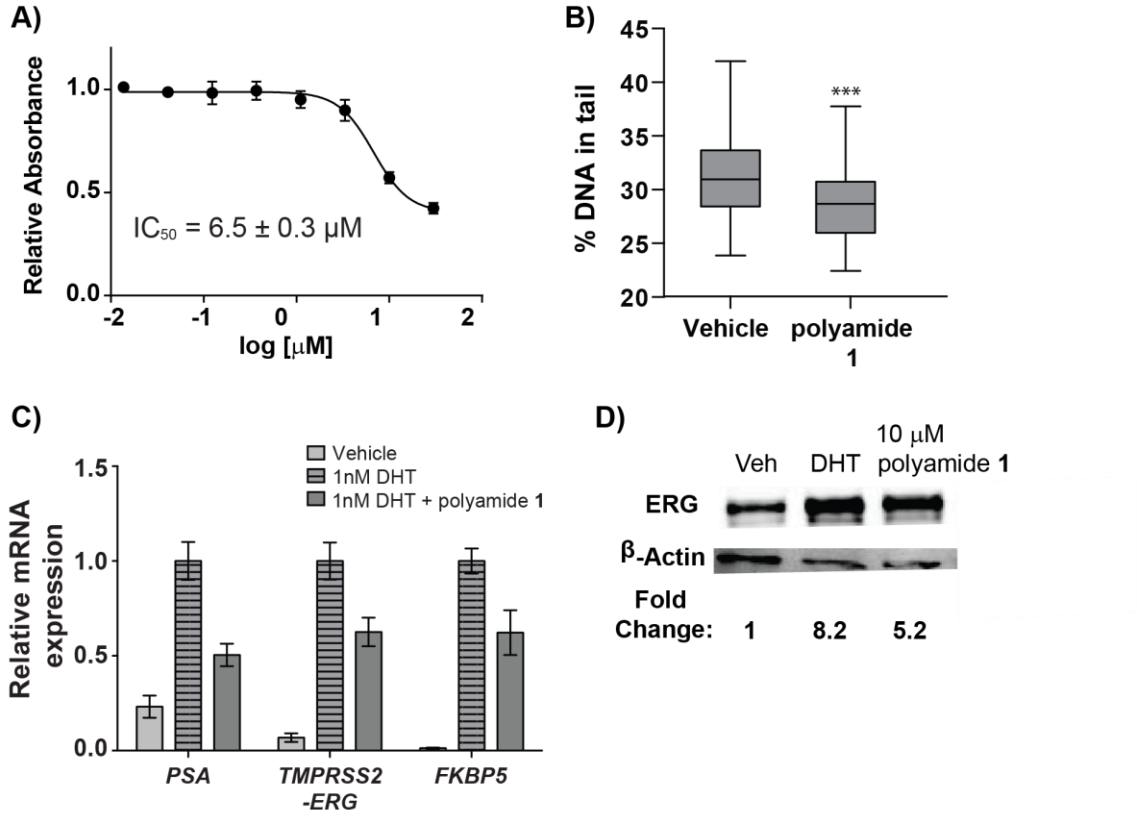

Figure 2.2 Cell culture characterization of polyamide **1** in VCaP cells. **A)** Cytotoxicity of polyamide **1** in VCaP cells after 96 h incubation. **B)** Quantification of 200 neutral comets from VCaP cells treated with 0.1% DMSO (vehicle) or 10 μM polyamide **1** for 72 h. Statistical significance was determined using two-way ANOVA analysis (Prism) where *** = $p < 0.001$ relative to vehicle. Boxes are bounded by the upper and lower quartile while whiskers represent the 1st and 99th percentile. **C)** Effect of 10 μM polyamide **1** on select androgen receptor regulated genes in VCaP cells under 1 nM DHT induction. **D)** Change in ERG protein caused by 0.1% DMSO vehicle, 1 nM DHT alone, and cotreatment of 10 μM **1** with 1 nM DHT.

Reduction of DNA damage in VCaP cells upon treatment with Py-Im polyamide

The effect of polyamide **1** on the high level of extant DNA damage in VCaP cells was also investigated. After incubation with polyamide, VCaP cells were submitted to the neutral Comet assay, which allows visualization of double-strand breaks through single cell electrophoresis (Fig 2.2B). The percentage of DNA in the "tail" of the comets was then compared using two-way ANOVA statistical analysis (Fig S2.4). A significant reduction in DNA damage ($p < 0.001$) was observed with polyamide **1** over the vehicle control.

ARE-targeted Py-Im polyamide downregulates AR-driven *TMPRSS2-ERG* expression

Next the effect of polyamide **1** on AR signaling in ERG-positive cells was examined. Dosage concentrations were chosen based on previous reports of polyamide gene expression effects in LNCaP. (28, 34) In VCaP cells, polyamide **1** was found to reduce the DHT-induced expression of the *TMPRSS2-ERG* fusion as well as other AR target genes, including *PSA* and *FKBP5* (Fig 2.2C). Corresponding decreased expression of ERG protein was confirmed by Western blot (Fig 2.2D). In the non-induced state, polyamide **1** was also found to reduce expression of several ERG influenced genes, including *PLAT* and *MYC* (Fig S2.5).

Diminished growth in VCaP xenografts upon polyamide treatment

We next moved from cell culture studies to investigations of polyamide **1** in a VCaP mouse xenograft tumor model. Xenograft experiments were conducted in male SCID mice bearing subcutaneous VCaP cell xenografts. Treatments were started after tumor sizes in each group of mice reached ~100 mm^3 and were administered three times per week through

subcutaneous injection in DMSO vehicle for three weeks for a total of 10 injections. Dose-dependent retardation of tumor growth was observed in mice treated with polyamide **1** (Fig 2.3). After 5 weeks of monitoring, tumors treated with vehicle grew to approximately 6-fold the initial volume of that group while tumors treated with polyamide **1** at 5.0 mg/kg grew to approximately 1.6-fold the initial volume of that cohort.

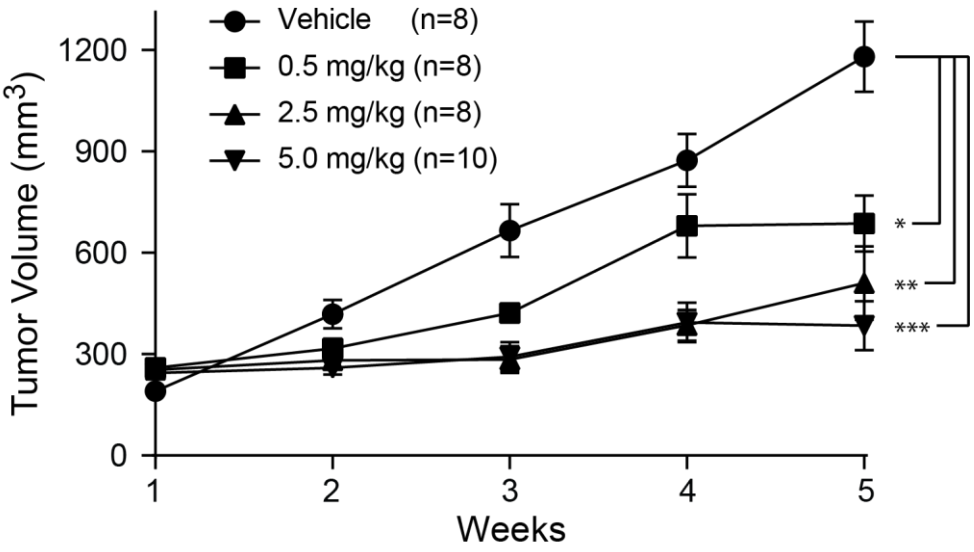

Figure 2.3 VCaP xenografts treated with polyamide **1** three times per week showed a dose dependent reduction in tumor growth. Tumor volume was determined by caliper measurements. Errors are SEM. *=<p<0.01, **=p<0.0005, *** = p<0.0001.

Genome wide expression analysis

RNA-seq analysis was performed after 96 hours of polyamide treatment in order to assess gene expression changes after prolonged exposure and to identify potential mechanisms of polyamide induced toxicity. Differential expression analysis using DESeq2 showed that of the genes with padj < 0.05 and |log2(fold change)| ≥ 1, 342 were upregulated and 399 were downregulated upon polyamide treatment (Fig 2.4A). Connectivity map analysis of these genes returned several compounds known to be topoisomerase inhibitors (Fig 2.4B), suggesting that the polyamide may also be interfering with topoisomerase activity. Analysis of a previously published genome wide data set from LNCaP cells treated with polyamide 1 shows similar results (Fig S2.6)[9].

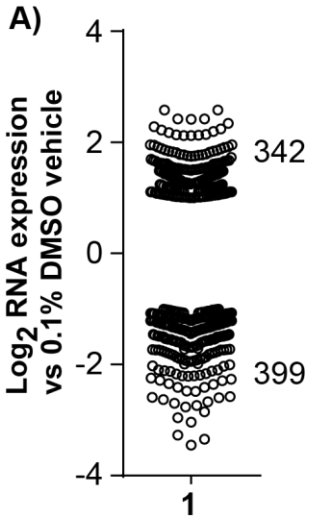

B)

	Compounds	Score
1	importazole	99.908
2	**SN-38**	99.781
3	pitavastatin	99.667
4	**amsacrine**	99.664
5	pyrvinium-pamoate	99.63
6	mitomycin-c	99.572
7	CD-437	99.303
8	**teniposide**	99.114
9	**camptothecin**	98.88
10	NSC-3852	98.559
11	**irinotecan**	98.552

Figure 2.4 Genome wide expression analysis of VCaP cells treated with 10 μM polyamide **1** for 96 h. **A)** Scatter plot of gene expression changes in VCaP cells after polyamide treatment. **B)** Connectivity map analysis of perturbagens that correlate with gene expression changes induced by polyamide **1**.

Inhibition of topoisomerases 1 and 2

Topoisomerase inhibitors have been shown to attenuate AR signaling in multiple cell lines. (35, 36) Similar results are also seen in VCaP cells, where treatment with etoposide and camptothecin is able to reduce DHT induced expression of select AR regulated genes (Fig S2.7). Based on the Connectivity map results, we examined the inhibitory effects of polyamide **1** against topoisomerase 1 and 2 *in vitro*. Topoisomerase 1 (Topo1) functions by relieving DNA supercoils generated by transcription and replication and is a therapeutic target in cancer. (37) To determine if polyamide **1** inhibits Topo1 mediated DNA cleavage, we titrated polyamide **1** with supercoiled pHOT1 plasmid and measured conversion to open circular plasmid or relaxation upon addition of purified Topo1. A reduction in DNA relaxation indicates polyamide **1** was able to attenuate Topo1 mediated cleavage of DNA (Fig 2.5A). To differentiate between open circular and relaxed DNA, samples were also run on an EtBr gel. Unlike camptothecin (CMT), which traps the Topo1 cleavage complex and generates nicked open circular DNA, treatment with polyamide **1** did not prevent DNA re-ligation. Topoisomerase II cleaves double stranded DNA in an ATP dependent manner and is essential for strand separation of tangled daughter chromosomes during replication. Like Topo1, Topo2 is targeted in cancer therapy. (38) Similar to results seen for Topo1, polyamide **1** was able to inhibit Topo2 cleavage of supercoiled pHOT1 plasmid in a concentration dependent manner (Fig 2.5B). Furthermore, samples were run with EtBr to allow unambiguous identification of linearized DNA, which allowed the identification of

Topo2 cleavage complex (Topo2cc) formation (Fig 2.5B, lanes 5 and 6). The lack of Topo2cc formation in polyamide **1** treated samples as compared to linearized DNA and etoposide-treated samples is consistent with disruption of Topo2 binding.

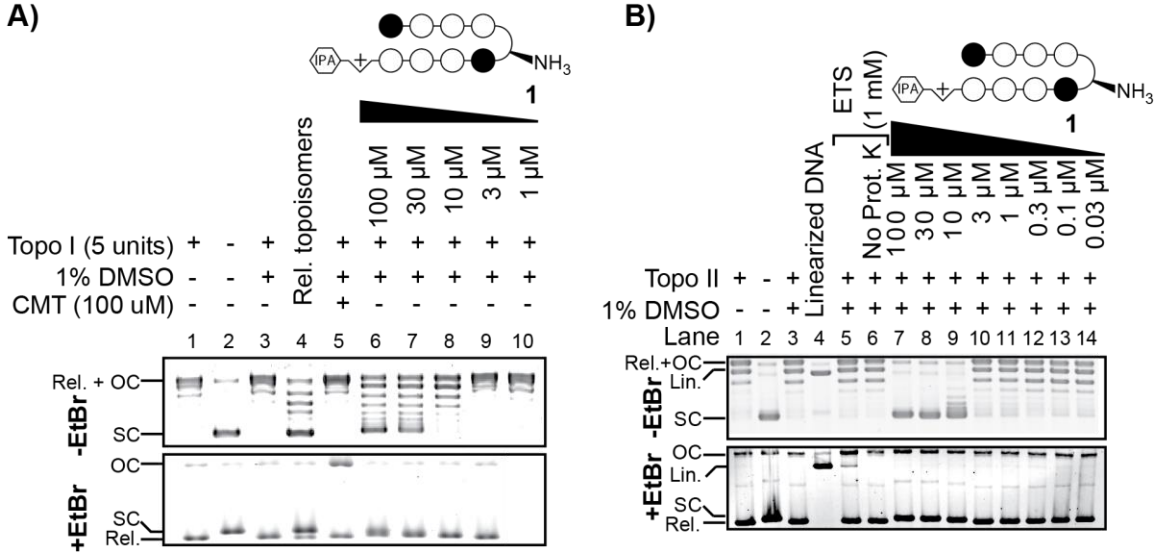

Figure 2.5 Inhibition of topoisomerase I and II by polyamide **1** *in vitro*. **A)** Supercoiled DNA relaxation assay for topoisomerase 1 treated with increasing concentrations of polyamide **1**. Camptothecin (CMT) is used as a positive control **B)** Supercoiled DNA relaxation assay for topoisomerase IIα–p170 fragment. Etoposide (ETS) is used as a control. Rel, relaxed; OC, open circular; SC, supercoiled; Lin, linear; Rel. topoisomers, relaxed topoisomers; Prot. K, proteinase K.

2.4 Discussion

In this study, we evaluated the activity of an ARE targeted polyamide in VCaP human prostate cancer cells. Polyamide **1** has been previously shown to exhibit antitumor activity in cell culture and in xenografts of the androgen sensitive LNCaP cell line (19), but there are several important genotypic differences between these two cell lines. First, VCaP cells possess an amplified AR region, leading to higher levels of AR protein than LNCaP cells. (30, 39, 40) Additionally, VCaP cells belong to a subtype of prostate cancer that possesses the

TMPRSS2:ERG fusion, resulting in the AR driven expression of *ERG*. (23) *ERG*, an oncogenic transcription factor, has been reported to increase double stranded DNA break formation in PrEC cells, while knockdown of *ERG* by siRNA in VCaP cells have been shown to decrease DNA breaks. (41) Studies have also shown that *ERG* overexpression increases cancer invasiveness and has been correlated to increased metastasis in the clinic. (25, 26)

In VCaP cell culture experiments, polyamide **1** exhibited antiproliferative activity and attenuated the DHT induced expression of select AR driven genes including *TMPRSS2:ERG*. Furthermore, in this cell line with high genomic instability due to *ERG* overexpression, treatment with polyamide **1** repressed the high level of DNA fragmentation found in the basal state, which may be attributed to diminished ERG protein. *In vivo*, VCaP xenografts treated with polyamide **1** exhibited reduced growth in a dosage dependent manner, demonstrating its potential as an anticancer therapeutic.

To further examine the mechanism of action for polyamide **1**, we conducted gene expression analysis of VCaP cells after exposure to polyamide **1** in the same time frame as the cytotoxic experiment. Connectivity map analysis of gene expression signatures from treated VCaP cells indicated overlap with expression profiles of several topoisomerase inhibitors. *In vitro* assays for inhibition of both Topo1 and Topo2 confirmed that polyamide **1** is able to attenuate enzymatic activity of both enzymes. Similar results have been reported for other minor groove binders. (42–47) Furthermore, the lack of topoisomerase 2 cleavage complex formation in the inhibition assays suggests polyamide **1** functions by

preventing protein-DNA interactions. This mechanism is in contrast to most drugs that target topoisomerases, which poison the enzymes. Drugs such as etoposide, doxorubicin, and camptothecin work by causing covalent adducts, which results in genotoxicity. (48)

In addition to inhibition of Topo1 and Topo2, polyamide **1** has been reported to antagonize AR signaling, block RNA polymerase II elongation, and affect DNA replication by impeding helicase processivity. (19, 21, 49) These effects may be related, as inhibition of Topo1 has been shown to lead to RNA polymerase II and DNA polymerase stalling (50), and treatment of prostate cancer cells with topoisomerase inhibitors has been shown to attenuate AR signaling. (35, 36, 51, 52) Taken together, these data suggest that by virtue of targeting DNA and DNA:protein interactions, polyamide **1** may exhibit antiproliferative effects on cancer cells through polypharmacological mechanisms without inducing genotoxic stress.

References

1. Kielkopf CL, Baird EE, Dervan PB and Rees DC. (1998) Structural basis for G.C recognition in the DNA minor groove. *Nat. Struct. Biol.*, **5**, 104–109.
2. Kielkopf CL, White S, Szewczyk JW, Turner JM, Baird EE, Dervan PB and Rees,D.C. (1998) A structural basis for recognition of A.T and T.A base pairs in the minor groove of B-DNA. *Science*, **282**, 111–115.
3. Chenoweth DM, and Dervan PB (2009) Allosteric modulation of DNA by small molecules. *Proc. Natl. Acad. Sci. U. S. A.*, **106**, 13175–13179.
4. Chenoweth DM, and Dervan PB (2010) Structural basis for cyclic Py-Im polyamide allosteric inhibition of nuclear receptor binding. *J. Am. Chem. Soc.*, **132**, 14521–14529.
5. Best TP, Edelson BS, Nickols NG, and Dervan PB (2003) Nuclear localization of pyrrole-imidazole polyamide-fluorescein conjugates in cell culture. *Proc. Natl. Acad. Sci. U. S. A.*, **100**, 12063–12068.
6. Edelson BS, Best TP, Olenyuk B, Nickols NG, Doss RM, Foister S, Heckel A and Dervan PB (2004) Influence of structural variation on nuclear localization of DNA-binding polyamide-fluorophore conjugates. *Nucleic Acids Res.*, **32**, 2802–2818.
7. Nickols NG, Jacobs CS, Farkas ME and Dervan PB (2007) Improved nuclear localization of DNA-binding polyamides. *Nucleic Acids Res.*, **35**, 363–370.
8. Muzikar KA, Nickols NG, and Dervan PB (2009) Repression of DNA-binding dependent glucocorticoid receptor-mediated gene expression. *Proc. Natl. Acad. Sci. U. S. A.*, **106**, 16598–16603.
9. Nickols NG, and Dervan PB (2007) Suppression of androgen receptor-mediated gene expression by a sequence-specific. *Proc. Natl. Acad. Sci. U. S. A.*, **104**, 10418–10423.
10. Nickols NG, Jacobs CS, Farkas ME and Dervan PB (2007) Modulating hypoxia-inducible transcription by disrupting the HIF-1-DNA interface. *ACS Chem. Biol.*, **2**, 561–571.
11. Olenyuk BZ, Zhang G-J, Klco JM, Nickols NG, Kaelin WGJ and Dervan PB (2004) Inhibition of vascular endothelial growth factor with a sequence-specific hypoxia response element antagonist. *Proc. Natl. Acad. Sci. U. S. A.*, **101**, 16768–16773.
12. Muzikar KA, Meier JL, Gubler DA, Raskatov JA and Dervan PB (2011) Expanding the repertoire of natural product-inspired ring pairs for molecular recognition of DNA. *Org. Lett.*, **13**, 5612–5615.
13. Raskatov JA, Meier JL, Puckett JW, Yang F, Ramakrishnan P and Dervan PB (2012) Modulation of NF-kappaB-dependent gene transcription using programmable DNA minor groove binders. *Proc. Natl. Acad. Sci. U. S. A.*, **109**, 1023–1028.
14. Chen CD, Welsbie DS, Tran C, Baek SH, Chen R, Vessella R, Rosenfeld MG and Sawyers CL (2004) Molecular determinants of resistance to antiandrogen therapy. *Nat. Med.*, **10**, 33–39.
15. Tsai MJ and O'Malley BW (1994) Molecular mechanisms of action of steroid/thyroid receptor superfamily members. *Annu. Rev. Biochem.*, **63**, 451–486.

16. Taylor BS, Schultz N, Hieronymus H, Gopalan A, Xiao Y, Carver BS, Arora VK, Kaushik P, Cerami E, Reva B, *et al.* (2010) Integrative genomic profiling of human prostate cancer. *Cancer Cell*, **18**, 11–22.
17. Tyagi RK, Lavrovsky Y, Ahn SC, Song CS, Chatterjee B and Roy AK (2000) Dynamics of intracellular movement and nucleocytoplasmic recycling of the ligand-activated androgen receptor in living cells. *Mol. Endocrinol. Baltim. Md*, **14**, 1162–1174.
18. Roche PJ, Hoare SA and Parker MG (1992) A consensus DNA-binding site for the androgen receptor. *Mol. Endocrinol. Baltim. Md*, **6**, 2229–2235.
19. Yang F, Nickols NG, Li BC, Marinov GK, Said JW and Dervan PB (2013) Antitumor activity of a pyrrole-imidazole polyamide. *Proc. Natl. Acad. Sci. U. S. A.*, **110**, 1863–1868.
20. Synold TW, Xi B, Wu J, Yen Y, Li BC, Yang F, Phillips JW, Nickols NG, and Dervan PB (2012) Single-dose pharmacokinetic and toxicity analysis of pyrrole-imidazole polyamides in mice. *Cancer Chemother. Pharmacol.*, **70**, 617–625.
21. Yang F, Nickols NG, Li BC, Szablowski JO, Hamilton SR, Meier JL, Wang C-M and Dervan PB (2013) Animal toxicity of hairpin pyrrole-imidazole polyamides varies with the turn unit. *J. Med. Chem.*, **56**, 7449–7457.
22. Perlmutter MA and Lepor H (2007) Androgen deprivation therapy in the treatment of advanced prostate cancer. *Rev. Urol.*, **9 Suppl 1**, S3-8.
23. Tomlins SA, Rhodes DR, Perner S, Dhanasekaran SM, Mehra R, Sun X-W, Varambally S, Cao X, Tchinda J, Kuefer R, *et al.* (2005) Recurrent fusion of TMPRSS2 and ETS transcription factor genes in prostate cancer. *Science*, **310**, 644–648.
24. Perner S, Demichelis F, Beroukhim R, Schmidt FH, Mosquera J-M, Setlur S, Tchinda J, Tomlins SA, Hofer MD, Pienta KG, *et al.* (2006) TMPRSS2:ERG fusion-associated deletions provide insight into the heterogeneity of prostate cancer. *Cancer Res.*, **66**, 8337–8341.
25. Demichelis F, Fall K, Perner S, Andren O, Schmidt F, Setlur SR, Hoshida Y, Mosquera J-M, Pawitan Y, Lee C, *et al.* (2007) TMPRSS2:ERG gene fusion associated with lethal prostate cancer in a watchful waiting cohort. *Oncogene*, **26**, 4596–4599.
26. Tomlins SA, Laxman B, Varambally S, Cao X, Yu J, Helgeson BE, Cao Q, Prensner JR, Rubin MA, Shah RB, *et al.* (2008) Role of the TMPRSS2-ERG gene fusion in prostate cancer. *Neoplasia N. Y. N*, **10**, 177–188.
27. Puckett JW, Green JT and Dervan PB (2012) Microwave assisted synthesis of Py-Im polyamides. *Org. Lett.*, **14**, 2774–2777.
28. Dose C, Farkas ME, Chenoweth DM, and Dervan PB (2008) Next generation hairpin polyamides with (R)-3,4-diaminobutyric acid turn unit. *J. Am. Chem. Soc.*, **130**, 6859–6866.
29. Li BC, Montgomery DC, Puckett JW and Dervan PB (2013) Synthesis of cyclic Py-Im polyamide libraries. *J. Org. Chem.*, **78**, 124–133.

30. Korenchuk S, Lehr JE, Mclean L, Lee YG, Whitney S, Vessella R, Lin DL and Pienta KJ (2001) VCaP, a cell-based model system of human prostate cancer. *Vivo Athens Greece*, **15**, 163–168.
31. Trapnell C, Roberts A, Goff L, Pertea G, Kim D, Kelley DR, Pimentel H, Salzberg SL, Rinn JL and Pachter,L (2012) Differential gene and transcript expression analysis of RNA-seq experiments with TopHat and Cufflinks. *Nat. Protoc.*, **7**, 562–578.
32. Anders S, Pyl PT and Huber W (2015) HTSeq--a Python framework to work with high-throughput sequencing data. *Bioinforma. Oxf. Engl.*, **31**, 166–169.
33. Love MI, Huber W and Anders S (2014) Moderated estimation of fold change and dispersion for RNA-seq data with DESeq2. *Genome Biol.*, **15**, 550.
34. Chenoweth DM, Harki DA, Phillips JW, Dose C and Dervan PB (2009) Cyclic pyrrole-imidazole polyamides targeted to the androgen response element. *J. Am. Chem. Soc.*, **131**, 7182–7188.
35. Haffner MC, Aryee MJ, Toubaji A, Esopi DM, Albadine R, Gurel B, Isaacs WB, Bova GS, Liu W, Xu J, *et al.* (2010) Androgen-induced TOP2B-mediated double-strand breaks and prostate cancer gene rearrangements. *Nat. Genet.*, **42**, 668–675.
36. Li H, Xie N, Gleave ME and Dong X (2015) Catalytic inhibitors of DNA topoisomerase II suppress the androgen receptor signaling and prostate cancer progression. *Oncotarget*, **6**, 20474–20484.
37. Pommier Y (2006) Topoisomerase I inhibitors: camptothecins and beyond. *Nat. Rev. Cancer*, **6**, 789–802.
38. Nitiss JL (2009) Targeting DNA topoisomerase II in cancer chemotherapy. *Nat. Rev. Cancer*, **9**, 338–350.
39. Makkonen H, Kauhanen M, Jaaskelainen T and Palvimo JJ (2011) Androgen receptor amplification is reflected in the transcriptional responses of Vertebral-Cancer of the Prostate cells. *Mol. Cell. Endocrinol.,* **331**, 57–65.
40. Liu W, Xie CC, Zhu Y, Li T, Sun J, Cheng Y, Ewing CM, Dalrymple S, Turner AR, Sun J, *et al.* (2008) Homozygous deletions and recurrent amplifications implicate new genes involved in prostate cancer. *Neoplasia N. Y. N*, **10**, 897–907.
41. Brenner JC, Ateeq B, Li Y, Yocum AK, Cao Q, Asangani IA, Patel S, Wang X, Liang H, Yu J, *et al.* (2011) Mechanistic rationale for inhibition of poly(ADP-ribose) polymerase in ETS gene fusion-positive prostate cancer. *Cancer Cell*, **19**, 664–678.
42. Kim S-O, Sakchaisri K, Thimmegowda NR, Soung NK, Jang J-H, Kim YS, Lee KS, Kwon YT, Asami Y, Ahn JS, *et al.* (2013) STK295900, a dual inhibitor of topoisomerase 1 and 2, induces G(2) arrest in the absence of DNA damage. *PloS One*, **8**, e53908.
43. Beerman TA, McHugh MM, Sigmund R, Lown JW, Rao KE and Bathini Y (1992) Effects of analogs of the DNA minor groove binder Hoechst 33258 on topoisomerase II and I mediated activities. *Biochim. Biophys. Acta*, **1131**, 53–61.
44. Beerman TA, Woynarowski JM, Sigmund RD, Gawron LS, Rao KE and Lown JW (1991) Netropsin and bis-netropsin analogs as inhibitors of the catalytic activity of mammalian

DNA topoisomerase II and topoisomerase cleavable complexes. *Biochim. Biophys. Acta*, **1090**, 52–60.

45. McHugh MM, Sigmund RD and Beerman TA (1990) Effects of minor groove binding drugs on camptothecin-induced DNA lesions in L1210 nuclei. *Biochem. Pharmacol.*, **39**, 707–714.
46. McHugh MM, Woynarowski JM, Sigmund RD and Beerman TA (1989) Effect of minor groove binding drugs on mammalian topoisomerase I activity. *Biochem. Pharmacol.*, **38**, 2323–2328.
47. Woynarowski JM, Sigmund RD and Beerman TA (1989) DNA minor groove binding agents interfere with topoisomerase II mediated lesions induced by epipodophyllotoxin derivative VM-26 and acridine derivative m-AMSA in nuclei from L1210 cells. *Biochemistry*, **28**, 3850–3855.
48. Pommier Y, Leo E, Zhang H and Marchand C (2010) DNA topoisomerases and their poisoning by anticancer and antibacterial drugs. *Chem. Biol.*, **17**, 421–433.
49. Martinez TF, Phillips JW, Karanja KK, Polaczek P, Wang C-M, Li BC, Campbell JL and Dervan PB (2014) Replication stress by Py-Im polyamides induces a non-canonical ATR-dependent checkpoint response. *Nucleic Acids Res.*, **42**, 11546–11559.
50. Tuduri S, Crabbe L, Conti C, Tourriere H, Holtgreve-Grez H, Jauch A, Pantesco V, De Vos J, Thomas A, Theillet C, *et al.* (2009) Topoisomerase I suppresses genomic instability by preventing interference between replication and transcription. *Nat. Cell Biol.*, **11**, 1315–1324.
51. Liu S and Yamauchi H (2010) Etoposide induces growth arrest and disrupts androgen receptor signaling in prostate cancer cells. *Oncol. Rep.*, **23**, 165–170.
52. Liu S, Yuan Y, Okumura Y, Shinkai N and Yamauchi H (2010) Camptothecin disrupts androgen receptor signaling and suppresses prostate cancer cell growth. *Biochem. Biophys. Res. Commun.*, **394**, 297–302.

2.5 Supplemental material

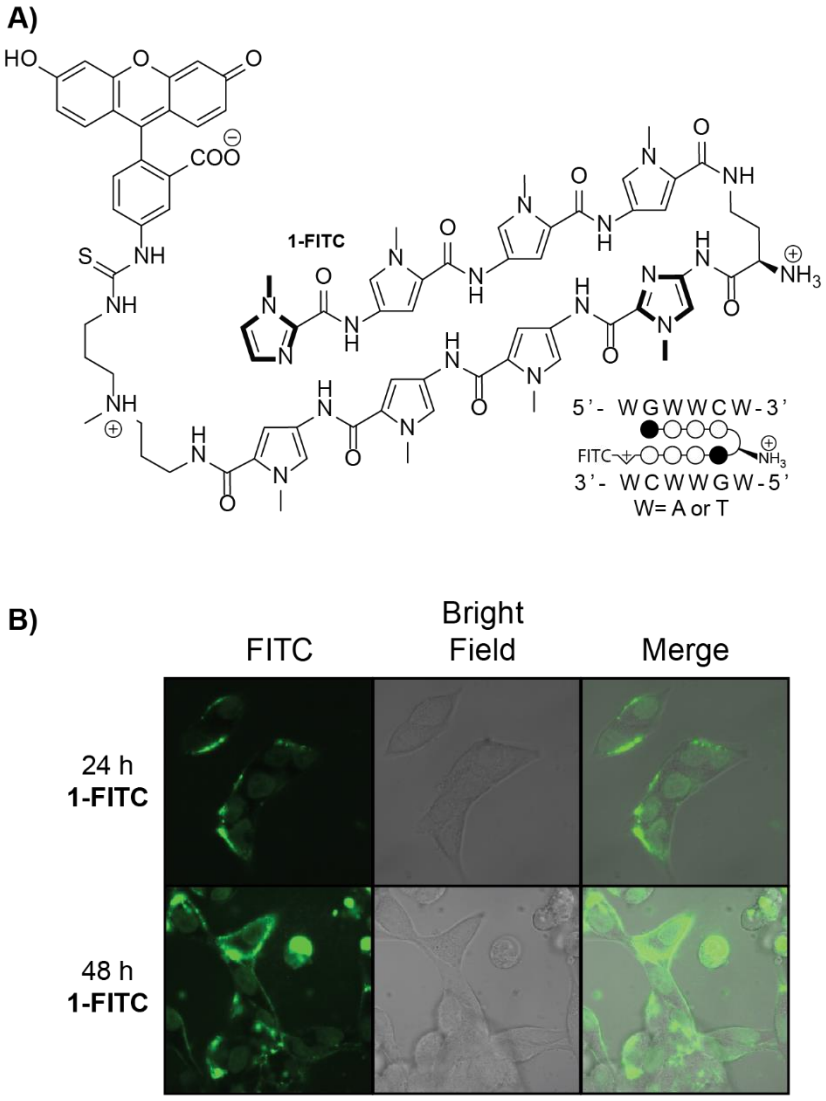

Figure S2.1 A) Chemical structure of **1-FITC**. **B)** Nuclear localization of **1-FITC** in VCaP cells after 24 h and 48 h incubation.

	Technique	Formula	Calculated Mass	Measured Mass (m/z)
1	MALDI-TOF	$C_{65}H_{77}N_{22}O_{12}$	$[M+H]^+$ 1357.6	1357.7
1-FITC	LCMS	$C_{78}H_{85}N_{23}O_{14}S$	$[M+H]^+$ 1599.6	533 (z = 3)
	MALDI-TOF	$C_{57}H_{73}N_{22}O_9$	$[M+H\text{-FITC}]^+$ 1209.6	1209.5

Figure S2.2 Mass spectrometry data for Py-Im polyamides used. All polyamides were characterized using high resolution MALDI-TOF. Because this method leads to cleavage of fluorescein, FITC functionalized polyamides were also characterized by liquid chromatography coupled mass spectrometry (LCMS) equipped with a low resolution ionization spectrometer.

qPCR (mRNA)	Sequence	Reference
AR-f	CAGTGGATGGGCTGAAAAAT	Yu JD, et al. Cancer Cell. 2010;17:443-54.
AR-r	GGAGCTTGGTGAGCTGGTAG	
cMYC-f	AGCGGGCGGGCACTTTGC	*
cMYC-r	GCGGGAGGCTGCTGGTTTTC	
ERG_ALL-f	CGCAGAGTTATCGTGCCAGCAGAT	Tomlins SA, et al. Science. 2005;310:644-8.
ERG_ALL-r	CCATATTCTTTCACCGCCCACTCC	
EZH2-f	TGCAGTTGCTTCAGTACCCATAAT	Yu JD, et al. Cancer Cell. 2010;17:443-54.
EZH2-r	ATCCCCGTGTACTTTCCCATCATAAT	
FKBP5-F	CGG AAA GGA GAG GGA TAT TCA	Meier JL, et al. Nucleic Acids Res. 2011;40:2345-56.
FKBP5-R	CCA CAT CTC TGC AGT CAA ACA	
GUSB-f	CTCATT TGGAATTTTGCCGATT	Jacobs CS, et al. J Med Chem. 2009;52:7380-8.
GUSB-r	CCGAGTGAAGATCCCCTTTTTA	
KLK3-f	TCTGCGGCGGTGTTCTG	Jacobs CS, et al. J Med Chem. 2009;52:7380-8.
KLK3-r	GCCGACCCAGCAAGATCA	
PLAT-f	GCAGAGCCCTCTCTTCATTG	*
PLAT-r	CTGGAGAGAAAACCTCTGCG	
PLAU-f	CCAGCTCACAATTCCAGTCA	*
PLAU-r	TGACCCACAGTGGAAAACAG	
SLC45A3-f	TCGTGGGCGAGGGGCTGTA	Lin C, et al. Cell. 2009;139:1069-83.
SLC45A3-r	CATCCGAACGCCTTCATCATAGTGT	
TMPRSS2-ERG-f	TAGGCGCGAGCTAAGCAGGAG	Tomlins SA, et al. Science. 2005;310:644-8.
TMPRSS2-ERG-r	GTAGGCACACTCAAACAACGACTGG	

Figure S2.3 Primer sequences for qPCR analysis. Sequences for mRNA analysis without a listed reference (*) were designed using qPrimerDepot (primerdepot.nci.nih.gov), and the single amplification products verified by agarose gel electrophoresis against the 1.1 kB NEB ladder.

Compare column means (main column effect)								
Number of families	1							
Number of comparisons per family	10							
Alpha	0.05							
Tukey's multiple comparisons test	**Mean Diff.**	**95% CI of diff.**	**Significant?**	**Summary**				
Vehicle vs. AR-1	2.452	1.254 to 3.650	Yes	****				
Test details	**Mean 1**	**Mean 2**	**Mean Diff.**	**SE of diff.**	**N1**	**N2**	**q**	**DF**
Vehicle vs. AR-1	31.16	28.7	2.452	0.4388	600	600	7.903	2000

Figure S2.4 Report of two-way ANOVA analysis from Prism software (GraphPad) for Comet assays in VCaP cells.

A)

Treatment	Conc.	DHT	AR	SLC45A3	EZH2	MYC	PLAT
Vehicle	-	-	2.13 ± 0.19	0.12 ± 0.04	1.08 ± 0.19	12.4 ± 4.06	*
1	10 μM	+	0.52 ± 0.13	0.69 ± 0.18	1.79 ± 0.46	1.40 ± 0.13	*

B)

Polyamide	Conc.	TMPRSS2-ERG	PSA	FKBP5	AR
1	1 μM	1.02 ± 0.08	0.81 ± 0.09	0.93 ± 0.09	0.96 ± 0.04
	10 μM	0.91 ± 0.05	0.68 ± 0.08	0.83 ± 0.04	1.09 ± 0.08

Polyamide	Conc.	ERG	PLAT	EZH2	MYC	SLC45A3
1	1 μM	0.84 ± 0.07	0.67 ± 0.06	1.00 ± 0.10	0.70 ± 0.04	0.98 ± 0.10
	10 μM	0.86 ± 0.05	0.42 ± 0.11	0.93 ± 0.03	0.49 ± 0.05	0.78 ± 0.07

Figure S2.5 A) Table of mRNA expression levels for AR-driven genes under DHT-induced conditions in response to 10 μM **1**. VCaP were cells plated at 31k/cm^2 treated with medium containing 0.1% DMSO (with or without polyamide) and charcoal-treated FBS (CT-FBS) for 72 h followed by induction with 1 nM dihydrotestosterone (DHT) or vehicle for an additional 24 h. * - mRNA expression levels below threshold. **B)** mRNA expression data for polyamides at 1 and 10 μM concentration. VCaP cells plated at 31k/cm2 were treated with medium containing 0.1% DMSO vehicle (with or without polyamide) for 72h. mRNA levels were measured by qPCR, referenced to GUSB, and the polyamide effects compared to vehicle treated samples. Data shown are the average of the fold changes (treated/untreated levels) for three or more biological replicates +/- standard error.

	Compounds	Score
1	**SN-38**	99.978
2	mitomycin-c	99.872
3	importazole	99.733
4	**irinotecan**	99.732
5	**teniposide**	99.573
6	**amsacrine**	99.547
7	SIB-1893	99.237
8	**camptothecin**	99.184
9	pyrvinium-pamoate	98.087
10	BRD-K39187410	98.623

Figure S2.6 Connectivity map analysis of perturbagens that correlate with gene expression changes induced by polyamide **1** in LNCaP cells. Bolded compounds are topoisomerase inhibitors.

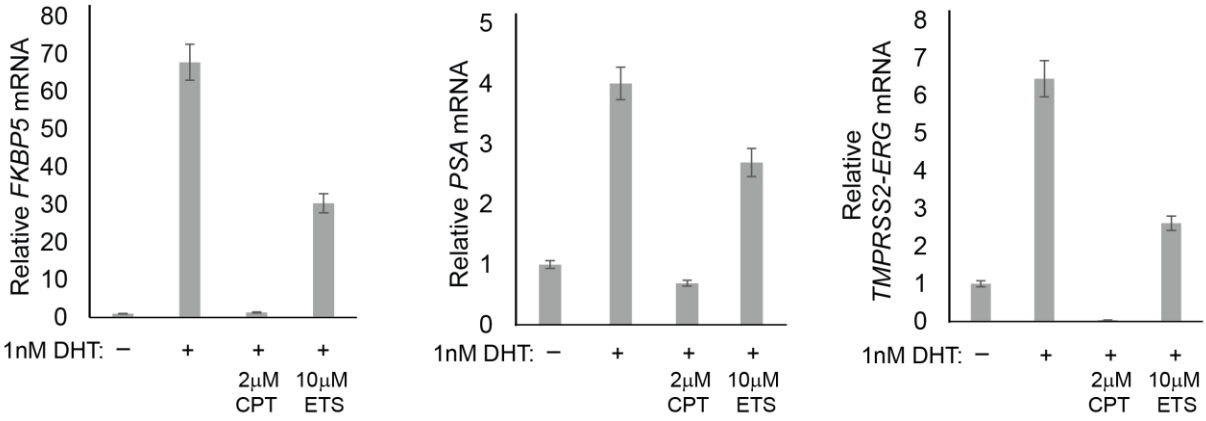

Figure S2.7 Effect of topoisomerase inhibitors on gene expression in VCaP cells. VCaP cells were plated at 31k/cm^2, incubated for 24 h, and then treated with medium containing 0.1% DMSO (with or without camptothecin or etoposide) and DHT for 16 h. mRNA levels were measured by qPCR, referenced to *GUSB*, and the effects compared to vehicle treated samples. Data shown are the average fold changes (treated/untreated) for three biological replicates +/- standard error.

Chapter 3

A Pyrrole-Imidazole Polyamide is Active against Enzalutamide-Resistant Prostate Cancer

The text of this chapter is taken from a manuscript coauthored with Fei Yang[1], Timothy R. Welch[1], Nicholas G. Nickols[2], and Peter B. Dervan[1].

1 Division of Chemistry and Chemical Engineering,
California Institute of Technology, Pasadena, CA

2 Department of Radiation Oncology,
David Geffen School of Medicine at UCLA, Los Angeles, CA

Kurmis AA, Yang F, Welch TR, Nickols NG and Dervan PB. (2017) A Pyrrole-Imidazole Polyamide is Active against Enzalutamide-Resistant Prostate Cancer. *Cancer Res.* 77:2207-2212. Doi: 10.1158/0008-5472.CAN-16-2503

Abstract

Effective treatment for enzalutamide-resistant prostate cancer is an unmet need. The LREX' prostate cancer model is resistant to the antiandrogen enzalutamide via activation of an alternative nuclear hormone receptor (NHR), glucocorticoid receptor (GR), which has similar DNA binding specificity to the androgen receptor (AR). Small molecules that target DNA to interfere with protein-DNA interactions may retain activity against enzalutamide-resistant prostate cancers where ligand binding domain antagonists are ineffective. A pyrrole-imidazole (Py-Im) polyamide designed to bind the consensus androgen response element half-site has antitumor activity against hormone sensitive prostate cancer. In enzalutamide-resistant LREX' cells this polyamide interferes with both androgen receptor and glucocorticoid receptor driven gene expression while enzalutamide interferes with only that of androgen receptor. Genomic analyses indicate immediate interference with the androgen receptor transcriptional pathway. Long-term treatment with the polyamide demonstrates a global decrease in RNA levels, consistent with inhibition of transcription. The polyamide is active against two enzalutamide-resistant xenografts with minimal toxicity.

3.1 Introduction

Prostate cancer is the second leading cause of cancer death in American men with 26,000 deaths annually (1), the majority from metastatic, castrate resistant prostate cancer (mCRPC), in which androgen deprivation therapy (ADT), which suppresses AR signaling, is ineffective. Enzalutamide, a potent AR-ligand binding domain (LBD) antagonist, is effective against mCRPC and is a current standard of care. (2) Unfortunately, *de novo* or acquired resistance to enzalutamide is common (3); overcoming this is an unmet need.

Mechanisms of enzalutamide resistance include restoration of AR signaling through LBD mutations or expression of transcriptionally active splice variants lacking the LBD(4), bypass of AR signaling through alternative nuclear hormone receptors (NHR; ref. (5)), or development of complete independence from AR signaling. (6) Glucocorticoid receptor (GR) is an NHR with a sequence preference similar to AR. (7) After enzalutamide treatment, the LREX' cell line highly expresses GR, which drives enzalutamide resistance by regulating gene expression significantly overlapping that of AR, suggesting prostate cancers co-opt GR to progress through AR antagonism. (5) Furthermore, GR expression in mCRPC associates with poor response to enzalutamide. (5) Therefore, interference with the NHR-DNA interface may overcome enzalutamide resistance.

A pyrrole-imidazole (Py-Im) polyamide (**ARE-1**) is effective against hormone sensitive LNCaP xenografts with minimal host toxicity. (8) Py-Im polyamides are minor groove DNA binding small molecules with modular sequence specificity and high affinity. (9) Polyamide-DNA

binding induces widening of the minor groove and compression of the opposing major groove (10), interfering with transcription factor-DNA interactions and the transcriptional machinery. (11, 12) A polyamide targeted to the ARE might prevent AR and GR signaling, and transcription.

We hypothesized that **ARE-1** may be effective against enzalutamide-resistant prostate cancer. We report **ARE-1** efficacy against enzalutamide-resistant VCaP and LREX' prostate cancer models in cell culture and xenografts. Mechanistic studies reveal immediate interference with androgen-induced gene expression and reduced transcription after long-term treatment.

3.2 Materials and Methods

Cell culture conditions and cytotoxicity assays. The LREX' and LNCaP/AR cell lines were gifts from Charles Sawyers (Memorial Sloan Kettering Cancer Center, New York, NY) and were received in 2014 and 2007, respectively. The VCaP cell line was a gift from Kenneth Pienta (University of Michigan Medical School, Ann Arbor, MI) and was received in 2012. Cells were maintained as previously described (5, 8, 11–13) and were used within 10 passages from thawing. Cells were validated to parental cell lines by STR profile at IDEXXX Bioresearch following experimentation and confirmed to be mycoplasma free. WST-1 assay (Roche) was used to measure cytotoxicity. Long-term toxicity in VCaP cells was assayed by cell counting.

Confocal imaging. Imaging was as described in ref. (8). Briefly, 2 μmol/L of **ARE-1-FITC** was added for 16 hours, washed with PBS, and imaged on a Zeiss LSM 5 Exciter.

Gene expression analysis. LNCaP/AR and LREX' cells were cultured for 72 hours after plating in phenol-red free RPMI1640 (10% CT-FBS) in six well plates at 4 x 10^4 and 5 x 10^4 cells/mL, respectively. LNCaP/AR cells were treated with 10 μmol/L **ARE-1**, bicalutamide, or enzalutamide (Aurum Pharmatech) for an additional 48, 2, and 2 hours, respectively, prior to treatment with 1 nmol/L DHT or ethanol for 16 hours. LREX' cells were treated with 10 μmol/L **ARE-1** for 16hours prior to induction with 1 nmol/L DHT or 100 nmol/L dexamethasone for 8 hours. RNA extraction (RNEasy columns, Qiagen), cDNA generation (Transcriptor First Strand cDNA Kit, Roche), and qRT-PCR (SYBR Green Master Mix, Applied Biosystems, ABI7300 instrument) were as described in refs. (8, 11, 12). Expression was normalized to β-glucuronidase.

RNA sequencing analysis. LREX' cells were plated at 5 × 10^4 cells/mL in 10-cm^2 dishes, treated with or without 10 μmol/L of **ARE-1** in fresh media, incubated 16 hours, and induced with 1 nmol/L DHT for 8 hours. Tumor samples were homogenized mechanically. Total RNA was Trizol extracted, sequenced (Illumina HiSeq2000), and mapped against the human genome (hg19) with Tophat2 using Ensembl GRCh37 gene annotations. Human and mouse reads from tumor samples were parsed with BBSplit and unique reads were mapped. Htseq-count was used for exon alignment and DESeq2 for differential expression. Gene set

enrichment analysis (GSEA) was performed on genes with $P_{adj} < 0.05$ and fold change ≥ 1.6 for cell samples and $P_{adj} < 0.05$ for tumor samples (SRP102746)

Nascent RNA measurement. LREX' cells were plated at 1×10^5 cells/mL in 96-well plates in RPMI1640 (20% FBS and 1 µmol/L enzalutamide), adhered for 24 hours, dosed with **ARE-1**, and incubated for 48 hours. The Click-iT RNA Alexa Fluor 488 HCS kit was used for dye conjugation, and incorporation of 5-ethynyl uridine (5-EU) was measured on a FlexStation 3 plate reader.

Flow cytometry. LREX' cells were plated at 1×10^5 cells/mL in 175-cm^2 flasks, adhered 24 hours, incubated with 10 µmol/L **ARE-1** 24, 48, and 72 hours, then with 300 µmol/L 5-EU in fresh media. Cells were detached by Accumax or Accutase, and Alexa Fluor 488 azide dye was conjugated. Cells were passed through a 35µm mesh prior to flow, sorted on a FACSCalibur instrument (Becton Dickinson), and analyzed using FlowJo.

Animal experiments. Animal experiments were performed at Caltech (Pasadena, CA) under IACUC approval. VCaP and LREX' cells were engrafted as 1:1 mixtures of $3x10^6$ cells in Matrigel (BD Biosciences) into the flanks of intact and castrated male SCID mice (Charles River Laboratories), respectively. LREX' engrafted mice received 10 mg/kg enzalutamide (oral gavage) daily. Once tumors were 100mm^3 (0.5*l*w*w), **ARE-1** was administered subcutaneously to opposing flanks in 20% DMSO:saline. For circulation studies, 4 C57BL6/J animals were injected subcutaneously with **ARE-1** at 30mg/kg and blood collected retro-

orbitally. Plasma concentrations of **ARE-1** were analyzed by HPLC, AUC approximated by the linear trapezoidal method, as described. (8)

Immunohistochemistry. Tumors were fixed in neutral-buffered formalin, paraffinized, sectioned, and stained as described. (12) Quantification of five random fields per slice was performed by ImmunoRatio.

Statistical analysis. Cell culture experiments represent ≥3 independent biological replicates, except sequencing analyses, which were duplicates for cell culture and quadruplicates for tumor samples. For xenografts, animals were randomly assigned to groups. For circulation experiments, concentrations of **ARE-1** were duplicate measurements. Measurements in cell culture, animal, and immunohistochemistry experiments were assessed by Student's t-test.

3.3 Results

ARE-1 is more potent than enzalutamide against prostate cancer cell growth and is not rescued by GR activation

ARE-1 (Fig. 3.1A) targets the sequence 5`-WGWWCW-3` (W=A or T), similar to the consensus half-site recognized by either AR or GR. Nuclear uptake in LNCaP/AR, LREX', and VCAP cells was evaluated using fluorescent analog **ARE-1-FITC** (Supplementary Fig. S3.1). The LNCaP/AR cell line overexpresses full length AR, modeling castration resistance. (14) **ARE-1** reduced proliferation of LNCaP/AR cells more than bicalutamide (Fig. 3.1B). The VCaP cell line overexpresses AR with modest GR expression, the activation of which reduces the

antiproliferative effects of enzalutamide. (5) **ARE-1** reduced proliferation of both VCaP and LREX' cells regardless of induction of AR signaling by 1 nmol/L DHT, induction of GR signaling by 100 nmol/L dexamethasone, or both (Fig. 3.1C-D). Long-term cell viability studies in VCaP cells show 10 µM **ARE-1** is more potent than enzalutamide and insensitive to GR activation (Fig. 3.1D).

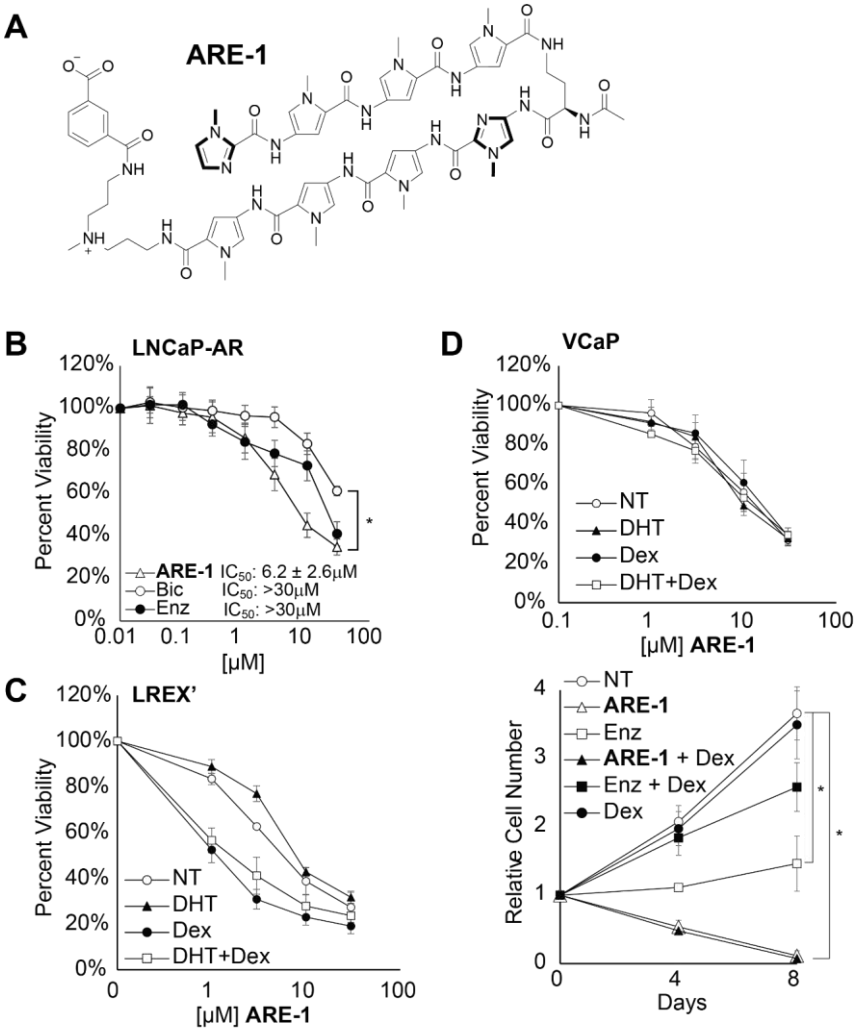

Figure 3.1. Structure of ARE-1 and antiproliferative activity against LNCaP/AR, LREX', and VCaP cells. A) Structure of polyamide **ARE-1**. **B)** Cytotoxicity of **ARE-1**, bicalutamide (Bic), and enzalutamide (Enz) in LNCaP/AR cells over 72 hours. **C)** Cytotoxicity of **ARE-1** in LREX' cells is not attenuated by AR or GR activation. **D)** Top, cytotoxicity of **ARE-1** in VCaP cells is not affected by dexamethasone (Dex); bottom, long-term incubation of **ARE-1** or Enz in VCaP cells. Results are in biological triplicate. Error bars are standard errors of the mean. * $P < 0.05$.

Py-Im polyamide attenuates androgen and glucocorticoid driven gene expression

In androgen-depleted conditions, bicalutamide activates AR in the LNCaP/AR cell line. (14) Enzalutamide and **ARE-1** demonstrate no agonist activity; **ARE-1** reduced baseline expression of *KLK3* (Fig. 3.2A). In LREX' cells, **ARE-1** represses *KLK3* and *HOMER2* expression, which are co-regulated by AR and GR (Fig. 3.2B). While enzalutamide was more potent than **ARE-1** in reducing DHT induced transcription, the opposite was observed with dexamethasone induction. Furthermore, co-administration of enzalutamide and **ARE-1** was additive, suggesting **ARE-1** may potentiate enzalutamide's activity.

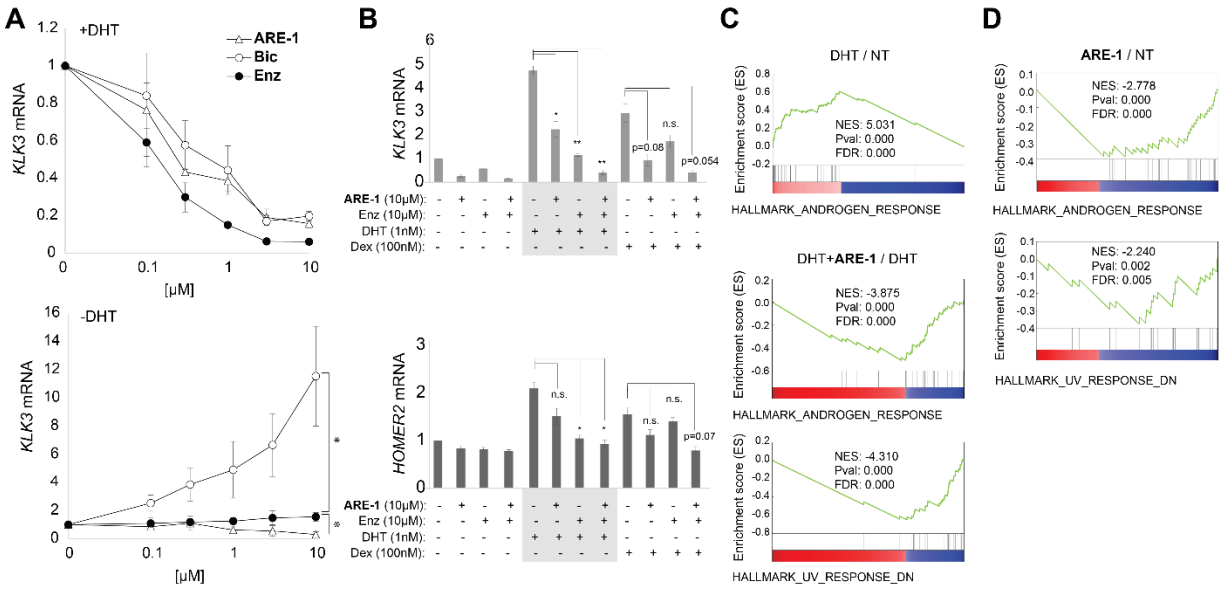

Figure 3.2 Gene regulation activity of ARE-1 in LNCaP/AR, LREX', and LNCaP cells. A) Effects of **ARE-1**, bicalutamide (Bic), and enzalutamide (Enz) on DHT induced *KLK3* mRNA in LNCaP/AR cells (top), and baseline (charcoal stripped media; bottom). **B)** effects of **ARE-1** and Enz against select genes co-regulated by AR and GR in LREX' cells. Dex: dexamethasone. **C)** GSEA analysis of gene expression profiles in LREX' cells. Top, DHT treatment of LREX' cells enriches for the androgen response. Bottom, treatment with **ARE-1** in the presence of DHT negatively enriches for androgen response as well as the UV response down. **D) ARE-1** treatment of parental LNCaP cells (maintained in 10% FBS without supplemented DHT) also negatively enriches for androgen response and the UV response down. NT: non-treated (i.e., vehicle only). * $P < 0.05$; n.s., not significant.

Global transcriptomic effects of Py-Im polyamide on enzalutamide sensitive and resistant CaP cells

We performed RNA sequencing analysis on three treatment conditions in LREX' cells: vehicle, DHT treatment, and co-treatment with **ARE-1** and DHT, and two conditions in parental LNCaP cells: vehicle and **ARE-1** treatment. GSEA of affected genes in LREX' cells using the hallmark pathways in the Molecular Signatures Database revealed DHT treatment enriched for the AR signaling pathway as expected (Fig. 3.2C, Supplementary Fig. S3.2; Supplementary Table S3.1). DHT-induced LREX' cells treated with **ARE-1** negatively enriched for the AR signaling pathway (NES -3.875; Fig. 3.2C, Supplementary Table S3.1), consistent with interference in AR driven gene expression by **ARE-1**. In addition, **ARE-1** treatment negatively enriched for the UV DNA damage response pathway down (NES -4.310; Fig. 3.2C). Similarly, **ARE-1** treatment in LNCaP cells negatively enriched for the AR signaling pathway (NES -2.778) and the UV DNA damage response pathway down (NES -2.240) (Fig. 3.2D, Supplementary Table S3.1). UV radiation induces DNA helical distortions through formation of pyrimidine dimers and 6-4 photoproducts, which arrest RNA polymerase II (RNAP2) during elongation, triggering degradation of RPB1. **ARE-1** reduced nascent RNA in LREX' cells as measured by 5-EU incorporation (Fig. 3.3), and we previously observed RPB1 degradation after long-term treatment with **ARE-1** and related polyamides. (8, 12) This suggests that long-term treatment with **ARE-1** reduces global transcription in LREX' cells.

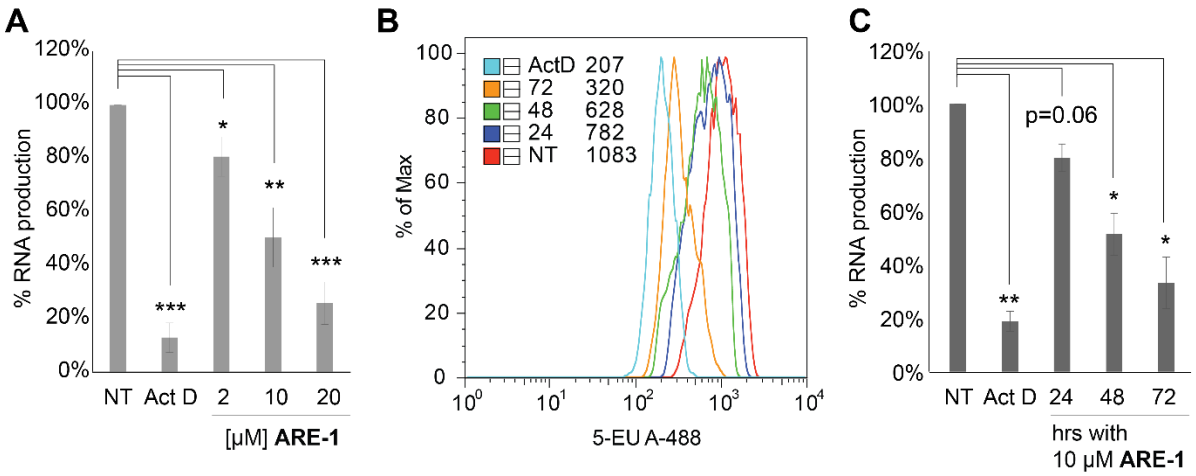

Figure 3.3 Effect of ARE-1 on RNA transcription. A) Measurement of nascent RNA in LREX' cells treated with **ARE-1** at 2, 10, and 20 μM for 48 hours. Actinomycin D (Act D) was used as a positive control. **B)** Measurement of nascent RNA in LREX' cells by flow cytometry after treatment with **ARE-1** at 10 μM for 24, 48, and 72 hours. **C)** Composite of flow cytometry results. Results are in biological triplicate. Error bars are SEM. * $P < 0.05$; ** $P < 0.005$; *** $P < 0.0005$.

Suppression of enzalutamide resistant CRPC *in vivo*

We further tested the efficacy of **ARE-1** in VCaP xenografts, which exhibit modest response to 10 mg/kg enzalutamide treatment, and in mice engrafted with enzalutamide-resistant LREX' cells. (5, 13) In VCaP xenografts, **ARE-1** dose dependently reduced tumor growth by 70% at 5 mg/kg compared with vehicle (Fig. 4A) without significant toxicity (Supplementary Fig. S3.3A). In castrated mice bearing LREX' tumors, **ARE-1** and enzalutamide cotreatment reduced growth by 80% compared with enzalutamide alone (Fig. 4B) without significant toxicity (Supplementary Fig. S3.3B). Enzalutamide was administered daily postengraftment at 10 mg/kg to maintain GR expression, which was confirmed by IHC. LNCaP tumors, which do not express GR, were used as controls (Fig. 3.4C). Furthermore, LREX' tumors treated with **ARE-1** and enzalutamide showed reduced *KLK3* expression (Supplementary Fig. S3.4C), elevated TUNEL, and reduced Ki67 staining compared to enzalutamide alone

(Supplementary Fig. S3.3D). GSEA of tumor expression profiles shows **ARE-1** treatment elicits similar UV response signatures as seen in cell culture and represses ontologies associated with DNA binding-dependent transcription (Supplementary Tables S3.2 and S3.3). Plasma concentration of **ARE-1** from terminal blood samples collected from LREX'-engrafted animals were compared with the plasma concentration in C57BL6/J animals treated with 30 mg/kg **ARE-1**; AUC was 25.9 and 189.9 μg*hr/mL, respectively (Supplementary Fig. S3.4). At 30 mg/kg mice experienced a 6% weight loss but recovered within 5 days without visible signs of distress (not shown).

3.4 Discussion

AR LBD mutations, expression of transcriptionally active splice variants lacking the LBD, co-option of NHRs with similar DNA binding specificities, or loss of reliance on AR, may drive enzalutamide resistance. (3) Furthermore, different metastatic foci within a patient may resist enzalutamide through different mechanisms (15), suggesting a successful treatment strategy might use multiple therapeutics that overcome a different resistance mechanism, or alternatively, a single therapeutic capable of overcoming multiple mechanisms. Therapeutic targeting of the NHR-DNA interface may overcome most known enzalutamide resistance mechanisms.

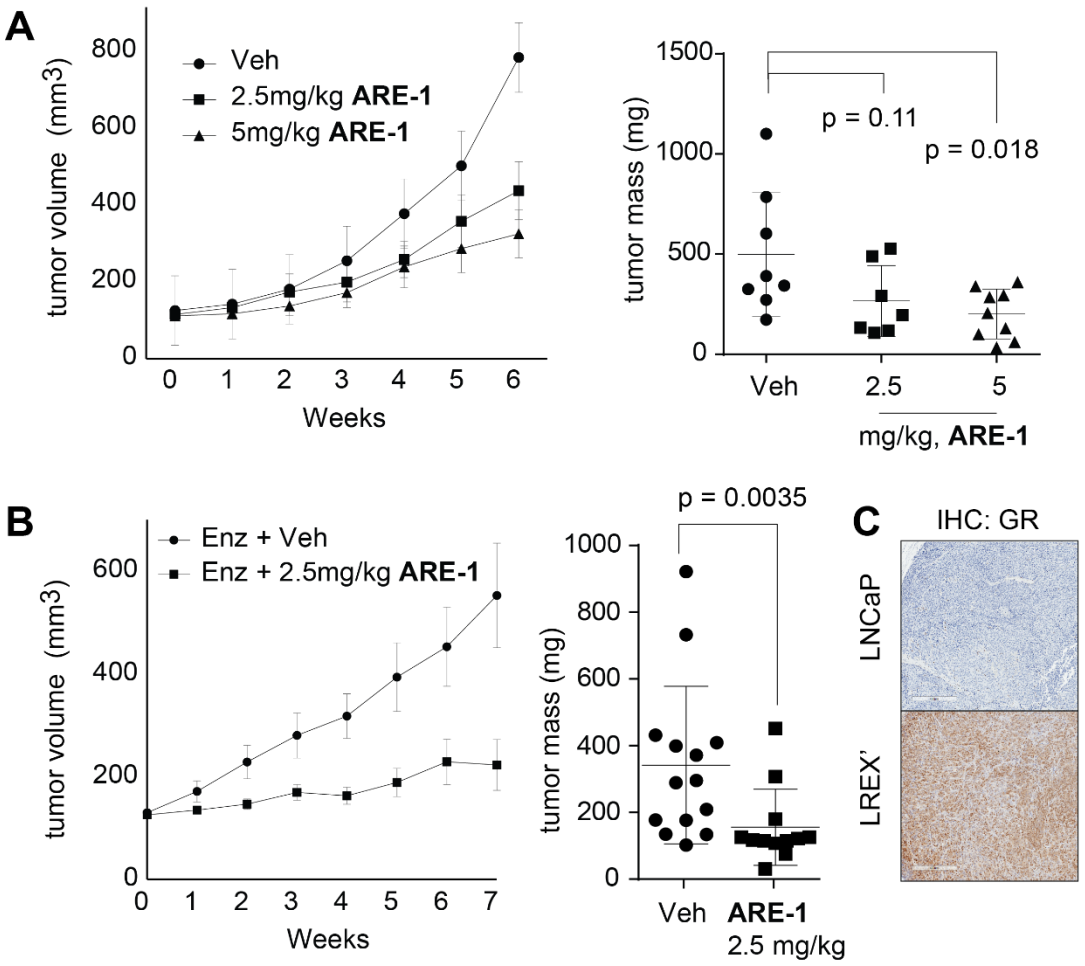

Figure 3.4 Mice were treated three times per week with **ARE-1** subcutaneously to flanks opposite engrafted tumor. **A)** Tumor volumes (left) and final tumor masses (right) of VCaP xenografts treated with vehicle (Veh; *n* = 8), 2.5 mg/kg (*n* = 7), and 5 mg/kg (*n* = 8) **ARE-1**. **B)** Tumor volumes (left) and final tumor masses (right) of LREX' xenografts in castrated animals treated daily with 10 mg/kg enzalutamide (Enz) and vehicle (*n* = 14) or enzalutamide and 2.5 mg/kg **ARE-1** (*n* = 12).**C)** GR staining of LREX' and LNCaP tumors. All LREX' tumors stained for GR. Errors for tumor volumes are SEM. Whisker plots represent means and standard deviations.

The GR antagonist mifepristone added to ADT was previously tested in mCRPC patients and was not effective. (16) Trials for mCRPC patients combining enzalutamide with mifepristone are underway. Other NHRs may also be active in refractory prostate cancer. (3) Notably, progesterone receptor inhibitors have entered clinical trials for mCRPC. Therapeutics targeting the N-terminal domain (NTD) of AR, or that mediate degradation of AR, may overcome treatment resistance due to AR splice variants. The NTD inhibitor EPI-506 has entered clinical trials. (17) However this approach may not overcome resistance due to cooption of alternate NHRs. Others have reported small molecules that interfere with the AR DNA-binding domain. (18) The clinical utility of this approach is unknown.

We report a Py-Im polyamide with activity against enzalutamide-resistant prostate cancer in cell and animal models. Polyamide **ARE-1**, targeted to the sequence 5'-WGWWCW-3', which is similar to the ARE and GRE half-site, attenuates ligand-induced AR and GR transcriptional activity, is more potent than enzalutamide and bicalutamide in cell culture, and is active against enzalutamide-resistant xenografts. Long-term treatment of LREX' cells with **ARE-1** also decreases nascent RNA synthesis. In biophysical experiments, polyamides can halt RNAP2 elongation directly upstream of a polyamide binding site. (19) We hypothesize this stalling of RNAP2 promotes ubiquitination and degradation of RPB1, ultimately interfering with RNA synthesis, which may contribute to efficacy against treatment-refractory prostate cancer. Other molecules that interfere with RNA synthesis are proposed as potential drug candidates for prostate cancer. (13, 20)

References

1. American Cancer Society. Cancer Facts & Figures 2016. Atlanta: American Cancer Society; 2016.
2. Beer TM, Armstrong, AJ, Rathkopf DE, Loriot Y, Sternberg CN, Higano CS, Iversen P, Bhattacharya S, Carles J, Chowdhury S, *et al.* (2014) Enzalutamide in Metastatic Prostate Cancer before Chemotherapy. *N. Engl. J. Med.*, **371**, 424–433.
3. Watson PA, Arora VK and Sawyers CL (2015) Emerging mechanisms of resistance to androgen receptor inhibitors in prostate cancer. *Nat. Rev. Cancer*, **15**, 701–711.
4. Ware KE, Garcia-Blanco MA, Armstrong AJ and Dehm SM (2014) Biologic and clinical significance of androgen receptor variants in castration resistant prostate cancer. *Endocr. Relat. Cancer*, **21**, T87–T103.
5. Arora VK, Schenkein E, Murali R, Subudhi SK, Wongvipat J, Balbas MD, Shah N, Cai L, Efstathiou E, Logothetis C, *et al.* (2013) Glucocorticoid Receptor Confers Resistance to Antiandrogens by Bypassing Androgen Receptor Blockade. *Cell*, **155**, 1309–1322.
6. Beltran H, Prandi D, Mosquera JM, Benelli M, Puca L, Cyrta J, Marotz C, Giannopoulou E, Chakravarthi BVSK, Varambally S, *et al.* (2016) Divergent clonal evolution of castration-resistant neuroendocrine prostate cancer. *Nat. Med.*, **22**, 298–305.
7. Meijsing SH, Pufall MA, So AY, Bates DL, Chen L and Yamamoto KR (2009) DNA binding site sequence directs glucocorticoid receptor structure and activity. *Science*, **324**, 407–410.
8. Yang F, Nickols NG, Li BC, Szablowski JO, Hamilton SR, Meier JL, Wang C-M and Dervan PB (2013) Animal toxicity of hairpin pyrrole-imidazole polyamides varies with the turn unit. *J. Med. Chem.*, **56**, 7449–7457.
9. Dervan PB and Edelson BS (2003) Recognition of the DNA minor groove by pyrrole-imidazole polyamides. *Curr. Opin. Struct. Biol.*, **13**, 284–299.
10. Chenoweth DM and Dervan PB (2009) Allosteric modulation of DNA by small molecules. *Proc. Natl. Acad. Sci. U. S. A.*, **106**, 13175–13179.
11. Nickols NG and Dervan PB (2007) Suppression of androgen receptor-mediated gene expression by a sequence-specific DNA-binding polyamide. *Proc. Natl. Acad. Sci. U. S. A.*, **104**, 10418–10423.
12. Yang F, Nickols NG, Li BC, Marinov GK, Said JW and Dervan PB (2013) Antitumor activity of a pyrrole-imidazole polyamide. *Proc. Natl. Acad. Sci. U. S. A.*, **110**, 1863–1868.
13. Asangani IA, Dommeti VL, Wang X, Malik R, Cieslik M, Yang R, Escara-Wilke J, Wilder-Romans K, Dhanireddy S, Engelke C, *et al.* (2014) Therapeutic targeting of BET bromodomain proteins in castration-resistant prostate cancer. *Nature*, **510**, 278–282.
14. Chen CD, Welsbie DS, Tran C, Baek SH, Chen R, Vessella R, Rosenfeld MG and Sawyers CL (2004) Molecular determinants of resistance to antiandrogen therapy. *Nat. Med.*, **10**, 33–39.

15. Gundem G, Van Loo P, Kremeyer B, Alexandrov LB, Tubio JMC, Papaemmanuil E, Brewer DS, Kallio HML, Högnäs G, Annala M, *et al.* (2015) The evolutionary history of lethal metastatic prostate cancer. *Nature*, **520**, 353–357.
16. Taplin M-E, Manola J, Oh WK, Kantoff PW, Bubley GJ, Smith M, Barb D, Mantzoros C, Gelmann EP and Balk SP (2008) A phase II study of mifepristone (RU-486) in castration-resistant prostate cancer, with a correlative assessment of androgen-related hormones. *BJU Int.*, **101**, 1084–1089.
17. Myung J-K, Banuelos CA, Fernandez JG, Mawji NR, Wang J, Tien AH, Yang YC, Tavakoli I, Haile S, Watt K, *et al.* (2013) An androgen receptor N-terminal domain antagonist for treating prostate cancer. *J. Clin. Invest.*, **123**, 2948–2960.
18. Dalal K, Roshan-Moniri M, Sharma A, Li H, Ban F, Hassona MD, Hessein M, Hsing M, Singh K, LeBlanc E, *et al.* (2014) Selectively targeting the DNA-binding domain of the androgen receptor as a prospective therapy for prostate cancer. *J. Biol. Chem.*, **289**, 26417–26429.
19. Xu L, Wang W, Gotte D, Yang F, Hare AA, Welch TR, Li BC, Shin JH, Chong J, Strathern JN, *et al.* (2016) RNA polymerase II senses obstruction in the DNA minor groove via a conserved sensor motif. *Proc. Natl. Acad. Sci.*, **113**, 12426–12431.
20. Peltonen K, Colis L, Liu H, Jäämaa S, Zhang Z, Af Hällström T, Moore HM, Sirajuddin P and Laiho M (2014) Small molecule BMH-compounds that inhibit RNA polymerase I and cause nucleolar stress. *Mol. Cancer Ther.* **13**, 2537–2546.

3.5 Supplemental material

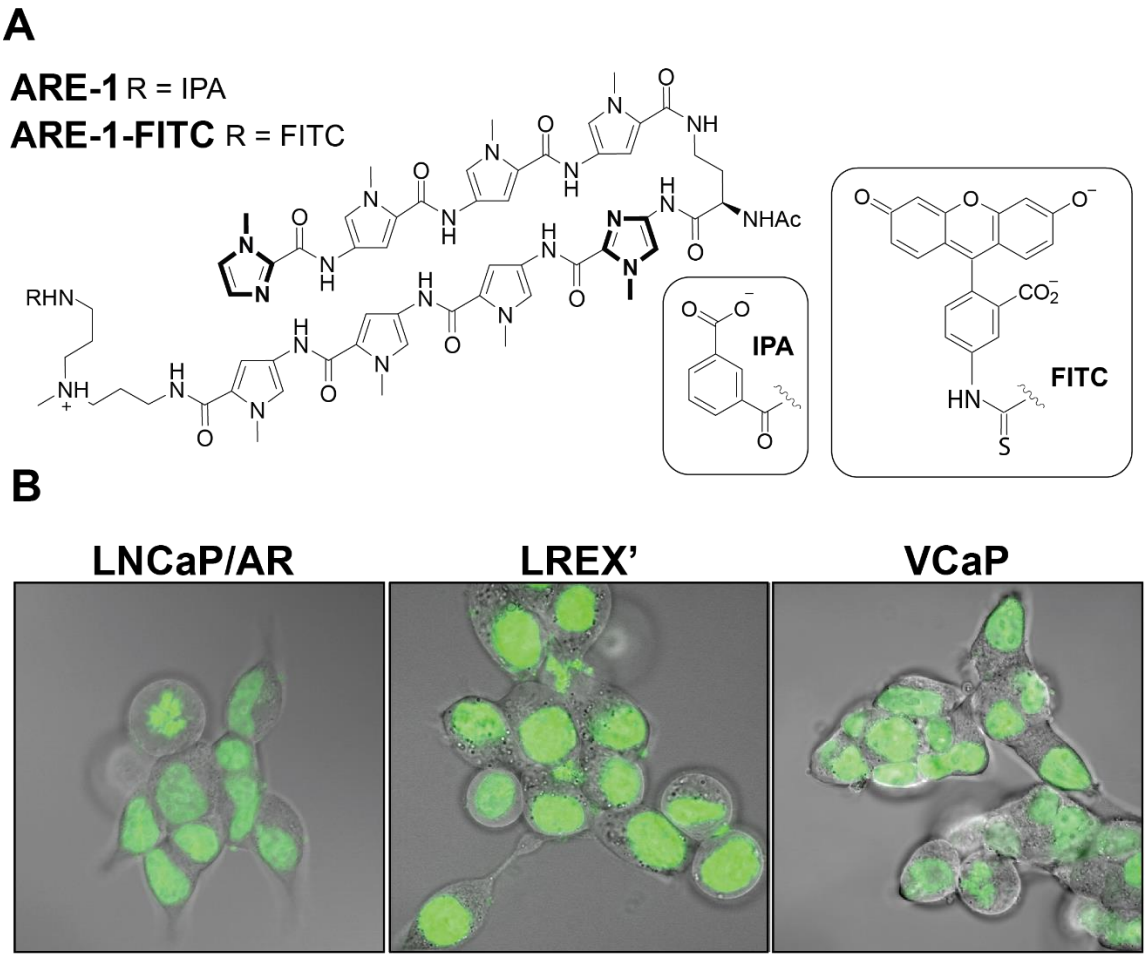

Figure S3.1 A) Chemical structure of **ARE-1** and **ARE-1-FITC**. **B)** Nuclear uptake of **ARE-1-FITC** in LNCaP/AR, LREX', and VCaP cells.

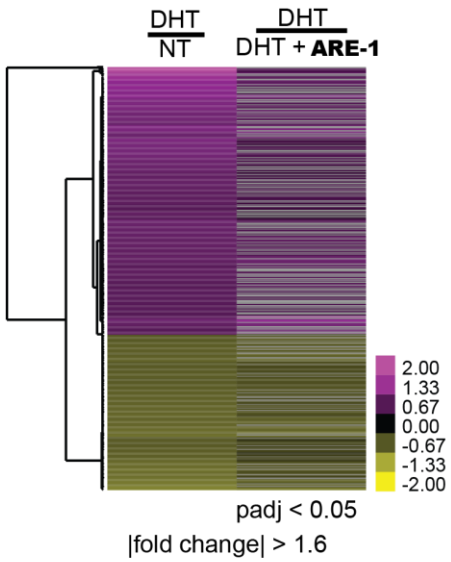

Figure S3.2 Heatmap of gene expression profile of LREX' cells for conditions DHT/NT and DHT/DHT+**ARE-1**.

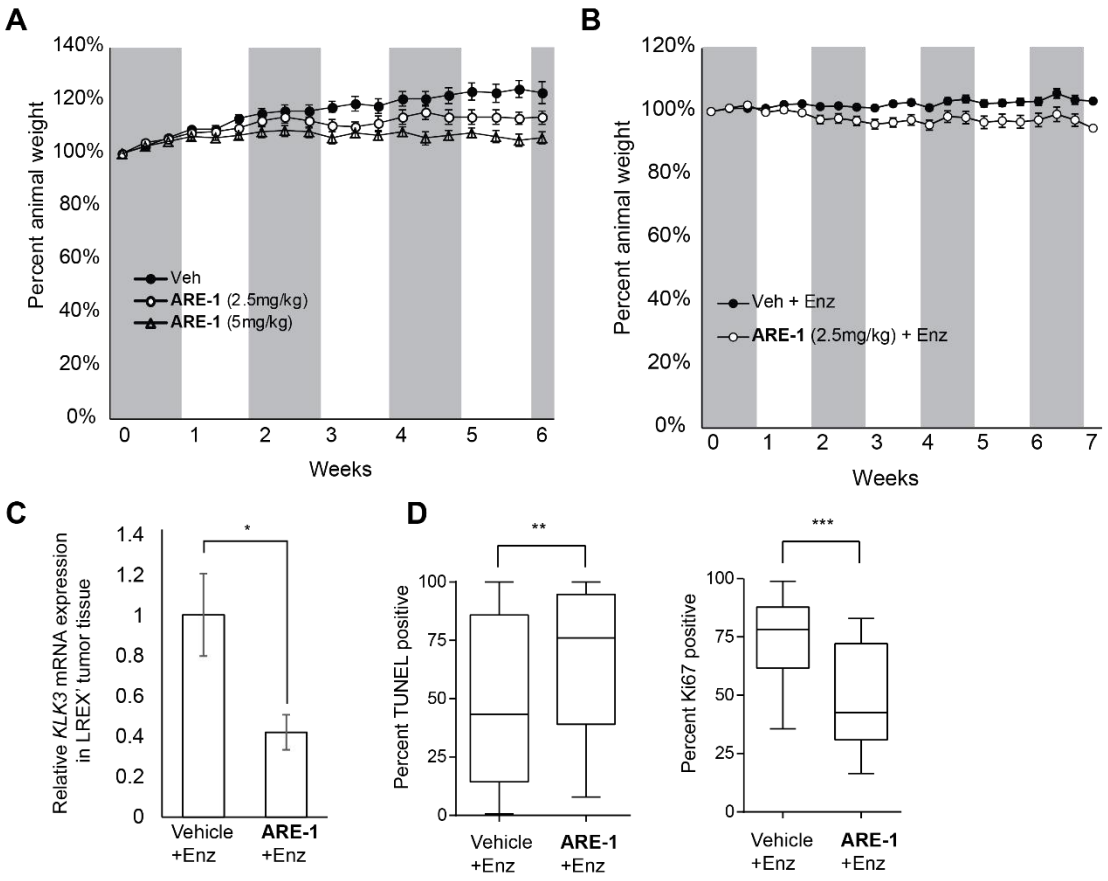

Figure S3.3 A) Weights of VCaP tumor bearing animals treated with **ARE-1**. **B)** Weights of LREX' tumor bearing animals treated with Enz or Enz + **ARE-1**. **C)** Expression of *KLK3* mRNA in tumor tissue. **D)** TUNEL and Ki67 analysis of LREX' tumors. For animal weights and *KLK3* expression, error bars are SEM. Whisker plots for TUNEL and Ki67 staining represent means, quartiles, and maxima/minima. * $P < 0.05$, ** $P < 0.005$, *** $P < 0.0005$.

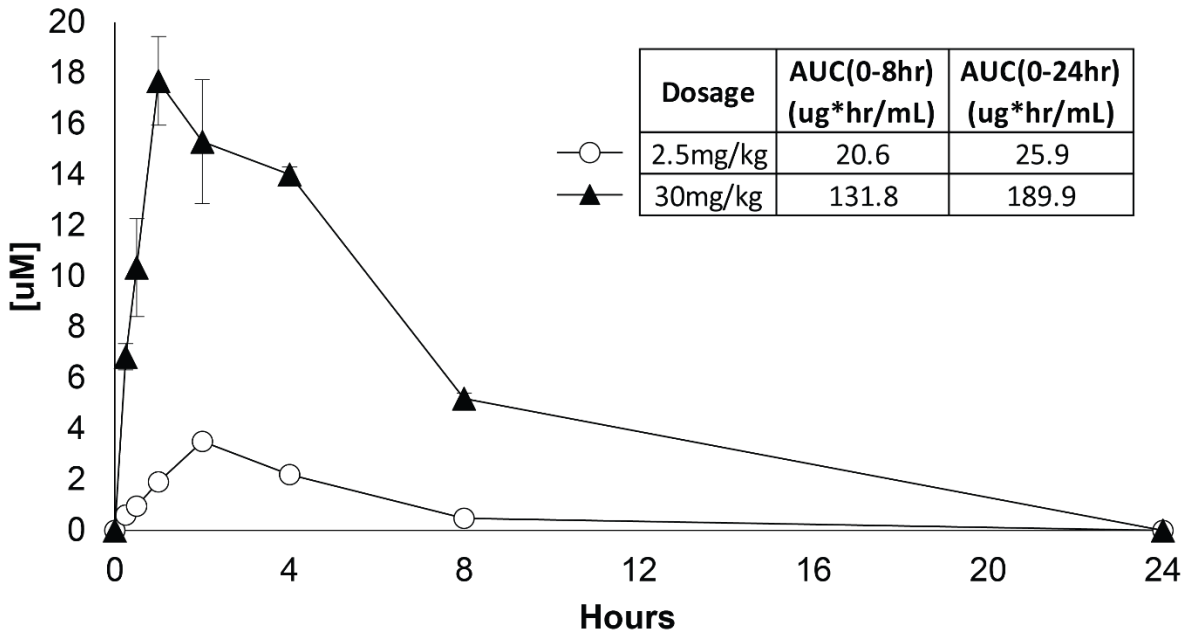

Figure S3.4 Plasma concentration of **ARE-1** at 2.5mg/kg and 30mg/kg in LREX' tumor bearing SCID mice and C57BL6/J mice, respectively.

Condition: LREX' DHT/NT			
Enrichment Terms	**NES**	**Pval**	**FDR**
HALLMARK ANDROGEN RESPONSE	5.0307606	0	0
HALLMARK PROTEIN SECRETION	2.8486454	0	0
HALLMARK TNFA SIGNALING VIA NFKB	2.7508241	0	0
HALLMARK UV RESPONSE DOWN	2.4962228	0	0.0010452
HALLMARK MYC TARGETS V2	-1.810043	0.018797	0.0436006
HALLMARK MYC TARGETS V1	-1.8610797	0.0056497	0.0482218
HALLMARK OXIDATIVE PHOSPHORYLATION	-2.1263347	0.0058594	0.0168776
Condition: LREX' DHT + **ARE-1**/DHT			
Enrichment Terms	**NES**	**Pval**	**FDR**
HALLMARK OXIDATIVE PHOSPHORYLATION	2.738261	0	0.0010684
HALLMARK UV RESPONSE UP	2.1734213	0.0020284	0.0192308
HALLMARK DNA REPAIR	2.0550299	0.0019608	0.0281339
HALLMARK INTERFERON GAMMA RESPONSE	2.0279558	0.004065	0.0224359
HALLMARK MYC TARGETS V1	2.0058489	0.0019763	0.0194444
HALLMARK APICAL JUNCTION	-2.1975774	0	0.005597
HALLMARK MITOTIC SPINDLE	-2.3021617	0	0.0037313
HALLMARK PROTEIN SECRETION	-2.4021989	0	0.0031095
HALLMARK ANDROGEN RESPONSE	-3.8752934	0	0
HALLMARK UV RESPONSE DOWN	-4.3098002	0	0
Condition: LNCaP **ARE-1**/NT			
Enrichment Terms	**NES**	**Pval**	**FDR**
HALLMARK P53 PATHWAY	3.7487608	0	0
HALLMARK TNFA SIGNALING VIA NFKB	3.2482756	0	0
HALLMARK INTERFERON GAMMA RESPONSE	3.0602648	0	0
HALLMARK APOPTOSIS	2.3234139	0.0019194	0.0005936
HALLMARK UV RESPONSE DOWN	-2.2403436	0.0017953	0.0048524
HALLMARK ANDROGEN RESPONSE	-2.7783908	0	0

Table S3.1 GSEA of DHT/NT and DHT + **ARE-1**/DHT condition in LREX' cells, and **ARE-1**/NT in LNCaP cells. Top 5 positively and negatively enriched Hallmark pathways with FDR < 0.05 are listed.

Enrichment Terms	NES	Pval	FDR
HALLMARK OXIDATIVE PHOSPHORYLATION	3.8754299	0	0
HALLMARK MYC TARGETS V1	2.7354496	0	0
HALLMARK DNA REPAIR	2.254965	0.0019685	0.0081733
HALLMARK XENOBIOTIC METABOLISM	1.9715754	0.0039761	0.0360503
HALLMARK FATTY ACID METABOLISM	1.915122	0.0059642	0.0395982
HALLMARK G2M CHECKPOINT	-1.9537216	0.0099206	0.0218211
HALLMARK UV RESPONSE DOWN	-2.3472996	0	0.0023326
HALLMARK HYPOXIA	-2.4245274	0	0.0018768
HALLMARK MITOTIC SPINDLE	-4.0181766	0	0

Table S3.2 GSEA of Enz+**ARE-1**/Enz+vehicle expression profiles of LREX' tumors. Top 5 positively and negatively Hallmark pathways with FDR < 0.05 are listed.

Gene Ontology Term	Nes	Pval	FDR
MITOCHONDRION	6.584773	0	0
ORGANONITROGEN COMPOUND METABOLIC PROCESS	5.958487	0	0
MITOCHONDRIAL PART	5.946175	0	0
MITOCHONDRIAL ENVELOPE	5.169817	0	0
ORGANELLE INNER MEMBRANE	4.9216123	0	0
ORGANONITROGEN COMPOUND BIOSYNTHETIC PROCESS	4.8149147	0	0
RIBOSOME	4.7787743	0	0
STRUCTURAL CONSTITUENT OF RIBOSOME	4.7411127	0	0
CELLULAR AMIDE METABOLIC PROCESS	4.7254405	0	0
MITOCHONDRION ORGANIZATION	4.686384	0	0
MACROMOLECULAR COMPLEX BINDING	-3.7259953	0	0
CHROMATIN BINDING	-3.7858937	0	0
CELL PROJECTION ORGANIZATION	-3.8129647	0	0
ZINC ION BINDING	-3.9227276	0	0
DOUBLE STRANDED DNA BINDING	-4.0743546	0	0
ADENYL NUCLEOTIDE BINDING	-4.2202587	0	0
REGULATION OF TRANSCRIPTION FROM RNA POLYMERASE II PROMOTER	-4.437626	0	0
REGULATORY REGION NUCLEIC ACID BINDING	-4.775455	0	0
SEQUENCE SPECIFIC DNA BINDING	-4.9900775	0	0
NUCLEIC ACID BINDING TRANSCRIPTION FACTOR ACTIVITY	-5.598217	0	0

Table S3.3 GSEA of gene ontology of LREX' tumor expression profiles.

Chapter 4
Sequence specific suppression of androgen receptor-DNA binding *in vivo* by a Py-Im polyamide

The text of this chapter is taken from a manuscript coauthored with Peter B. Dervan[1].

1 Division of Chemistry and Chemical Engineering,
California Institute of Technology, Pasadena, CA

Kurmis AA and Dervan PB. (2019) Sequence specific suppression of androgen receptor-DNA binding in vivo by a Py-Im polyamide. *Nucleic Acids Research.* Doi: 10.1093/nar/gkz153

Abstract

The crucial role of androgen receptor in prostate cancer development is well documented, and its inhibition is a mainstay of prostate cancer treatment. Here we analyze the perturbations to the androgen receptor cistrome caused by a minor groove binding molecule that is designed to target a sequence found in a subset of androgen response elements. We find treatment with this pyrrole-imidazole polyamide exhibits sequence selectivity in its repression of androgen receptor binding *in vivo*. Differentially changed loci are enriched for sequences resembling ARE half-sites that match the Py-Im polyamide binding preferences determined *in vitro*. Comparatively, permutations of ARE half-site bearing single or double mismatches to the Py-Im polyamide binding sequence are not enriched. This study represents an indirect determination of Py-Im polyamide binding preference *in vivo* using an unbiased approach.

4.1 Introduction

Transcription factors regulate cellular gene expression and the loss of this regulatory balance can lead to a myriad of genetic diseases including cancer. The role of androgen receptor in prostate cancer is one of the most well characterized examples. Early work in 1941 by Charles Huggins and Clarence Hodges showed that the progression of prostate cancer can be controlled by androgen deprivation through castration or hormonal therapy with estrogen. (1) Later the discovery of the first anti-androgen, cyproterone acetate, allowed direct inhibition of androgen binding to the androgen receptor. (2) Since then, the androgen receptor has remained the primary target for systemic therapeutics for prostate cancer patients. (3, 4) In recent years, newer anti-androgens including enzalutamide and apalutamide have already been approved and others are in late-stage clinical development. (5–7)

Metastatic prostate cancers treated with androgen suppressive therapy will ultimately progress to a disease state termed castration-resistant prostate cancer (CRPC). Second-line AR directed therapeutics, such as enzalutamide, are often effective against CRPC, but a second disease progression is almost inevitable. Two mechanisms that have been documented to confer resistance to second-line AR directed therapies are mutations to the AR C-terminal ligand binding domain and expression of AR splice variants lacking the ligand binding domain. (8–10) Multiple approaches have been explored to overcome these resistance mechanisms, as reviewed recently by Jung and colleagues. (11) These include AR

transcription activation domain inhibitors such as EPI-506 and AR DNA binding domain inhibitors, such as pyrvinium pamoate. (11) In addition, our lab has previously reported the use of DNA binders to allosterically modulate the binding of androgen receptor at the protein-DNA interface. (12) We have shown this approach to be efficacious in several prostate cancer models, including anti-androgen resistant models. (13, 14)

Py-Im polyamides are DNA minor groove binding molecules with modular sequence specificity that bind to target sites with affinities comparable to DNA binding proteins. (15, 16) Minor groove sequence recognition is determined by the pairing of N-methylimidazole (Im) and N-methylpyrrole (Py); the target sequence of a particular polyamide is dependent on the location of the Im and Py monomers within the hairpin structure. (17) An Im/Py pair will recognize a G•C pair in the DNA, Py/Im will recognize C•G, and Py/Py will bind to either A•T or T•A. (18–20) Upon binding to the minor groove, Py-Im polyamides cause an expansion of the minor groove and a corresponding compression in the opposing major groove. (21) Py-Im polyamides have been shown to interfere with DNA dependent processes such as gene expression, RNA polymerase II elongation, DNA polymerase replication, and topoisomerase activity. (13, 22–24) They have also been shown to activate p53 and induce apoptosis without genotoxicity, and to have antitumor activity in prostate cancer cell lines and xenograft models. (13, 14, 23) **ARE-1** is a Py-Im polyamide designed to target the sequence 5'-WGWWCW-3', which is found in a subset of response elements common to AR and GR.

In this study, we evaluate the anti-proliferative effects of **ARE-1** in the setting of enzalutamide resistant LNCaP-95 cells, and in the context of AR signaling. We further examine the disruption pattern to the cistrome caused by **ARE-1** treatment. We find that at loci where AR binding is reduced by **ARE-1** treatment, the consensus ARE motif bears closer resemblance to the **ARE-1** target sequence, whereas the native consensus motif has more sequence degeneracy.

4.2 Materials and Methods

Cell culture

The LNCaP-95 cell line was obtained from the laboratory of Dr. Jun Luo at Johns Hopkins School of Medicine. The cells were received at passage 3 and maintained in phenol red free RPMI 1640 (Gibco 11835-030) with 10% charcoal treated FBS. All experiments were performed below passage 20, and cells were validated to parental cell line and confirmed mycoplasma free by ATCC following experimentation.

Cell uptake

Cell uptake was confirmed by confocal imaging, as previously described. Briefly, LNCaP-95 cells were plated in 35-mm optical dishes (MatTek) at 7.5×10^4 cells per dish and allowed to adhere for 24 h. Cells were treated with 2 μM **ARE-1-FITC** for 16 hours, washed with PBS, and imaged at the Caltech Biological Imaging Facility using a Zeiss LSM 710 inverted laser scanning confocal microscope equipped with a 63x oil immersion lens.

Cytotoxicity assay

LNCaP-95 cells were plated at 7.5 x 10^3 per well in 96 well plates. Cells were allowed to adhere for 24 hours, and media was then replaced with fresh media containing vehicle or polyamide **ARE-1**. After 72 hours, an equivalent volume of CellTiter-Glo (CTG) reagent (Promega) was added to each well. Luminescence was allowed to stabilize for ten minutes at room temperature, according to manufacturer instructions, and then measured on a FlexStation3 plate reader (Molecular Devices). Background subtracted luminescence of polyamide treated cells was normalized to vehicle treated cells, and non-linear regression analysis (Prism software, Graphpad) was performed to determine IC_{50} value.

Gene expression analysis by quantitative RT-PCR (qPCR)

LNCaP-95 cells were cultured for 24 hours after plating in six well plates at 7.5 x 10^4 cells/mL. Cells were treated with 10 μM **ARE-1** with 10 nM DHT or DMSO for 24 hours before harvest. RNA extraction (RNEasy columns, Qiagen), cDNA generation (ProtoScript II First Strand cDNA Synthesis Kit, NEB), and qRT-PCR (PowerUp SYBR Green Master Mix, Life Technologies, ABI7300 instrument) were done following manufacturer recommendations. Expression was normalized to β-glucuronidase.

Bioavailability in new formulation

All animal experiments were performed at the California Institute of Technology (Pasadena, CA) with prior IACUC approval. To evaluate a new formulation for polyamide delivery, **ARE-1** was injected at 10 mg/kg in a 1% polyvinylpyrrolidone K17 (PVP), 50 mM Tris, 0.9% saline

vehicle into the right flank of 6 C57BL/6J mice. Mice were anesthetized using isoflurane and blood collected retroorbitally at 30 min, 1h, 3h, 6h, 12h, and 24h after injection. Blood samples were centrifuged at 6000 rpm for 5 minutes to collect the serum, which was processed as previously published and analyzed by HPLC to determine polyamide concentration. (25) 9-aminoacridine was used as an internal standard.

Xenograft assay

Male SCID hairless outbred (SHO) mice (4-6 weeks old) were obtained from Charles River Laboratories. LNCAP-95 cells (3×10^6) were injected into the flanks of the mice as a 1:1 mixture in Matrigel (BD Biosciences). Mice were monitored for the appearance of tumors and calipered twice weekly once tumors appeared. When tumors reached 100 mm^3 (using 0.5*l*w*w), animals were castrated by veterinary staff. Following surgery, animals were monitored daily for 3 days, and allowed to recover for 7-10 days prior to the start of treatment. After the recovery period, animals were randomly assigned to treated or vehicle groups, and injected 3 times per week with 2.5 mg/kg **ARE-1** or vehicle (1% polyvinylpyrrolide K17 (PVP), 50 mM Tris, 0.9% saline) for 3 weeks. Tumor growth was monitored weekly by calipers, and growth compared to starting size. Animals were anesthetized with 2-5% isoflurane/air when necessary, and sterile technique was used for all procedures. Animal health was monitored daily by veterinary staff, and any animals exhibiting signs of distress were euthanized by administration of isoflurane followed by carbon dioxide.

Chromatin immunoprecipitation

Genomic occupancy of full length AR was determined by chromatin immunoprecipitation (ChIP) with the PG21 antibody (Millipore). LNCAP-95 cells were plated at 20 million cells per plate in phenol red free RPMI 1640 supplemented with 10% CTFBS and allowed to adhere for 24 hours. The cells were treated with 10 μM **ARE-1** with either 10 nM DHT or DMSO for 24 hours. Formaldehyde crosslinking was performed and chromatin was immunoprecipitated by previously published methods. (12) DNA was then harvested by phenol chloroform extraction and purified using the Monarch PCR & DNA Cleanup kit (NEB). Quantitative PCR was used to validate enrichment at the KLK3 ARE I site (5'-TGCATCCAGGGTGATCTAGT-3' and 5'-ACCCAGAGCTGTGGAAGG-3') compared to a negative internal locus (5'-TAGAAGGGGGATAGGGGAAC-3' and 5'-CCAGAAAACTGGCTCCTTCTT-3') prior to submission for sequencing. Each sample was immunoprecipitated as 3 technical replicates, which were combined for sequencing on an Illumina HiSeq2500. Biological replicates of each treatment condition were acquired. Input DNA (not immunoprecipitated) was also extracted and purified using the same methods and submitted for sequencing.

ChIP-Seq analysis

At least 29.7 million reads were sequenced for each sample. Reads were mapped to the human genome (hg19) using Bowtie2 v 2.2.3 and converted to BAM format with SAMtools. (26, 27) Peak calling was performed using the model-based analysis of ChIP-Seq (MACS2) program for each replicate. (28) Peaks from each replicate of each condition were

compared using IDR to determine a set of reproducible peaks, which was then submitted to MEME-ChIP (http://meme-suite.org/tools/meme-chip) for motif analysis. (29–31) Peaks selected by IDR were converted to bigWig format for viewing in the UCSC genome browser (http://genome.ucsc.edu).

Differential analysis between treatment conditions was conducted using PePr. (32) PePr results were used for all further analysis. BEDtools was used for overlap analysis and peak annotation was performed using ChIPseeker. (33, 34) Differentially changed peaks were submitted to MEME-ChIP for motif finding as above. Based on the MEME-ChIP results, Homer was used to examine the density of specific motifs within peaks. (35) Data has been deposited and can be accessed in GEO (GSE125552).

Thermal stabilization assay

Melting temperature analysis of the DNA oligos 5′-TTGTAGAACACGTT-3′, 5′-TTGTAGGACACGTT-3′, 5′-TTGTGGAACACGTT-3′, and 5′-TTGTGGGACACGTT-3′ in the presence of **ARE-1** was conducted as previously described. (36)

Statistical analysis

All statistical analysis was performed in GraphPad Prism. Gene expression data was normalized to the DHT induced condition and ANOVA analysis was performed on three biological replicates using the Dunnett's test for multiple comparisons. Statistical analysis of tumor percentage growth between vehicle and **ARE-1** treated groups (N=11 per group) was performed using the unpaired t-test. All reported p-values are two-sided.

4.3 Results

Nuclear uptake and cytotoxicity

Py-Im polyamide **ARE-1** has been previously shown to exhibit antiproliferative activity towards several models of prostate cancer including LNCaP, LNCaP-AR, VCaP, and LREX'. (14, 22) We further evaluate the activity of **ARE-1** in LNCaP-95 cells, which derive their resistance from the expression of AR splice variants. (37) Nuclear localization of **ARE-1** (Figure 4.1A) was confirmed using a fluorescein analog, **ARE-1-FITC** (Figure S4.1), in LNCaP-95 cells (Figure 4.1B). Antiproliferative effect of **ARE-1** towards LNCaP-95 cell growth was evaluated using the CTG assay and compared against the antiandrogen enzalutamide and pyrvinium pamoate (pyrvinium), a molecule that has been reported to bind to the AR DNA binding domain to prevent AR-DNA interactions. (38) Results from the assay show the 72hr growth inhibition IC_{50}s for **ARE-1**, enzalutamide, and pyrvinium to be 20.1 μM, >30 μM, and 44 nM, respectively. A synergistic effect was observed when a subtoxic concentration of enzalutamide (5 μM) was combined with polyamide, and the IC_{50} was reduced to 3.4 μM. Changes to *KLK3* gene expression was also evaluated in LNCaP-95 cells treated with **ARE-1**, enzalutamide, pyrvinium, and a combination of **ARE-1** with pyrvinium or enzalutamide (Figure 4.1D). After 24hr of treatment, the greatest reduction in *KLK3* expression from treatment with a single agent came from **ARE-1**, and combining either additional agent with **ARE-1** further reduced gene expression. Based on these cell culture results, we further evaluated the antitumor effects of **ARE-1** in LNCaP-95 xenografts using an optimized

formulation that increased the subcutaneous bioavailability when compared to the previously used DMSO/saline vehicle (Figure S4.2A). Animals were engrafted with LNCaP-95 cells and monitored until palpable tumors were observed. Once tumors reached 100mm^3, the animals were castrated, allowed to recover for approximately one week, and then randomized before treatment (Figure 4.1E). The animals were treated with either vehicle or 2.5mg/kg **ARE-1** subcutaneously MWF for 3 weeks. The vehicle treated group grew approximately 380%, while the **ARE-1** treated group grew 225%, for a 40% reduction in tumor size in the polyamide treated mice (Figure 4.1F). Animal weight was measured at each injection and was not adversely affected (Figure S4.2B).

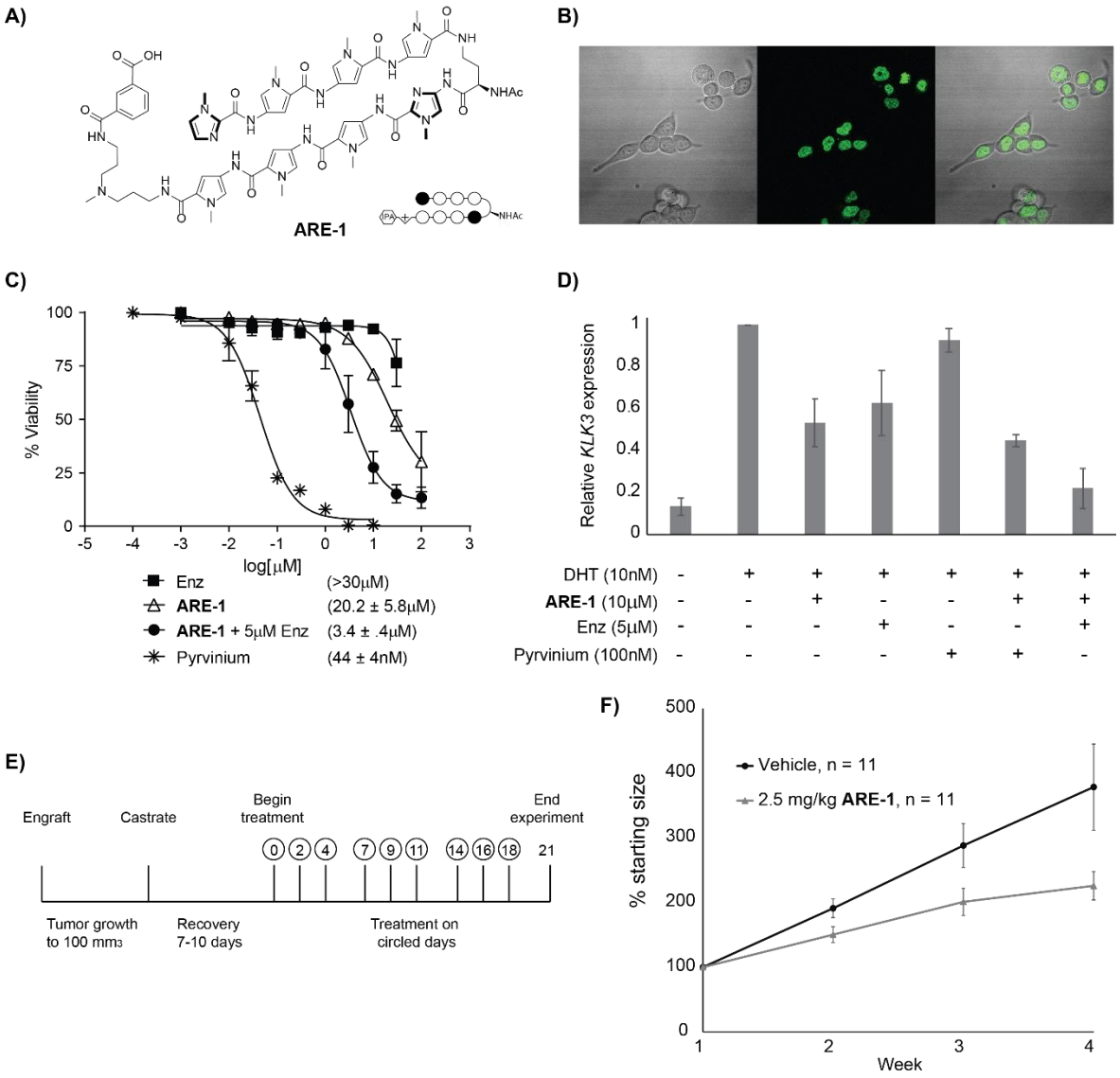

Figure 4.1 A) Structure of Py-Im polyamide **ARE-1. B)** Nuclear localization of **ARE-1-FITC** in LNCaP-95 cells after 16h treatment. **C)** Cell viability as determined by CellTiterGlo assay after 72h treatment. IC_{50} is indicated in parentheses. **D)** Relative expression of *KLK3* in LNCaP-95 cells after the indicated treatments. Cells were co-treated with **ARE-1**, enzalutamide, or pyrvinium pamoate and DHT at the indicated concentrations and RNA harvested at 24h. **E)** Schedule of LNCaP-95 xenograft experiment. Animals were engrafted, allowed to grow tumors, castrated, allowed to recover for 7-10 days, and then treated with **ARE-1** or vehicle at indicated times. **F)** Tumor volumes of LNCaP-95 xenografts in castrated mice treated with vehicle or 2.5 mg/kg **ARE-1** as shown in E. N=11 for both groups. * $P < 0.05$, ** $P < 0.01$, **** $P < 0.0001$.

Genomic perturbation of androgen receptor occupancy

The effects of Py-Im polyamide treatment on androgen receptor occupancy on chromatin have previously been explored by chromatin immunoprecipitation experiments. A related Py-Im polyamide, targeting the same sequence as **ARE-1**, has previously been shown to decrease occupancy of AR at the KLK3 promoter and enhancer in LNCaP cells. (12) In LNCaP-95 cells, a similar reduction at the KLK3 promoter ARE I is seen after 24hr of cotreatment with **ARE-1** and 10nM DHT (Figure S4.3A). In this study, we explored the genomic effect **ARE-1** treatment has on AR occupancy using ChIP-Seq analysis. Sequencing results of biological duplicates of non-treated (NT), 10nM DHT treated (DHT), and 10nM DHT and 10μM **ARE-1** treated (DHT+**ARE-1**) showed approximately 30 million reads mapping for all samples (Figure S4.3B). Sequencing reads were aligned to hg19 and select AR target genes are shown (Figure 4.2A-B). Motif analysis by MEME discovered the forkhead binding motif in all samples, and the complete androgen response element (ARE) was discovered in the DHT and DHT + **ARE-1** samples (Figure S4.3C). Differential binding of DHT/NT and DHT/(DHT+**ARE-1**) was calculated using PePr. Analysis revealed 16,015 peaks increased in DHT over non-treated (DHT/NT) and 6,343 differentially changed DHT/(DHT+**ARE-1**) peaks, of which 4,921 overlapped with DHT inducible peaks (Figure 4.2C). Correlation of peak location to genomic regions, conducted by ChIPseeker, showed no difference between the DHT/NT, DHT/(DHT+**ARE-1**), and overlap peaks, suggesting that **ARE-1** does not have a regional binding preference (Figure 4.2D). Motif analysis of peaks unique to DHT/NT

revealed the canonical ARE where the first half-site is 5′-RGNACA-3′. In this motif, the first position is selective for A or G (R) and the third position is degenerate for any base (N) (Figure 4.2E). Motif analysis of the overlapping peaks between DHT/NT and DHT/(DHT+**ARE-1**) also revealed a complete ARE; however, the first half-site has the sequence 5′-RGWACA-3′, where the third position shows selectivity for A or T (Figure 4.2E); additional motifs can be found in the supplemental information (Figure S4.4A). Comparison of the letter probability matrix between the DHT/NT unique peaks and the overlapping peaks show more A character in the first position and reduced C and G character in the third position in the overlapping motif (Figure S4.4B).

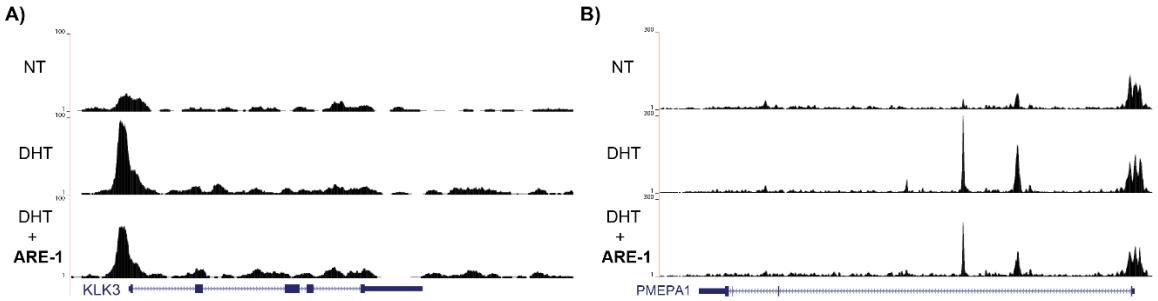

C)

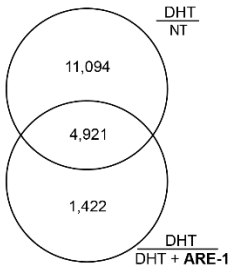

D)

	DHT / NT	DHT / DHT + ARE-1	Overlap
5' UTR	0.3%	0.2%	0.2%
Promoter	3.4%	2.3%	2.1%
1st Exon	0.2%	0.1%	0.2%
Other Exon	2.2%	1.5%	1.6%
1st Intron	16.5%	16.3%	16.9%
Other Intron	32.0%	33.0%	32.7%
Downstream	0.7%	0.7%	0.7%
3' UTR	1.7%	1.7%	1.7%
Distal Intergenic	43.1%	44.3%	44.0%

E)

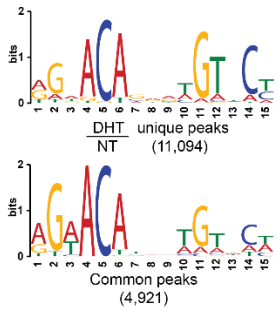

Figure 4.2 ChIP-seq analysis of the *KLK3* promoter ARE I **(A)** and PMEPA1 **(B)**. **C)** Overlap of peaks differentially changed in DHT relative to NT, and peaks changed in DHT relative to DHT and **ARE-1**. **D)** Identified peaks were annotated by genomic region by ChIPseeker. **E)** Top ARE motif found by MEME in the indicated peak sets.

Of the possible permutations of the first ARE half-site, **ARE-1** is expected to have the strongest binding to the sequences 5′-AGWACA-3′. Based on Py-Im polyamide pairing rules, **ARE-1** is expected to have lower binding to the sequences 5′-GGWACA-3′ and 5′-AGGACA-3′, which contain single base mismatches, and to have little binding to the sequence 5′-GGGACA-3′, which contains two mismatches (Figure 4.3A). (17–20) DNA thermal stability experiments confirmed this trend and showed **ARE-1** stabilized match sequences by ~9°C; single mismatches reduced thermal stability by ~2-4°C. **ARE-1** showed no significant thermal stabilization to a double mismatch sequence (Figure 4.3B).

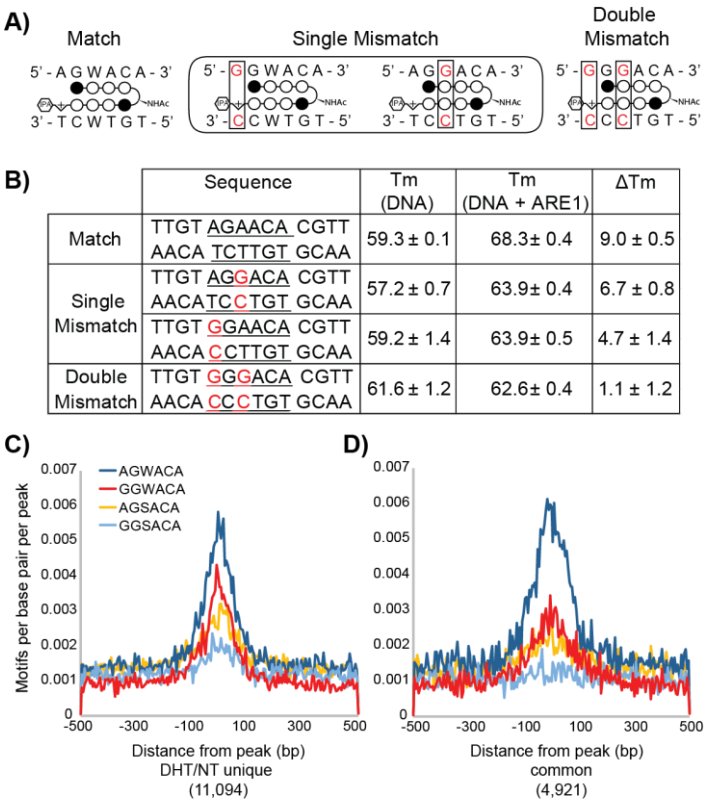

	Sequence	Tm (DNA)	Tm (DNA + ARE1)	ΔTm
Match	TTGT AGAACA CGTT AACA TCTTGT GCAA	59.3 ± 0.1	68.3± 0.4	9.0 ± 0.5
Single Mismatch	TTGT AGGACA CGTT AACA TCCTGT GCAA	57.2 ± 0.7	63.9± 0.4	6.7 ± 0.8
	TTGT GGAACA CGTT AACA CCTTGT GCAA	59.2 ± 1.4	63.9± 0.5	4.7 ± 1.4
Double Mismatch	TTGT GGGACA CGTT AACA CCCTGT GCAA	61.6 ± 1.2	62.6± 0.4	1.1 ± 1.2

Figure 4.3 A) Illustration of match and mismatch **ARE-1** binding sites. Mismatches are shown in red and boxed. **B)** Melting temperature analysis of match and mismatch sequences shown in **A. C + D)** Motif density analysis of possible ARE half sites in peaks unique to DHT/NT **(C)** and overlapping between DHT/NT and DHT/DHT + **ARE-1 (D)**.

The ARE half-site sequence 5′-RGNACA-3′ can be split into four sequences: 5′-AGWACA-3′, 5′-GGWACA-3′, 5′-AGSACA-3′, and 5′-GGSACA-3′, where S represents G or C. Density analysis of these 4 motifs revealed 5′-AGWACA-3′ to be significantly enriched around the peak center of DHT/NT and DHT/(DHT+**ARE-1**) overlap peaks compared to the other possible motifs. A lesser effect was found for the DHT/NT unique peaks (Figure 4.3 C-D).

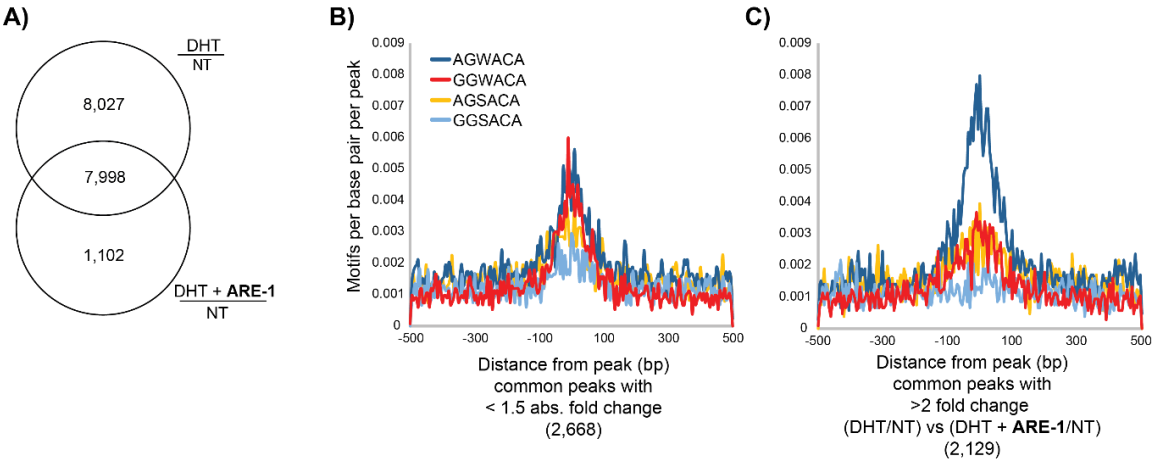

Figure 4.4 A) Venn diagram showing the overlap of peaks differentially changed in DHT as compared to NT with peaks changed by DHT and **ARE-1** as compared to NT. **B + C)** Density analysis of overlapping peaks with < 1.5 absolute fold change between DHT/NT and DHT+**ARE-1**/NT **(B)** and peaks with > 2 fold change when comparing DHT/NT to DHT+**ARE-1**/NT **(C)**.

To confirm that the enrichment for 5′-AGWACA-3′ was only present in regions where AR peaks are affected by **ARE-1**, we examined common peaks between DHT/NT and (DHT+**ARE-1**)/NT samples (Figure 4.4A). Of the 7,998 overlapping peaks, 2,668 peaks had an absolute change of less than 1.5 fold. Motif density analysis in these unchanged regions showed no enrichment of 5′-AGWACA-3′ (Figure 4.4B). Comparatively, 5′-AGWACA-3′ was significantly enriched in 2,129 peaks showing greater than 2 fold change between DHT/NT and (DHT+**ARE-1**)/NT.

4.4 Discussion

Py-Im polyamides have been shown to inhibit the signaling of oncogenic transcription factors and reduce their binding at select loci in ChIP experiments. (12, 39, 40) Genomic binding of Py-Im polyamides linked to DNA alkylators have also been examined. (41, 42) In this study, we elucidate the genome-wide effects of polyamide treatment on the androgen receptor on chromatin. Py-Im polyamide **ARE-1** is a cell permeable molecule that exerts anti-proliferative effects towards several prostate cancer models, including the castration and enzalutamide resistant models LREX' and now LNCaP-95.

In this present study, we find that **ARE-1** localizes to LNCaP-95 nucleus within 16 hrs of dosing, and is able to repress ligand-induced gene expression after 24 hrs of co-treatment with DHT. In this time frame, our ChIP-Seq results show **ARE-1** is able to repress ~30% of DHT inducible peaks. Motif analysis of these AR peaks repressed by **ARE-1**, which is selective for the sequence 5'-WGWWCW-3', indicates that these loci are enriched for canonical AREs with 5'-RGWACA-3' as the first half-site compared to the common 5'-RGNACA-3' half-site. Thus, the differential effects on AR-DNA binding events *in vivo* reflect the DNA target sequence binding preference of **ARE-1** *in vitro*. These experiments provide evidence of the *in vivo* sequence selectivity of **ARE-1**, and provide a snapshot of how **ARE-1** modulates the AR cistrome.

References

1. Huggins C and Hodges CV (1941) Studies on Prostatic Cancer. I. The Effect of Castration, of Estrogen and of Androgen Injection on Serum Phosphatases in Metastatic Carcinoma of the Prostate. *Cancer Res*, **1**, 293.
2. Giorgi EP, Shirley IM, Grant JK and Stewart JC (1973) Androgen dynamics in vitro in the human prostate gland. Effect of cyproterone and cyproterone acetate. *Biochem. J.*, **132**, 465–474.
3. Heinlein CA and Chang C (2004) Androgen Receptor in Prostate Cancer. *Endocrine Reviews*, **25**, 276–308.
4. Sharifi N (2005) Androgen Deprivation Therapy for Prostate Cancer. *JAMA*, **294**, 238.
5. Tran C, Ouk S, Clegg NJ, Chen Y, Watson PA, Arora V, Wongvipat J, Smith-Jones PM, Yoo D, Kwon A, *et al.* (2009) Development of a Second-Generation Antiandrogen for Treatment of Advanced Prostate Cancer. *Science*, **324**, 787–790.
6. Clegg NJ, Wongvipat J, Joseph JD, Tran C, Ouk S, Dilhas A, Chen Y, Grillot K, Bischoff ED, Cai L, *et al.* (2012) ARN-509: A Novel Antiandrogen for Prostate Cancer Treatment. *Cancer Research*, **72**, 1494–1503.
7. Shore ND, Tammela TL, Massard C, Bono P, Aspegren J, Mustonen M and Fizazi K (2018) Safety and Antitumour Activity of ODM-201 (BAY-1841788) in Chemotherapy-naïve and CYP17 Inhibitor-naïve Patients: Follow-up from the ARADES and ARAFOR Trials. *Eur Urol Focus*, **4**, 547–553.
8. Chen CD, Welsbie DS, Tran C, Baek SH, Chen R, Vessella R, Rosenfeld MG and Sawyers CL (2004) Molecular determinants of resistance to antiandrogen therapy. *Nat. Med.*, **10**, 33–39.
9. Dehm SM and Tindall DJ (2011) Alternatively spliced androgen receptor variants. *Endocr. Relat. Cancer*, **18**, R183-196.
10. Korpal M, Korn JM, Gao X, Rakiec DP, Ruddy DA, Doshi S, Yuan J, Kovats SG, Kim S, Cooke VG, *et al.* (2013) An F876L mutation in androgen receptor confers genetic and phenotypic resistance to MDV3100 (enzalutamide). *Cancer Discov*, **3**, 1030–1043.
11. Elshan NGRD, Rettig MB and Jung ME (2018) Molecules targeting the androgen receptor (AR) signaling axis beyond the AR-Ligand binding domain: ELSHAN ET AL. *Medicinal Research Reviews*, 10.1002/med.21548.
12. Nickols NG and Dervan PB (2007) Suppression of androgen receptor-mediated gene expression by a sequence-specific DNA-binding polyamide. *Proceedings of the National Academy of Sciences of the United States of America*, **104**, 10418–10423.
13. Hargrove AE, Martinez TF, Hare AA, Kurmis AA, Phillips JW, Sud S, Pienta KJ and Dervan PB (2015) Tumor Repression of VCaP Xenografts by a Pyrrole-Imidazole Polyamide. *PLoS ONE*, **10**, e0143161.

14. Kurmis AA, Yang F, Welch TR, Nickols NG and Dervan PB (2017) A Pyrrole-Imidazole Polyamide Is Active against Enzalutamide-Resistant Prostate Cancer. *Cancer Research*, **77**, 2207–2212.
15. Trauger JW, Baird EE and Dervan PB (1996) Recognition of DNA by designed ligands at subnanomolar concentrations. *Nature*, **382**, 559–561.
16. Hsu CF, Phillips JW, Trauger JW, Farkas ME, Belitsky JM, Heckel A, Olenyuk BZ, Puckett JW, Wang CCC and Dervan PB (2007) Completion of a Programmable DNA-Binding Small Molecule Library. *Tetrahedron*, **63**, 6146–6151.
17. White S, Baird EE and Dervan PB (1997) On the pairing rules for recognition in the minor groove of DNA by pyrrole-imidazole polyamides. *Chemistry & Biology*, **4**, 569–578.
18. Kielkopf CL, White S, Szewczyk JW, Turner JM, Baird EE, Dervan PB and Rees DC (1998) A structural basis for recognition of A.T and T.A base pairs in the minor groove of B-DNA. *Science*, **282**, 111–115.
19. Kielkopf CL, Baird EE, Dervan PB and Rees DC (1998) Structural basis for G.C recognition in the DNA minor groove. *Nat. Struct. Biol.,* **5**, 104–109.
20. Foister S, Marques MA, Doss RM and Dervan PB (2003) Shape selective recognition of T.A base pairs by hairpin polyamides containing N-terminal 3-methoxy (and 3-chloro) thiophene residues. *Bioorg. Med. Chem.*, **11**, 4333–4340.
21. Chenoweth DM and Dervan PB (2010) Structural Basis for Cyclic Py-Im Polyamide Allosteric Inhibition of Nuclear Receptor Binding. *Journal of the American Chemical Society*, **132**, 14521–14529.
22. Yang F, Nickols NG, Li BC, Szablowski JO, Hamilton SR, Meier JL, Wang C-M and Dervan PB (2013) Animal toxicity of hairpin pyrrole-imidazole polyamides varies with the turn unit. *Journal of Medicinal Chemistry*, **56**, 7449–7457.
23. Yang F, Nickols NG, Li BC, Marinov GK, Said JW and Dervan PB (2013) Antitumor activity of a pyrrole-imidazole polyamide. *Proceedings of the National Academy of Sciences of the United States of America*, **110**, 1863–1868.
24. Martinez TF, Phillips JW, Karanja KK, Polaczek P, Wang C-M, Li BC, Campbell JL and Dervan PB (2014) Replication stress by Py-Im polyamides induces a non-canonical ATR-dependent checkpoint response. *Nucleic Acids Res*, **42**, 11546–11559.
25. Raskatov JA, Hargrove AE, So AY and Dervan PB (2012) Pharmacokinetics of Py-Im Polyamides Depend on Architecture: Cyclic versus Linear. *Journal of the American Chemical Society*, **134**, 7995–7999.
26. Langmead B, Trapnell C, Pop M and Salzberg SL (2009) Ultrafast and memory-efficient alignment of short DNA sequences to the human genome. *Genome Biology*, **10**, R25.
27. Li H, Handsaker B, Wysoker A, Fennell T, Ruan J, Homer N, Marth G, Abecasis G, Durbin R and 1000 Genome Project Data Processing Subgroup (2009) The Sequence Alignment/Map format and SAMtools. *Bioinformatics*, **25**, 2078–2079.

28. Zhang Y, Liu T, Meyer CA, Eeckhoute J, Johnson DS, Bernstein BE, Nusbaum C, Myers RM, Brown M, Li W, *et al.* (2008) Model-based analysis of ChIP-Seq (MACS). *Genome Biol.*, **9**, R137.
29. Li Q, Brown JB, Huang H and Bickel PJ (2011) Measuring reproducibility of high-throughput experiments. *The Annals of Applied Statistics*, **5**, 1752–1779.
30. Machanick P and Bailey TL (2011) MEME-ChIP: motif analysis of large DNA datasets. *Bioinformatics*, **27**, 1696–1697.
31. Bailey TL, Boden M, Buske FA, Frith M, Grant CE, Clementi L, Ren J, Li WW and Noble WS (2009) MEME SUITE: tools for motif discovery and searching. *Nucleic Acids Research*, **37**, W202–W208.
32. Zhang Y, Lin Y-H, Johnson TD, Rozek LS and Sartor MA (2014) PePr: a peak-calling prioritization pipeline to identify consistent or differential peaks from replicated ChIP-Seq data. *Bioinformatics*, **30**, 2568–2575.
33. Quinlan AR and Hall IM (2010) BEDTools: a flexible suite of utilities for comparing genomic features. *Bioinformatics*, **26**, 841–842.
34. Yu G, Wang L-G and He Q-Y (2015) ChIPseeker: an R/Bioconductor package for ChIP peak annotation, comparison and visualization. *Bioinformatics*, **31**, 2382–2383.
35. Heinz S, Benner C, Spann N, Bertolino E, Lin YC, Laslo P, Cheng JX, Murre C, Singh H and Glass CK (2010) Simple combinations of lineage-determining transcription factors prime cis-regulatory elements required for macrophage and B cell identities. *Mol. Cell*, **38**, 576–589.
36. Dose C, Farkas ME, Chenoweth DM and Dervan PB (2008) Next generation hairpin polyamides with (R)-3,4-diaminobutyric acid turn unit. *J Am Chem Soc*, **130**, 6859–6866.
37. Liu LL, Xie N, Sun S, Plymate S, Mostaghe ,E and Dong X (2014) Mechanisms of the androgen receptor splicing in prostate cancer cells. *Oncogene*, **33**, 3140–3150.
38. Jones JO, Bolton EC, Huang Y, Feau C, Guy RK, Yamamoto KR, Hann B and Diamond MI (2009) Non-competitive androgen receptor inhibition in vitro and in vivo. *Proceedings of the National Academy of Sciences*, **106**, 7233–7238.
39. Nickols NG, Jacobs CS, Farkas ME and Dervan PB (2007) Modulating hypoxia-inducible transcription by disrupting the HIF-1-DNA interface. *ACS Chem Biol*, **2**, 561–571.
40. Muzikar KA, Nickols NG and Dervan PB (2009) Repression of DNA-binding dependent glucocorticoid receptor-mediated gene expression. *Proc Natl Acad Sci U S A*, **106**, 16598–16603.
41. Erwin GS, Grieshop MP, Bhimsaria D, Do TJ, Rodríguez-Martínez JA, Mehta C, Khanna K, Swanson SA, Stewart R, Thomson JA, *et al.* (2016) Synthetic genome readers target clustered binding sites across diverse chromatin states. *Proc. Natl. Acad. Sci. U.S.A.*, **113**, E7418–E7427.
42. Chandran A, Syed J, Taylor RD, Kashiwazaki G, Sato S, Hashiya K, Bando T and Sugiyama H (2016) Deciphering the genomic targets of alkylating polyamide conjugates using high-throughput sequencing. *Nucleic Acids Research*, **44**, 4014–4024.

4.5 Supplemental material

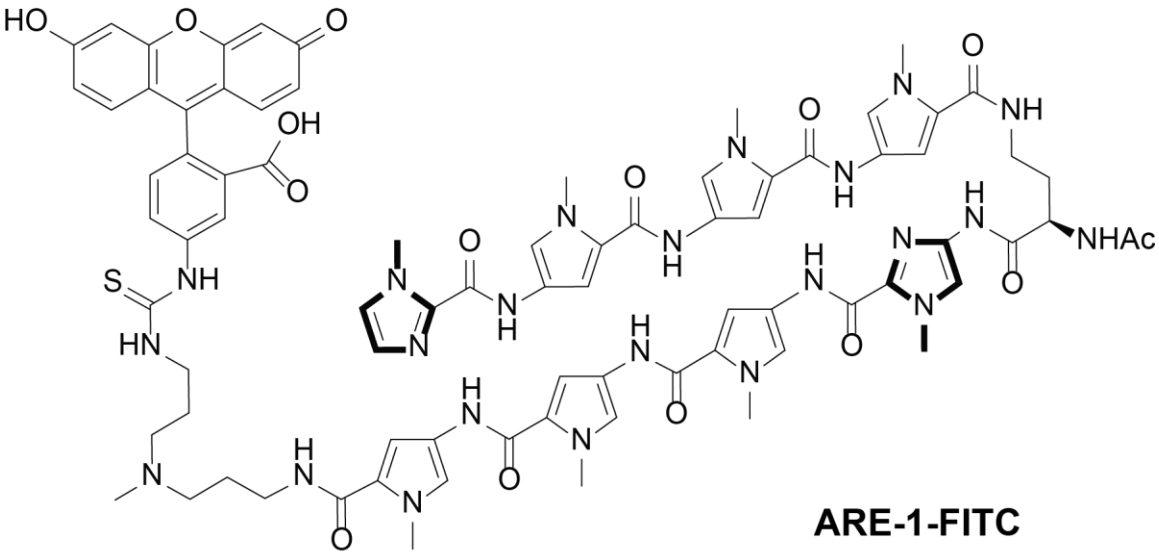

Figure S4.1 Chemical structure of **ARE-1-FITC.**

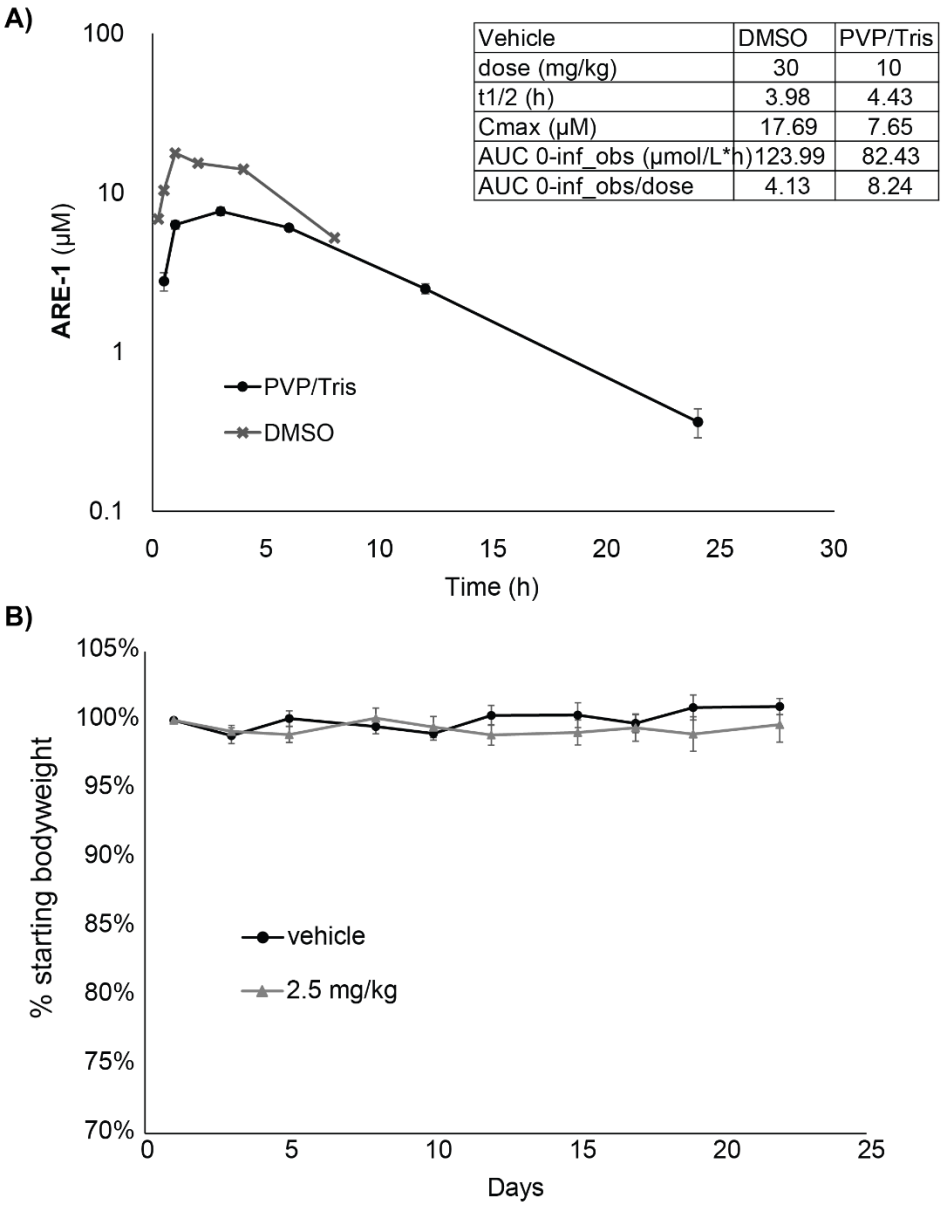

Figure S4.2 A) Pharmacokinetic analysis of **ARE-1** in PVP/Tris formulation compared to DMSO/saline formulation. **B)** Body weight changes of animals in LN95 xenograft experiment.

A)

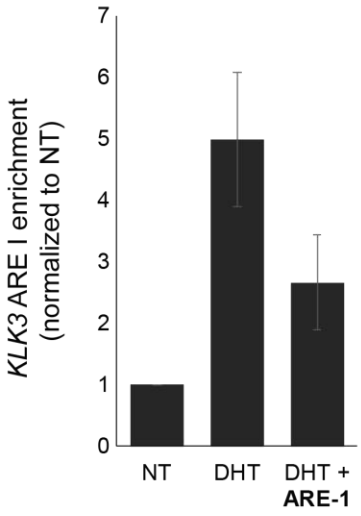

B)

	NT	DHT	DHT + **ARE-1**
Reads mapped (millions):			
rep 1	30.2	29.7	33.1
rep 2	30.0	43.5	44.5
(30 million recommended)			
Peaks:			
IDR	14,812	50,445	35,856
(rep 1)	(35,723)	(62,770)	(55,009)
(rep 2)	(24,801)	(84,015)	(45,102)

C)

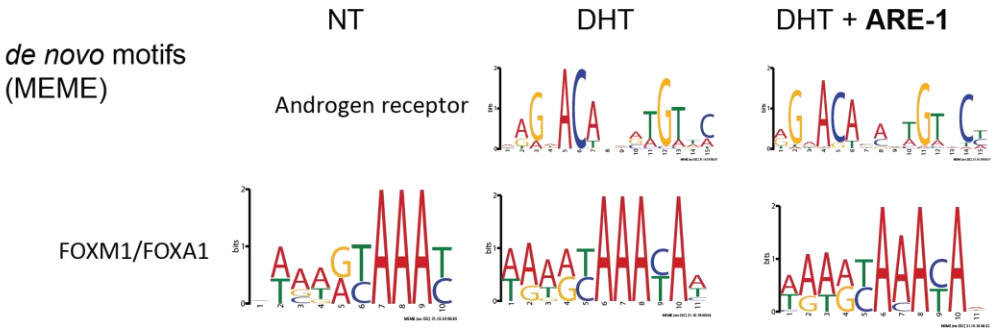

Figure S4.3 A) AR occupany of *KLK3* ARE I as determined by ChIP. **B)** Sequencing results from AR ChIP experiments of indicated conditions. **C)** *De novo* motif discovery by MEME of reproducible peaks as determined by IDR analysis.

A)

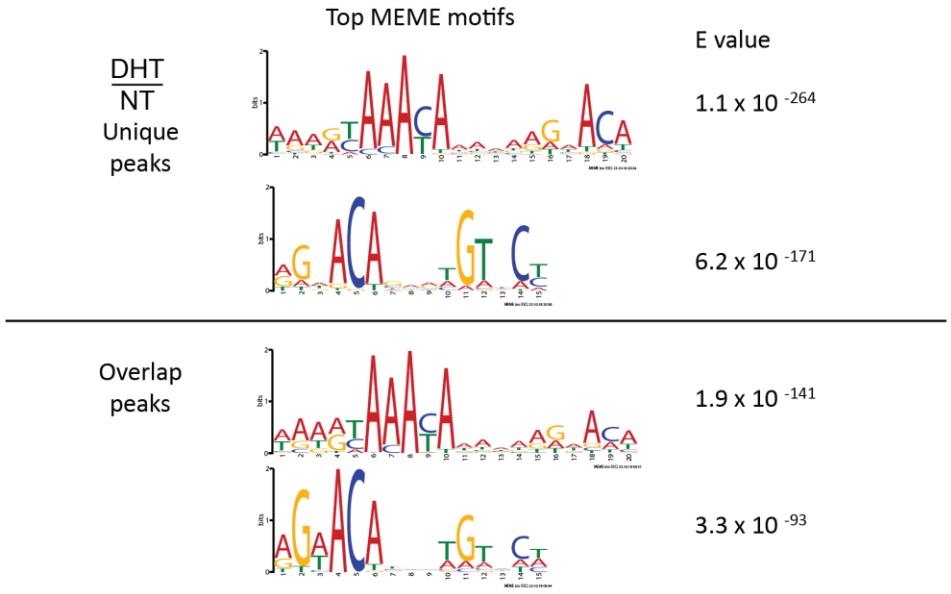

B)

DHT/NT unique				Overlap			
A	**C**	**G**	**T**	**A**	**C**	**G**	**T**
0.426237	0.000000	0.405094	0.168669	**0.632749**	0.000000	**0.270216**	0.097035
0.137914	0.017780	0.756367	0.087938	0.000000	0.000000	0.923854	0.076146
0.398606	0.093224	0.192456	0.315714	**0.578841**	0.057278	**0.000000**	0.363881
0.894762	0.005766	0.068957	0.030514	1.000000	0.000000	0.000000	0.000000
0.000000	0.974291	0.025709	0.000000	0.000000	1.000000	0.000000	0.000000
0.913023	0.003364	0.002643	0.080971	0.884097	0.000000	0.027628	0.088275
0.142960	0.227775	0.481019	0.148246	0.134097	0.237871	0.216981	0.411051
0.414224	0.143681	0.253484	0.188611	0.333558	0.201482	0.165094	0.299865
0.420471	0.140317	0.302739	0.136473	0.281671	0.327493	0.145553	0.245283
0.265738	0.160500	0.028111	0.545651	0.274259	0.062668	0.047170	0.615903
0.063671	0.010332	0.925997	0.000000	0.125337	0.066712	0.807951	0.000000
0.135031	0.035560	0.032436	0.796973	0.210916	0.099057	0.068059	0.621968
0.225613	0.181643	0.194858	0.397886	0.377358	0.194744	0.152965	0.274933
0.120855	0.849351	0.000000	0.029793	0.195418	0.645553	0.000000	0.159030
0.135992	0.364969	0.007448	0.491591	0.371968	0.229111	0.000000	0.398922

Figure S4.4 A) Motif analysis of differentially bound sites using MEME-ChIP. Top two results are shown for peaks unique to DHT/NT and overlapping betwen DHT/NT and DHT/DHT+**ARE-1**. **B)** Motif matrix of androgen response element motif logo presented in **(A).** Positions 1 and 3 are highlighted in red.

Appendix A

Influence of structure on aqueous solubility of hairpin Py-Im polyamides

A.1 Introduction

The biological activity of Py-Im polyamides has been extensively explored in the context of enzymatic and cell culture experiments. (1–7) Py-Im polyamides have also shown efficacy against multiple xenograft models. (7–9) The subcutaneous administration of polyamides to animals, however, requires high levels of DMSO, typically 20% (10, 11) The goal of this study was to improve the aqueous solubility of a hairpin Py-Im polyamide by chemical modifications for use in future animal studies. Three Py-Im polyamides were selected for this purpose; their structures are shown in Figure A.1. Polyamides **1** and **2** contain a 2,2'-(Ethylenedioxy)diethylamine (PEG) linker connecting the core to the C-terminal isophthalic acid (IPA), and polyamide **3** contains the 3,3'-Diamino-N-methyldipropylamine (triamine) linker.

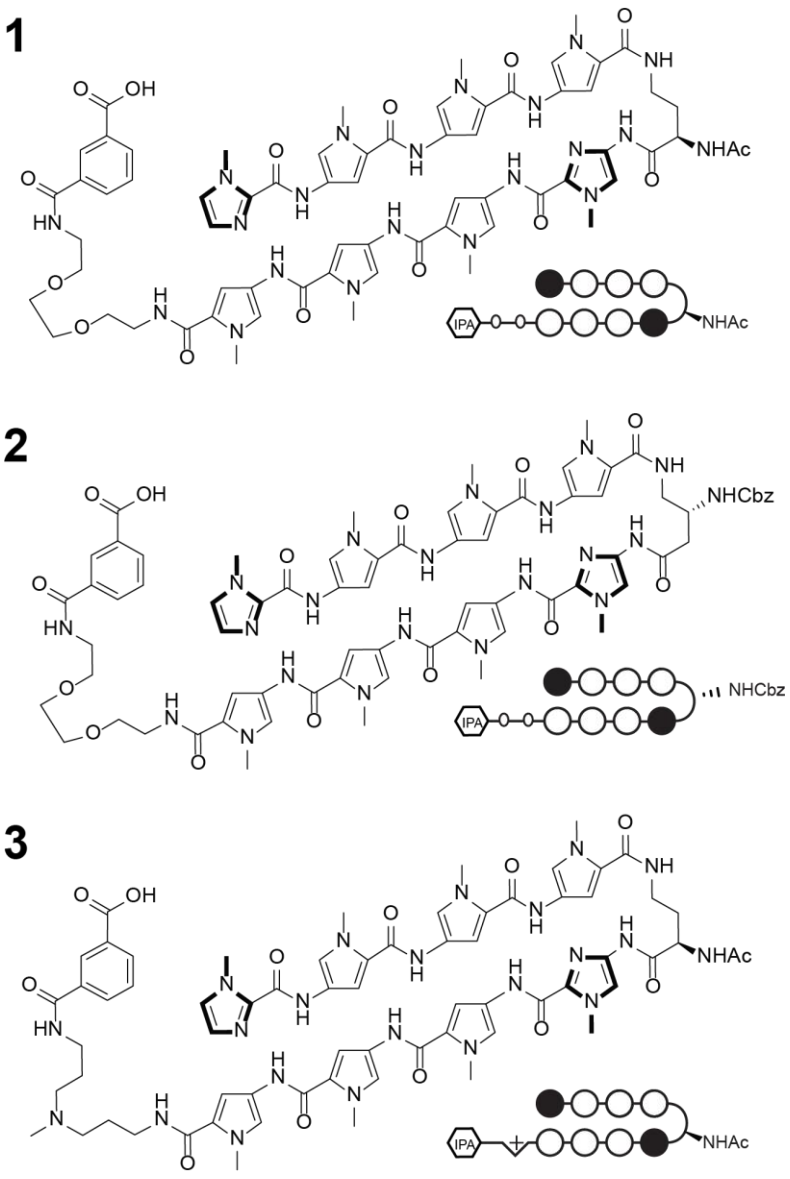

Figure A.1 Structure of Py-Im polyamides **1**-**3**.

A.2 Results

Aqueous solubility

The net charge of a molecule influences its aqueous solubility, and the pH of the solution can alter the charge. The standard hairpin polyamide carries a positive charge on the tertiary amine of the C-terminus and the adjacent IPA is negatively charged at physiological pH, leading to a net charge of 0, as shown in Figure A.2 A. Previously, it has been shown that replacing the triamine linker with a PEG linker results in similar biological activity. (12) This modification removes the positive charge, leaving the molecule with a net charge of -1 at physiological pH (Fig A.2 B). The solubility of polyamides **1** and **3** was tested in water at three pH levels, and two additional solutions at basic pHs (Figure A.2 C and D), where the target concentration was 1 mM. Polyamide **1** was found to be completely insoluble at low pH, but at least 70% soluble at pH 7 and above, in water, Tris, and PBS. In contrast, polyamide **3** was most soluble in water at a pH of 12, with solubility significantly decreased in other conditions. While the PEG linker improves solubility, the DNA thermal stabilization of polyamide **1** was much lower than that of polyamide **3** (table A.1).

5'-TTGC**TGTTCT**GCAAA-3'		
	Tm	**Δ**Tm
DNA	60.2	
Polyamide **3**	69.7	9.6
Polyamide **1**	65.1	4.9

Table A.1 Melting temperature analysis of polyamides **1** and **3**.

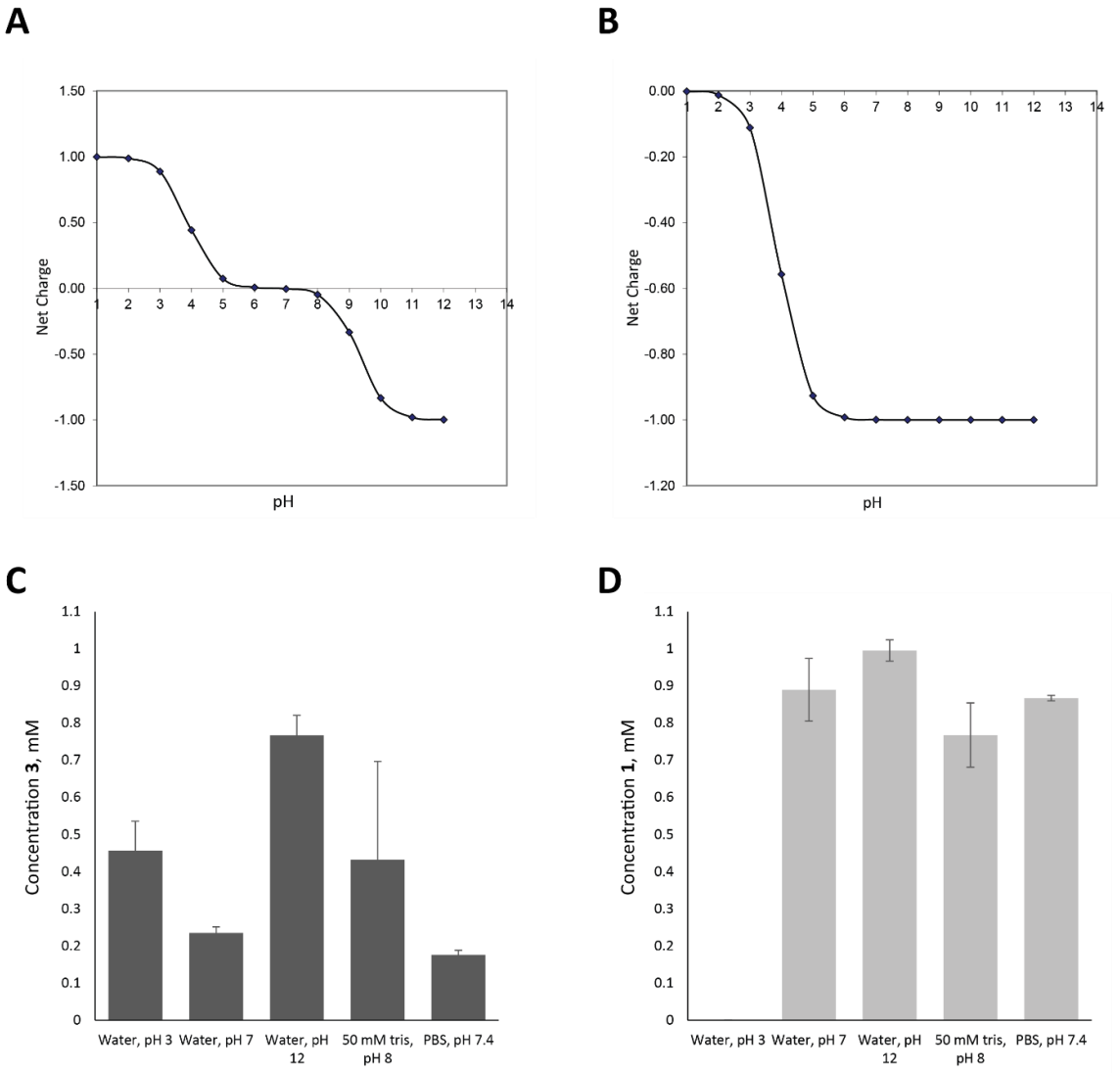

Figure A.2 Calculated net charge and aqueous solubility of Py-Im polyamides **3 (A+C)** and **1 (B+D)**.

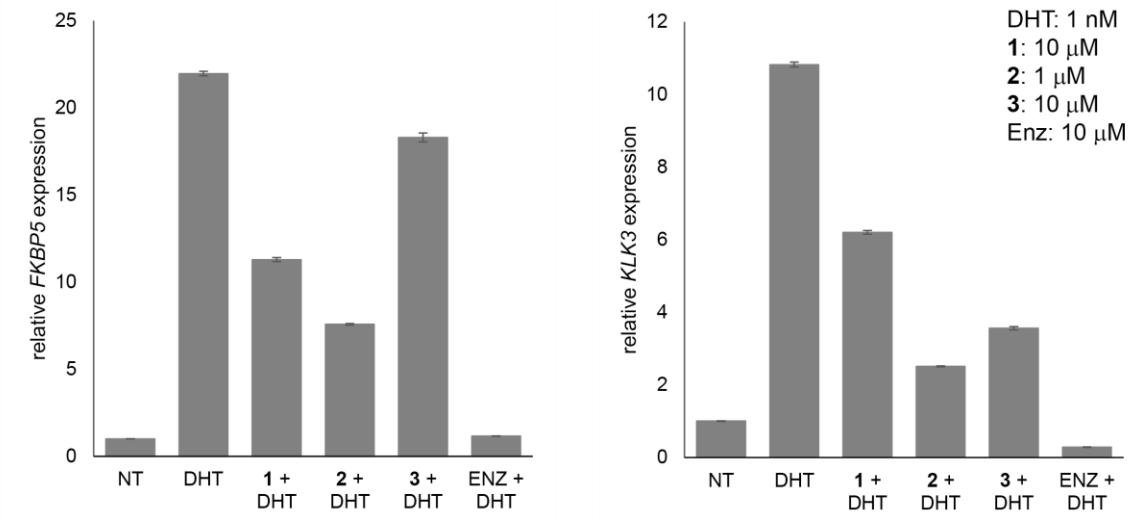

Figure A.3 Effect of polyamides **1**-**3** and enzalutamide on DHT-induced expression of *FKBP5* (left) and *KLK3* (right) in LNCaP-AR cells. Data shown represents one of two biological replicates.

Gene expression

Polyamide **3** has been shown to be toxic to multiple prostate cancer cell lines, both in cell culture and xenograft models, and to regulate expression of certain androgen receptor driven genes, including *KLK3* (PSA) and *FKBP5*. (8, 7, 9) The increased aqueous solubility of polyamide **1** compared to polyamide **3** at physiological pH makes it an attractive candidate for further development. Polyamide **2** was also evaluated to investigate if the effect of the PEG linker applies to other polyamide structures; polyamides with aryl (R)-3,4-diaminobutyric acid turns have been shown to be more biologically active than polyamides with (R)-2,4-diaminobutyric acid turns. (11) The effect of polyamides **1**-**3** on DHT induced gene expression was analyzed in LNCaP-AR cells. Cells were plated in charcoal treated FBS and allowed to adjust for 72 hours prior to treatment. All three polyamides reduced expression of both *KLK3* and *FKBP5* to below the DHT induced condition. Of the three,

polyamide **2** had the greatest effect, although only enzalutamide reduced expression of both genes to pre-induction levels.

Cytotoxicity

Cytotoxicity was assessed in a human prostate cancer cell line previously shown to be sensitive to polyamide **3** (Figure A.4 A). (9) Using the WST1 assay, polyamide **3** demonstrates toxicity at 72 hours in LNCaP-AR cells, with an IC_{50} of 6.2 ± 2.6 μM. At the same time point, there is no apparent toxicity caused by polyamide **1**. Viability was then investigated at 96 hours and found to be unchanged (Figure A.4 B). A cell counting experiment was then conducted to evaluate the cytotoxicity of polyamides **1** and **3** over a longer term. Cells were dosed with 10 μM polyamide **1** or **3**, and counted at days 0, 3, and 6. While polyamide **3** reduced growth by approximately 33% on day 3 and 60% on day 6, cells treated with polyamide **1** grew at the same rate as cells treated only with vehicle. (Figure A.4 C)

Cytotoxicity of polyamide **1**-**3** was also assessed by WST1 in a human pancreatic cancer cell line, AsPC1. After 72 hours of treatment, polyamide **1** was found to actually increase cell viability at the highest dose of 30 μM. Polyamide **3** did not demonstrate significant toxicity, and an IC_{50} value could not be calculated. Polyamide **2**, however, was extremely toxic, with an IC_{50} of 328 nM (Figure A.4 D).

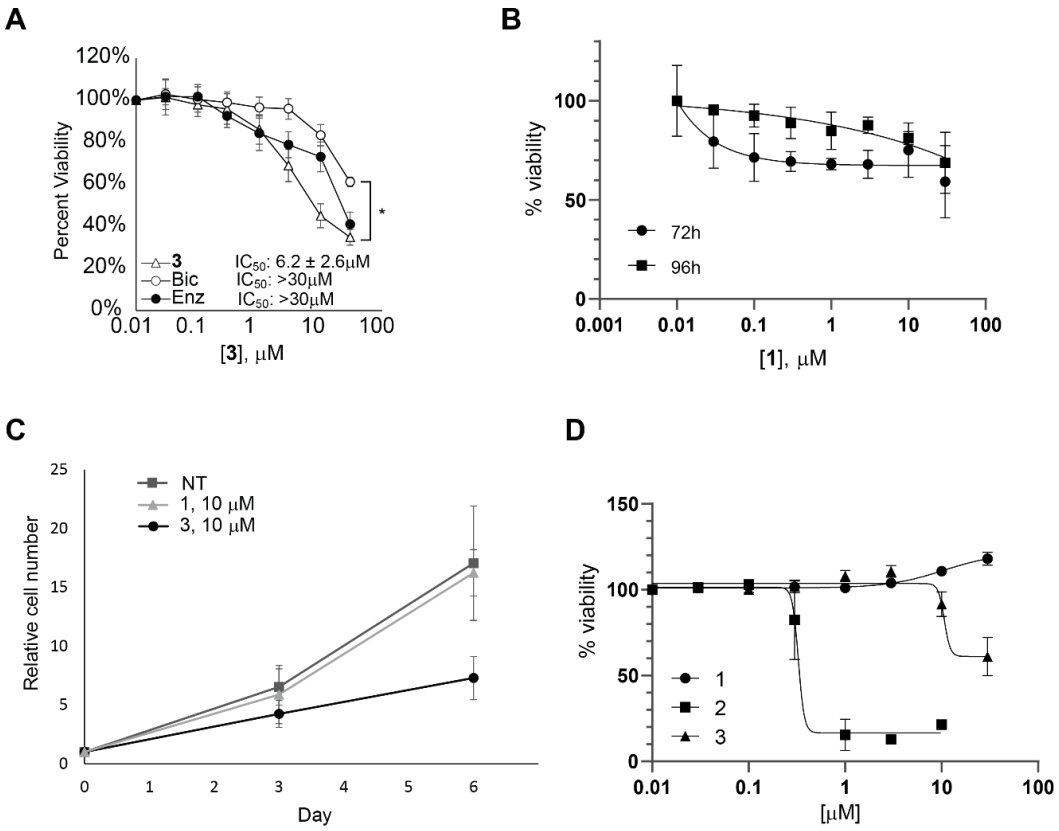

Figure A.4 Cytotoxicity of polyamides **1**-**3**. **A)** Cytotoxicity of polyamide **3**, enzalutamide, and bicalutamide in LNCaP-AR cells over 72 hours. IC_{50} = 6.2 ± 2.6 μM. Reproduced from Figure 3.1 B. **B)** Cytotoxicity of polyamide **1** in LNCaP-AR cells at 72 and 96 hours.No IC_{50}. **C)** Cell counting experiment in LNCaP-AR. Cells were dosed with indicated polyamide or vehicle on day 0 and counted on days 0, 3, and 6. **D)** Cytotoxicity of polyamides **1**-**3** in AsPC1 human pancreatic cancer cell line over 72 hours. Polyamide **2** IC_{50} = 328 nM.

In vivo toxicity

Based on the gene expression and cytotoxicity results, polyamide **2** was chosen for further assessment in animal models and preliminary toxicity experiments were conducted in healthy C57Bl6/J mice. For toxicity studies, animals were injected subcutaneously with polyamide **2** at 0.3 or 1 mg/kg in a single dose or daily until adverse reactions were observed. Animals were monitored daily for signs of toxicity and weight loss. After a slight initial dip, both animals that received a single injection returned to their starting weights.

The animal receiving 1 mg/kg daily injections experienced a significant weight loss after only 3 injections and was euthanized on day 4. The animal receiving daily 0.3 mg/kg injections was losing weight as well and injections were stopped after day 4. After a brief increase, the animal's weight continued to decrease until the experiment was ended on day 9.

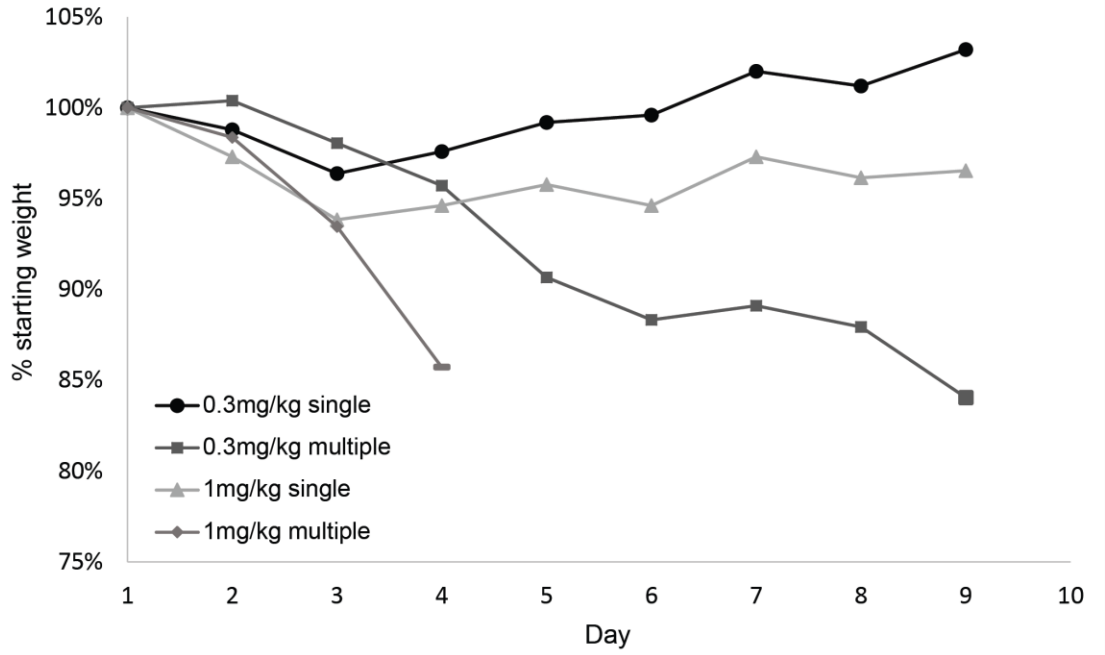

Figure A.5 Weight of animals injected with the indicated dose of polyamide **2**. Single injections were administered on day 1. Animals receiving multiple injections were dosed once per day until day 3 (1 mg/kg) or day 5 (0.3 mg/kg).

A.3 Methods

Aqueous solubility

Aqueous solubility was determined according to previously published procedures. (10) Polyamides were dissolved in the minimum possible amount of DMSO and quantified by UV-vis. Polyamide stock and additional DMSO were added to test solvents (water at pH 3, 7, or 12, 50 mM tris(hydroxymethyl)aminomethane at pH 8, or phosphate buffered saline

at pH 7.4) to reach 1 mM polyamide and 2% DMSO. Solutions were briefly vortexed, then sonicated for 20 minutes, incubated for 2 hours at room temperature, and centrifuged for 20 minutes at 15,700 x *g*. To determine final concentration in solution, sample was analyzed by analytical HPLC and compared to a standard curve, using 9-aminoacridine as an internal standard. Data shown is the average of two replicates; error is SEM.

Cytotoxicity

Cytotoxicity was investigated in two human prostate cancer cell lines, LNCaP-AR and 22Rv1, and one human pancreatic cancer cell line (AsPC1). For WST1 assays, cells were plated at 4 x 10^5, 1 x 10^6, and 5 x 10^5 per mL, respectively, allowed to adhere for 24 hours and then dosed with polyamide. Viability was measured at 72 hours for all cell lines, and also at 96 hours for LNCaP-AR and 22Rv1. All medium was removed following polyamide incubation at the indicated time points and replaced with one volume of WST-1 reagent (Roche) in medium according to manufacturer instructions. After 2 h of incubation at 37°C, the absorbance was measured on a FlexStation3 plate reader (Molecule Devices). Absorbance was normalized to the nontreated condition. Non-linear regression analysis (Prism software, Graphpad) was performed to determine IC_{50} values.

Cytotoxicity was also assessed by a cell counting assay in LNCaP-AR. Cells were plated in 6 well plates 4 x 10^4 cells/mL, allowed to adhere 24 hours, and dosed with 10 µM polyamide **1** or **3**. Cells were harvested and counted at time of dosing (day 0) and at days 3 and 6 after dosing.

Gene expression

LNCaP-AR cells were plated at 4 x 10^4 cells/mL in phenol-red free RPMI 1640 supplemented with 10% CTFBS and allowed to adjust for 72 hours prior to treatment. Cells were then co-treated with ethanol (vehicle) or DHT (1 nM) and polyamide or enzalutamide at 10 μM (polyamides **1**, **3**, and enzalutamide) or 1 μM (polyamide **2**). Cells were harvested 8 hours after treatment. RNA extraction (RNeasy, Qiagen), cDNA generation (Transcriptor First Strand cDNA Kit, Roche), and qRT-PCR (SYBR Green Master Mix, Applied Biosystems, ABI7300 instrument) were performed according to manufacturer instructions and expression was normalized to β–glucuronidase.

Thermal stabilization assay

Melting temperature analysis of the DNA oligo 5'-TTGCTGTTCTGCAAA-3' in the presence of polyamides **1** and **3** was conducted as previously described. (13)

***In vivo* toxicity**

All animal experiments were conducted with prior IACUC approval. For toxicity analysis, mice were injected subcutaneously with 0.3 mg/kg (n = 2) or 1 mg/kg (n = 2) polyamide **2** in a 1% polyvinylpyrrolidone/50 mM tris vehicle. One animal per dose was injected only on day one, and one animal was injected daily (3 days for 1 mg/kg and 5 days for 0.3 mg/kg). Animal weight was monitored daily for 9 days, and any animal exhibiting signs of toxicity (including weight below 85% initial weight) was euthanized by CO_2 inhalation.

A.4 Conclusions

While the PEG linker afforded polyamide **1** greater solubility at physiological pH than the triamine containing polyamide **3**, the DNA thermal stabilization was greatly compromised. A concurrent reduction in cytotoxicity was also observed, but this did not affect inhibition of DHT induced gene expression. Polyamide **2** exhibited the most favorable profile in gene regulation and cytotoxicity, but was proven too toxic in animal studies to continue evaluation.

References

1. Olenyuk BZ, Zhang G-J, Klco JM, Nickols NG, Kaelin WGJ and Dervan PB (2004) Inhibition of vascular endothelial growth factor with a sequence-specific hypoxia response element antagonist. *Proc. Natl. Acad. Sci. U. S. A.*, **101**, 16768–16773.
2. Nickols NG and Dervan PB (2007) Suppression of androgen receptor-mediated gene expression by a sequence-specific DNA-binding polyamide. *Proc. Natl. Acad. Sci. U. S. A.*, **104**, 10418–10423.
3. Nickols NG, Jacobs CS, Farkas ME and Dervan PB (2007) Modulating hypoxia-inducible transcription by disrupting the HIF-1-DNA interface. *ACS Chem. Biol.*, **2**, 561–571.
4. Hsu CF and Dervan PB (2008) Quantitating the concentration of Py-Im polyamide-fluorescein conjugates in live cells. *Bioorg. Med. Chem. Lett.*, **18**, 5851–5855.
5. Raskatov JA, Meier JL, Puckett JW, Yang F, Ramakrishnan P and Dervan PB (2012) Modulation of NF-kappaB-dependent gene transcription using programmable DNA minor groove binders. *Proc. Natl. Acad. Sci. U. S. A.*, **109**, 1023–1028.
6. Martinez TF, Phillips JW, Karanja KK, Polaczek P, Wang C-M, Li BC, Campbell JL and Dervan PB (2014) Replication stress by Py-Im polyamides induces a non-canonical ATR-dependent checkpoint response. *Nucleic Acids Res.*, **42**, 11546–11559.
7. Hargrove AE, Martinez TF, Hare AA, Kurmis AA, Phillips JW, Sud S, Pienta KJ and Dervan PB (2015) Tumor Repression of VCaP Xenografts by a Pyrrole-Imidazole Polyamide. *PloS One*, **10**, e0143161.
8. Yang F, Nickols NG, Li BC, Marinov GK, Said JW and Dervan PB (2013) Antitumor activity of a pyrrole-imidazole polyamide. *Proc. Natl. Acad. Sci. U. S. A.*, **110**, 1863–1868.
9. Kurmis AA, Yang F, Welch TR, Nickols NG and Dervan PB (2017) A Pyrrole-Imidazole Polyamide Is Active against Enzalutamide-Resistant Prostate Cancer. *Cancer Res.*, **77**, 2207–2212.
10. Hargrove AE, Raskatov JA, Meier JL, Montgomery DC and Dervan PB (2012) Characterization and solubilization of pyrrole-imidazole polyamide aggregates. *J. Med. Chem.*, **55**, 5425–5432.
11. Meier JL, Montgomery DC and Dervan PB (2012) Enhancing the cellular uptake of Py-Im polyamides through next-generation aryl turns. *Nucleic Acids Res.*, **40**, 2345–2356.
12. Nickols NG, Jacobs CS, Farkas ME and Dervan PB (2007) Improved nuclear localization of DNA-binding polyamides. *Nucleic Acids Res.*, **35**, 363–370.
13. Dose C, Farkas ME, Chenoweth DM and Dervan PB (2008) Next generation hairpin polyamides with (R)-3,4-diaminobutyric acid turn unit. *J. Am. Chem. Soc.*, **130**, 6859–6866.
14. Yang F, Nickols NG, Li BC, Szablowski JO, Hamilton SR, Meier JL, Wang C-M and Dervan PB (2013) Animal toxicity of hairpin pyrrole-imidazole polyamides varies with the turn unit. *J. Med. Chem.*, **56**, 7449–7457.

Appendix B
Solubility and stability of hairpin polyamides in pharmaceutical excipients

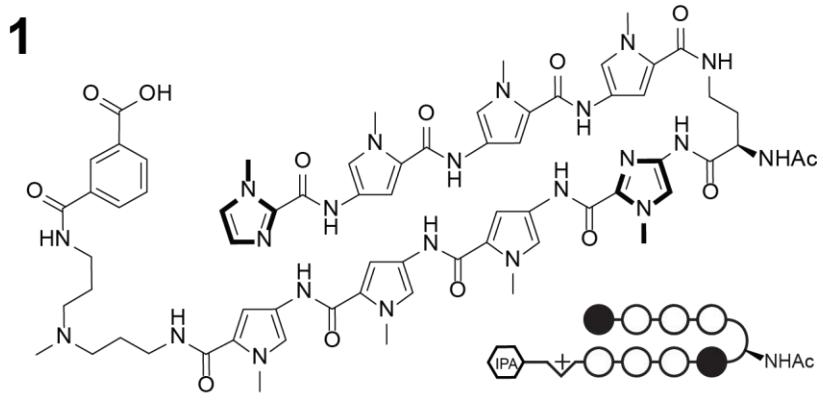

Figure B.1 Structure of Py-Im polyamide **1**.

Py-Im polyamide **1** (Figure B.1) has shown efficacy in several prostate cancer xenograft studies. It has typically been administered in a 20% dimethylsulfoxide (DMSO)/saline solution. This appendix contains the results of several excipient screens conducted with the goal of finding a replacement for DMSO for use in animal studies.

Three commercially available kits (Solubility and Stability, Solubility and Stability 2, and Slice pH, Hampton Research) were used to test a wide range of potential excipients. Polyamide **1** was added to 96 well plates, lyophilized, and solutions from kits added for a final polyamide concentration of 50 µM. Plates were sonicated for 20 minutes, incubated for two hours at room temperature, and absorbance at 315 nm measured by a FlexStation3 plate reader (Molecular Devices). Background at 700 nm was subtracted, and absorbance

from a control (solution only) plate was subtracted from each well. Next, each well was normalized to the highest absorbance well on the same plate to determine relative solubility. Stability was determined by incubating the plates for 10 days at room temperature and analyzing high solubility wells for the presence of polyamide **1** by analytical HPLC. Results are shown in Tables B.1-3. Solutions with the greatest relative solubility were cross-referenced with the FDA Inactive Ingredients list to determine acceptable levels to be used for subcutaneous injection, and to exclude non-FDA approved excipients. Excipients scoring high in relative solubility and stability were tested for their ability to dissolve polyamide **1** at 1 mM, both alone and in combination with each other. A combination of 1% polyvinylpyrrolidone (PVP) and 0.6% tris(hydroxymethyl)aminomethane (Tris) achieved full solubility and this combination was chosen for animal experiments.

Solubility and Stability Screen 1				
Identity	**% maximum solubility**	**Concentration**	**Stable**	**Approved**
tetraethylammonium bromide	100	12.5% w/v	yes	no
polyvinylpyrrolidone K 15	100	1% w/v	yes	yes
non detergent sulfobetaine 256 (NDSB-256)	95	400 mM	mostly	no
non detergent sulfobetaine 221 (NDSB-221)	94	500 mM	no	no
1-butyl-3-methylimidazolium chloride	93	12.5% w/v	yes	no
non detergent sulfobetaine 195 (NDSB-195)	91	500 mM	no	no
pentaerythritol ethoxylate (15/4 EO/OH)	91	12.5% w/v	no	no
6-O-α-D-maltosyl-β-cyclodextrin	91	50 mM	no	no
polyethylene glycol monomethyl ether 750	90	2.5% w/v	no	yes
n-methylformamide	89	15% w/v	no	no
non detergent sulfobetaine 201 (NDSB-201)	89	500 mM	no	no
glutaric acid	88	250 mM	no	no
urea	88	250 mM	no	yes
1-ethyl-3-methylimidazolium acetate	88	12.5% w/v	no	no
non detergent sulfobetaine 211 (NDSB-211)	85	500 mM	no	no
formamide	83	25% w/v	no	no
triethylene glycol	81	5% w/v	no	no
polypropylene glycol P 400	81	25% w/v	yes	yes
glycerol	80	25% w/v	no	no
spermidine	78	250 mM	yes	no

Table B.1 Results of Hampton Research Solubility and Stability screening kit.

Solubility and Stability 2						
Buffer (0.05 M)	**Ion source**	**Ion concentration**	**% maximum solubility**	**pH**	**Stable**	**Approved**
Glycine	Sodium chloride	0.05 M	100	9.5	yes	yes
Glycine	Sodium chloride	1 M	99	9.5	yes	yes
Glycine	-	0	98	9.5	yes	yes
Glycine	Sodium chloride	0.5 M	97	9.5	yes	yes
Sodium citrate tribasic dihydrate	Sodium chloride	1 M	97	5	no	yes
AMPD	Sodium chloride	0.5 M	96	9	yes	no
Imidazole	Sodium chloride	1 M	95	7	no	no
BIS-TRIS propane	Sodium chloride	0.5 M	94	8.5	yes	no
BIS-TRIS propane	Sodium chloride	1 M	92	8.5	yes	no
Tris	Sodium chloride	1 M	92	8	yes	yes
AMPD	-	0	91	9	yes	no
BIS-TRIS	Sodium chloride	0.2 M	91	6.5	yes	no
Succinic acid	Sodium chloride	1 M	91	5.5	no	yes
HEPES	Sodium chloride	0.5 M	89	7.5	no	yes
AMPD	Sodium chloride	0.05 M	88	9	yes	no
Tris	Sodium chloride	0.2 M	88	8	yes	yes
Tris	Sodium chloride	0.5 M	88	8	yes	yes
BIS-TRIS propane	Sodium chloride	0.25 M	87	8.5	yes	no
Sodium citrate tribasic dihydrate	Sodium chloride	0.5 M	87	5	yes	yes
BIS-TRIS	Sodium chloride	0.5 M	87	6.5	no	no

Table B.2 Results of Hampton Research Solubility and Stability 2 screening kit.

Slice pH				
Buffer	**% maximum solubility**	**pH**	**Stable**	**Approved**
500 mM MOPS	100	6.8	no	no
500 mM MOPS	99	7.1	no	no
500 mM BIS-TRIS propane	98	7	yes	no
500 mM MOPS	97	6.5	no	no
500 mM BIS-TRIS propane	96	6.7	yes	no
500 mM BIS-TRIS propane	96	7.3	yes	no
500 mM BIS-TRIS propane	95	8.5	yes	no
500 mM HEPES	93	7.7	no	yes
500 mM TRIS hydrochloride	93	7.5	no	no
500 mM BIS-TRIS propane	93	9.1	yes	no
500 mM TRIS hydrochloride	92	8.1	yes	no
500 mM BIS-TRIS	91	5.7	yes	no
500 mM Tris	91	7.3	no	yes
500 mM BIS-TRIS propane	91	9.4	yes	no
500 mM MES monohydrate	90	5.9	no	no
500 mM BIS-TRIS	90	6.3	yes	no
500 mM MOPS	90	7.7	no	no
500 mM AMPD	89	9.6	yes	no
500 mM AMPD	88	9	yes	no
500 mM Tris	87	8.2	yes	yes
500 mM Tris	87	8.5	yes	yes

Table B.3 Results of Hampton Research Slice pH screening kit.

Animals were subcutaneously injected with 10 mg/kg polyamide **1** in 1% PVP/0.6% tris/saline and blood drawn retroorbitally at 1, 2, 4, 6, 12, and 24 hours. Plasma concentration was determined using analytical HPLC as described in chapter 4, and compared to a previous experiment where animals were injected with 30 mg/kg polyamide **1** in 20% DMSO (Figure B.2). AUC/dose was significantly improved by the new formulation and it was subsequently adopted for the xenograft experiment described in Chapter 4.

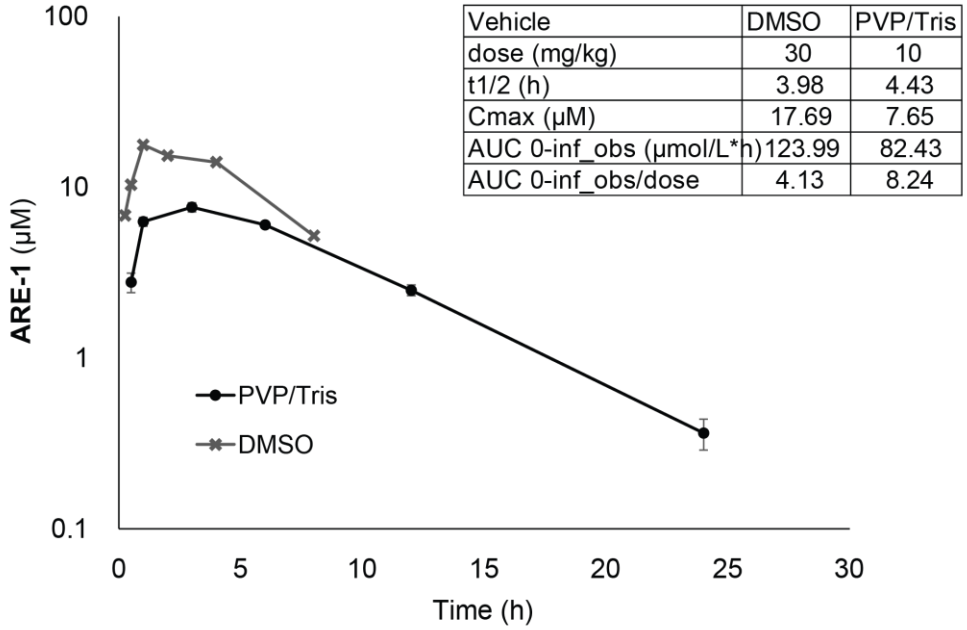

Vehicle	DMSO	PVP/Tris
dose (mg/kg)	30	10
t1/2 (h)	3.98	4.43
Cmax (μM)	17.69	7.65
AUC 0-inf_obs (μmol/L*h)	123.99	82.43
AUC 0-inf_obs/dose	4.13	8.24

Figure B.2 Pharmacokinetic analysis of polyamide **1** in PVP/Tris formulation compared to DMSO/saline formulation. Reproduced from Figure S4.2 A.